Patterns of Soil Instability and Sediment Delivery from the peri-urban Red House Gill catchment, County Durham

Thesis submitted for Master of Science

Department of Geography, Durham University

Alex Rebecca Peters

I. Abstract

Catchment urbanisation raises important concerns over surface water management and potential negative impacts on erosion and the ecological status of rivers. Red House Gill is a small peri-urban sub-catchment of the River Wear, Northern England, which over the past 50 years has undergone extensive urban growth. This research assesses the effects of urbanisation on sediment delivery from this catchment. A sediment budget approach is used to investigate spatial patterns of fine sediment delivery from three main sub-catchments (East, Middle and West streams). Processes were monitored over a six month period using direct stream flow gauging and spatial sampling (with a network of nine Time-Integrated Mass Samplers- TIMS) together with fixed point photography of sediment sources and terrestrial laser scanning. Historic patterns of soil movement were indirectly assessed by measuring the basal trunk angle of 340 trees across the wooded catchment and a detailed dendrochronologic analysis of eight trees.

Results demonstrate that the steep catchment is highly sensitive to high rainfall which leads to rapid discharge (peaks up to 4 $m^3 s^{-1}$) and large suspended sediment loads. Over the study period 80% of suspended sediment load was transported in 2% of the time. Peaks in erosion observed from the static photography and high suspended sediment flux from the TIMS show good temporal agreement. The network of TIMS demonstrates that the majority of sediment is delivered from the Middle stream (55%), which has the second largest catchment area, steepest channel and valley side slopes. In contrast the West stream has the lowest channel gradient and least steep side slopes and consequently delivers the least suspended sediment (3%). Trees growing on steeper slopes generally show greater tilt but the rate of tilt is not significantly correlated with local slope. Results from the dendrochronology demonstrate that soil creep is continually occurring in the catchment, with only a few brief periods where tree rings suggest reduced rates. The preliminary sediment budget demonstrates that over the course of the monitoring period, 482 t of sediment was eroded from the hillslope and delivered to the stream, while 493 t of sediment has been transported by the stream. The 11 t (3%) discrepancy is likely to be caused by in-channel erosion. Assuming a similar annual sediment yield, this equates to a specific annual sediment load of 386 t km^{-2} yr^{-1}, which is close to the maximum reported sediment yields from other UK catchments. Erosion can be potentially managed by reducing peak flows and limiting sediment supply to the stream.

Table of Contents

II. List of Figures

III. List of Tables

IV. Declaration

This thesis and all material presented within it has not been previously submitted for a degree at Durham University or at any other university. Where relevant all work produced by other people has been acknowledged.

I. Acknowledgements

I am incredibly grateful for the support and patience I have received from my supervisors, Dr Jeff Warburton and Dr Nick Rosser. Jeff has been invaluable during every stage of this project while Nick was always on hand offering technical guidance. Along with my supervisors, this project wouldn't have been completed without the help and advice of the Geography Technicians especially: Merv Brown, Paul West, Alison Clark, Kathryn Melvin and Chris Longley.

Special thanks must also be given to Hannah Joyce who was always brilliant in the field along with Mark Kincey, Bishnu Sharma, Rosie Fewings and Richard Boothroyd. I am also incredibly grateful to Catherine Kelham for our discussions in The Dungeon.

I would also like to thank Graham Stenson, who has been incredibly helpful.

1 Introduction

1.1 Research rationale

Urbanisation continues to increase at an alarming rate; predictions suggest that by 2030, 83% of people living in developed countries will occupy urban areas (Cohen, 2003). In England there is a steady demand for housing and related urban services, with just short of 100,000 new homes developed in 2012 (National Statistics, 2012). Typically this expansion is accommodated on the urban periphery, leading to development on green-field agricultural or natural land. The result is a catchment which consists of a mixture of urban, agricultural and natural land, and these are typically referred to as peri-urban watersheds (Braud et al., 2013). In extreme cases, the creation of urban infrastructure can set in motion a cascade of negative hydrological changes, often resulting in increased run-off and diffuse pollution (Jacobson, 2011). This has lead Meyer et al. (2005) to coin the term 'urban stream syndrome' describing the commonly observed ecological degradation of streams draining urban areas (Figure 1.1).

Of particular concern for stream ecology is growing awareness of the management problems caused by elevated levels of fine sediment delivery. Fine sediment can act as a potential carrier and storage agent for many hazardous contaminants including: phosphorous (P), pesticides, heavy metals and pathogens, which then pass through the fluvial system. (SedNet, 2004, Walling, 2005). Elevated levels of fine sediment also create a number of aquatic problems. For example, clogging the gills of aquatic animals, interfering with feeding regimes, ruining the habitat of bottom-dwelling creatures and decreasing light penetration, limiting photosynthesis and consequently decreasing primary productivity for the whole ecosystem (Wood and Armitage, 1997). Figure 1.1 illustrates the general relationship between urbanisation, increased fine sediment delivery and the detrimental impacts on ecology within the fluvial network.

Predicted increases in rainfall and storm intensity caused by anthropogenically induced climate change could further amplify the effects of urban development on fine sediment delivery (Praskievicz and Chang, 2009). However, within the UK's regulatory system there is no explicit legislative framework for sediment management (Walling and Webb, 1987). Instead sediment is indirectly regulated by

a range of legislative and non-legislative drivers including: catchment sensitive farming programmes, Salmon Action Plans (SAPs), Sustainable Urban Drainage Systems (SUDS) and Biodiversity Action Plans (BAPs) (Casper, 2008). The EU Water Framework Directive also doesn't ask member states to specifically monitor suspended sediment. However, the directive catchment characterisation process has identified sediment delivery as a diffuse source pressure, with 21% of surface water bodies in England and Wales either 'at risk' or 'probably at risk' of failing ecological objectives, due to high suspended sediment concentrations (Casper, 2008). Given the lack of direct legislative frameworks in place to monitor suspended sediment, a group of environmental specialists have formed SedNet, which has the aim of informing policies about sediment management (SedNet, 2013).

Although previous research has looked at both the short-term dynamics of fine sediment delivery and the longer term context (Duijsings, 1987, Pawlik et al., 2013) there is still considerable scope to better understand these processes, especially within peri-urban environments. Like most of the UK, the Northeast of England is currently experiencing high levels of urbanisation, creating a mixture of rural, urban and peri-urban catchments. The aim of this research is to investigate the impact of catchment urbanisation on patterns of soil instability and sediment delivery in a peri-urban headwater catchment using a sediment budget approach.

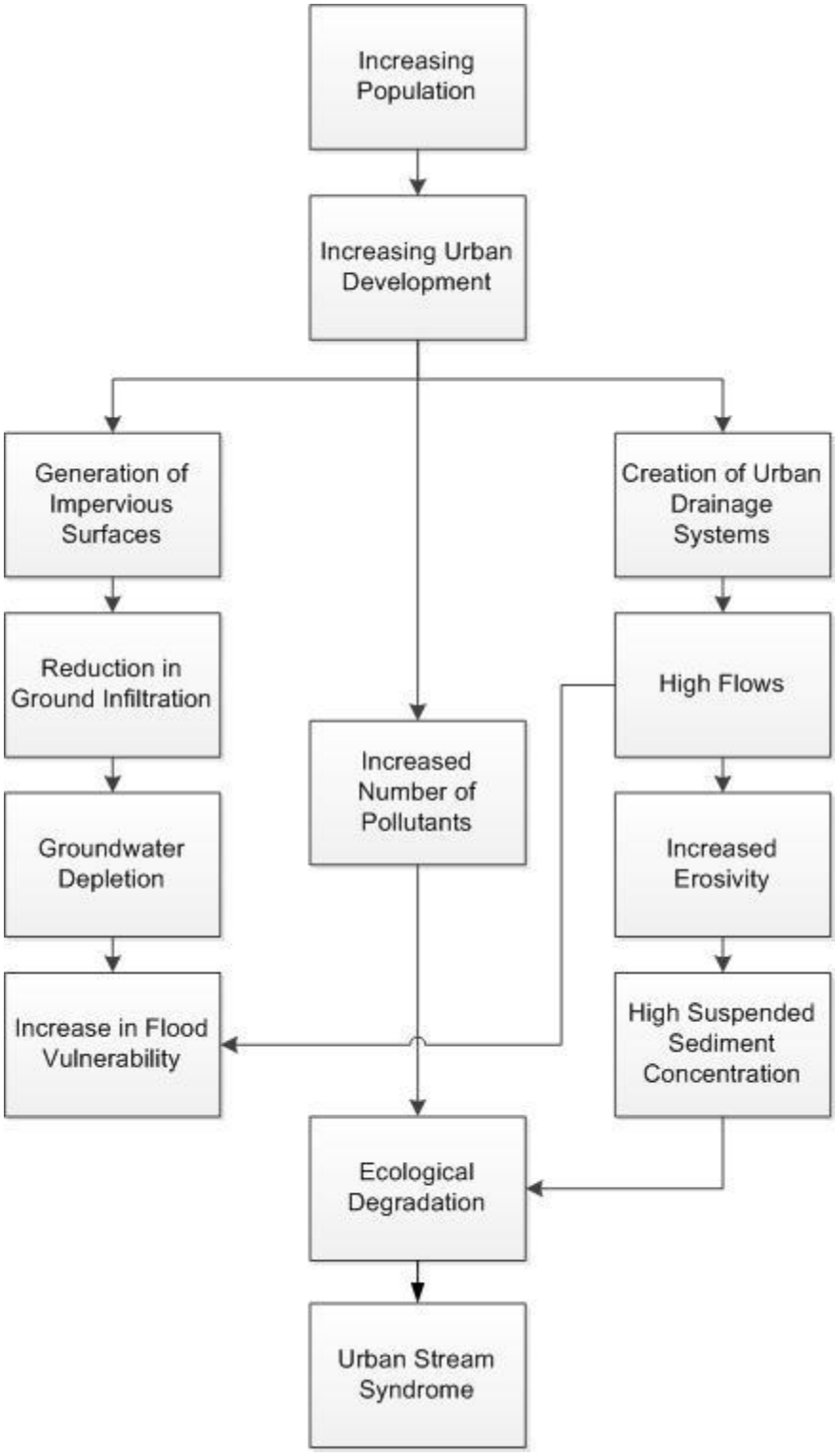

Figure 1.1-Flowchart illustrating the links between catchment urbanisation fine sediment and ecological degradation.

1.2 Case Study Site: Red House Gill, County Durham

Red House Gill is a small tributary (2.5 km^2) of the River Wear in County Durham (Figure 1.2). Since the 1960's, the catchment has undergone a range of land use changes, converting natural and agricultural land into houses and local services, including an out of town retail park called the Arniston Centre. During this period of catchment urbanisation, local fishermen have raised concerns over high flow events resulting in severe erosion and extensive bankside landslips along the stream course. However, in the lower reaches of the River Wear, where the underlying geology and local topography create a setting susceptible to erosion and landslips an important question arises as to whether the erosion within the Red House Gill catchment is natural or exacerbated by the urban development. Concerns are now growing regarding the ecological damage caused by deposition of eroded sediment in the River Wear downstream of the confluence with Red House Gill. This has ignited a debate between local stakeholders and responsible authorities regarding management schemes including sustainable urban drainage (SUDS), which aim to deal with storm water run-off in terms of quantity and quality close to source (Freni et al., 2010).

Red House Gill is a small tributary catchment of the lower reaches of the River Wear highlighted by the Environment Agency local fisheries stakeholders as having chronic erosion problems. In the lower Wear Valley any tributary catchments display similar physical characteristics such as steep slopes and highly erodible superficial geology and are also undergoing rapid urbanisation. Therefore, Red House Gill is not unique and provides a topical and relevant catchment to investigate the spatial and temporal patterns of fine sediment flux as a result of urbanisation.

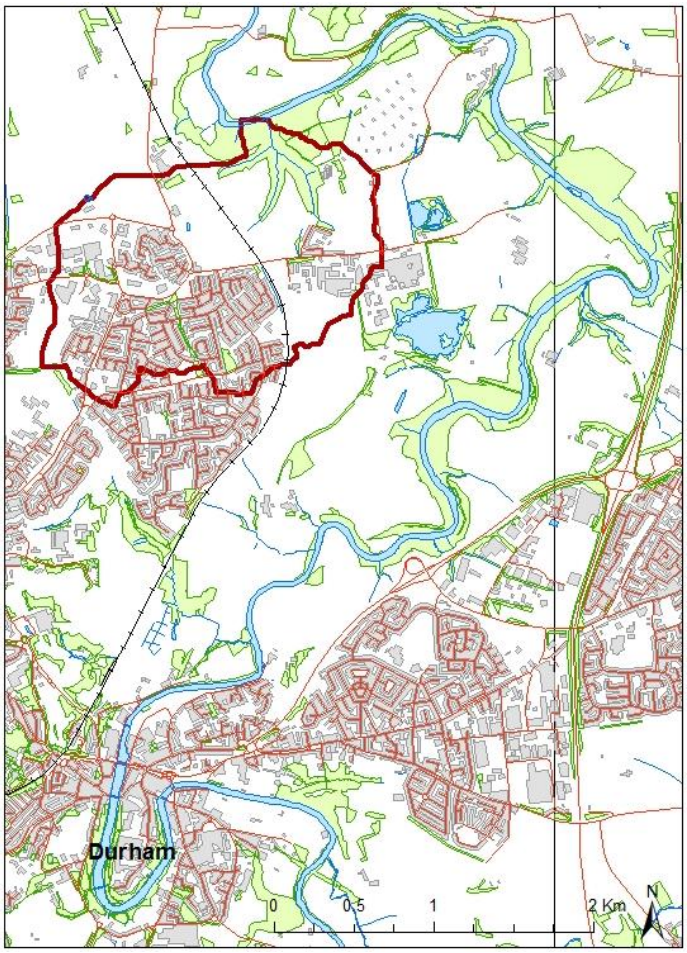

Figure 1.2-Location of the Red House Gill catchment (bold red line) in relation to the Durham city centre. The focus of the sediment budget study is the wooded stream network in the north-eastern part of the catchment.

1.3 Research aims and objectives

The general aim of this project is to assess the dynamics of fine sediment delivery from the Red House Gill catchment to the River Wear. This involves the consideration of the short-term sediment dynamics and longer term geomorphological evolution of the catchment. This information can then be used to inform and create effective management strategies for future development within the catchment.

This will be achieved through the following five research objectives:

1. Produce a time series of fine sediment flux from the catchment to the River Wear; identifying flow events; and periods and conditions leading to enhanced fine sediment delivery.

Previous research suggests 50% of total suspended sediment can be transported in as little as 1% of the time, while 90% can be transported in under 5% of the time (Walling et al., 1992). Therefore it is important to create a time series of suspended sediment concentrations, taking into account river stage and the spatial pattern of sediment movement, providing information on circumstances surrounding delivery.

2. Carry out local surveys using fixed point photography and a terrestrial laser scanner (TLS) to characterise hotspots of bank instability and lateral slope instability.

In order to assess the impact of high flows on lateral bank stability, static photography and terrestrial laser scanning will be used. Repeat photographs at numerous locations throughout the catchment will be collected documenting processes causing erosion. While terrestrial laser scanning at one location will be used to supplement this data, looking at the feasibility of monitoring erosion in a steep wooded catchment using this method.

3. Map areas of catchment soil instability using tree deformation and dendrochronology to determine historical patterns of soil creep.

As part of this research it is necessary to understand the spatial and temporal controls of fine sediment being supplied to the stream from the surrounding landscape. To assess the spatial controls of fine sediment, tree deformation will be mapped and used as a proxy for soil creep throughout the wooded catchment. Dendrochronology is a useful tool for interpreting temporal patterns of instability (Speer, 2010) and will therefore be used to provide historical insight into the patterns of soil creep.

4. Produce a geomorphic map summarising key sediment sources within the eroding catchment.

To help inform sustainable management strategies it is important to understand the connections between fine sediment sources, pathways and deposition downstream. This can be done by creating a geomorphic map (Cooke and Doornkamp, 1990). Based on site visits, landslides, bank erosion and collapse throughout the catchment will be mapped.

5. Use these data to assess the longer term spatial and temporal context of observed sediment delivery patterns and construct a preliminary sediment budget characterising fine sediment delivery in the catchment.

Sediment budgets offer a conceptual simplification of a variety of processes, conveying the sources, sinks and pathways of eroded material (Reid and Dunne, 1996). In this research, suspended sediment sampling along with static photography provide information on contemporary sediment movement throughout the catchment over a six month period.

These objectives will be realised through an integrated field measurement framework designed to satisfy the main data requirements (Table 1.1).

Measurement Technique	**Dominant Geomorphic Process**	**Data Acquired**	**Relevant Research Question**				
			1	2	3	4	5
Turbidity Sensor and Stage Recording	Fluvial – fine sediment	Suspended sediment concentration time series					
Time Integrated Mass Samplers	Fluvial – fine sediment	Spatial pattern of suspended sediment delivery					
Automatic Water Sampler	Fluvial – fine sediment	Suspended sediment concentration					
Static Photography and Terrestrial Laser Scanning	Slope – failure	Slope change analysis					
Tree Curvature	Slope – soil creep	Angle Measurement					
Tree Cores	Slope – soil creep	Temporal Pattern of Soil Creep					

Table 1.1-The different measurement techniques and relevance to the key research objectives.

1.4 Thesis Structure

This thesis consists of eight chapters. Following the introduction Chapter 2 reviews the existing literature regarding the spatial controls of fine sediment dynamics and

the associated ecological degradation using a range of case studies. Following on from this, Chapter 3 provides details about the Red House Gill catchment before Chapter 4 summarises the key research methods explaining both field and laboratory techniques. The next two chapters describe the results; Chapter 5 describes contemporary patterns of fine sediment erosion and delivery while Chapter 6 explains historic patterns of instability by characterising catchment wide soil creep. Chapter 7 then discusses the results, bringing all the data together to create a preliminary sediment budget for the catchment while deliberating potential management options. The conclusion of this research is then expressed in Chapter 8.

2 Literature review

This focus of this chapter is to briefly review literature relevant to hillslope processes occurring at Red House Gill and fine suspended sediment dynamics. This chapter will be broken down into four sections. The first section looks at the effects of urbanisation on river catchments (Section 2.1) before explaining the sediment budget approach which will be used in the research to look at the interactions between hillslope processes and fine suspended sediment (Section 2.2). The final sections discuss hillslope processes and how they will be monitored (Section 2.3), before explaining how fine suspended sediment will be measured (Section 2.4).

2.1 Catchment Urbanisation

Catchment urbanisation produces many important hydrological changes. An increase in impervious surfaces resulting from urban development significantly alters the hydrological response of streams, by reducing the lag time between peak rainfall and discharge creating a 'flashy' hydrograph (Dunne and Leopold, 1978). Research by McMahon et al. (2003) compared hydrograph characteristics including rising and falling limb rates with measures of urbanisation. Results from watersheds in Boston, Massachusetts and Birmingham, Alabama showed a positive correlation between 'flashy' hydrographs and urbanisation. However, a third watershed in Salt Lake City, Utah showed a less convincing correlation. Unlike the other areas studied, the catchment in Salt Lake City is occupied by isolated clusters of urbanisation separated by different types of land cover, which helps mitigate the effects of urbanisation. Within peri-urban watersheds (Section 1.1), urban areas have far more efficient drainage compared to agricultural or natural land (Burns et al., 2012). Miller et al. (2014) investigated changes in run-off resulting from the transformation of rural landscapes to peri-urban areas in two sub-catchments in Swindon, UK. The Rodburn catchment is highly urbanised but still has natural drainage routes whereas the Haydon Wick catchment is peri-urban containing two areas of distinct drainage, one with storm drainage and natural drainage routes (FBC) and one comprised entirely of storm drainage (CWS). The Haydon Wick FBC sub-catchment, demonstrated a peak flow of 0.8 m^3 s^{-1}, compared to a peak flow of 2.9 m^3 s^{-1} for the CWS sub-catchment comprised entirely of storm drainage. Hydrographs for Haydon Wick FBC and the Rodburn catchment are very similar which is expected as both receive run-off from sub-surface pathways and storm

drainage. Haydon Wick CWS has a higher peak discharge, due to the efficient storm drainage. This efficiency can be explained by Manning's equation (Equation 2.1):

$$V = \frac{R^{\frac{2}{3}} S^{1/2}}{n}$$

Equation 2.1

Where V is average velocity (m/s), R is the hydraulic radius (m), S is water surface slope (m/m), and n is roughness coefficient. Therefore, water velocity is indirectly proportional to the land surface roughness, so storm water run-off easily crosses smooth impervious surfaces and can be quickly routed through smooth drains and concrete-lined channels.

Over a 50 year period, Rose and Peters (2001) compared stream flow characteristics for urbanised and rural watersheds in Atlanta, Georgia. Their results show that peak flows are between 30-100% higher in urbanised catchments. As this water moves, potential energy is transformed into kinetic energy, which has the ability to significantly alter the character of the fluvial environment through erosional processes (Knighton, 1999). An increase in the erosional power of streams is typically followed by an increase in suspended sediment and increases in suspended sediment have biological and chemical effects. Biological effects include reduction of light penetration and therefore photosynthesis and clogging fish gills (Gordon et al., 2004). Research by Roy et al. (2003), looked at the effects of urbanisation on ecology by examining the relationship between land cover and macro-invertebrate assemblage indices in several streams within Georgia, USA. Results demonstrated that catchment urbanisation leads to less diverse and more tolerant stream macro-invertebrate assemblages due to increased sediment load. Chemical effects have also been widely reported. For example, Owens and Walling (2002) explained how total phosphorus content of sediment increased with urbanisation in three British catchments. While work by Robertson et al. (2003), demonstrated that road derived sediments from Manchester, UK contained high metal concentrations, which discharge into river systems through urban drainage. There was also a clear spatial pattern of lead concentration, with higher concentrations in inner cities compared to outer city sites, which reflects the different levels of vehicle activity (Robertson et al., 2003). Goodwin et al. (2003),

compared sediment yields for a small rural catchment and urban catchment in Bradford, UK. Their results demonstrated that for individual storms, the sediment yields from the urban catchment were higher. However, over the course of the annual monitoring program sediment yields from the rural catchment were comparable. In terms of environmental quality, instantaneous sediment concentrations were far higher from the urban part of the catchment as a result of the Combined Sewage Overflow (CSO) and therefore contained high levels of organic material, which can lead to oxygen depletion (Goodwin et al., 2003). Lawler et al. (2006) measured turbidity and five water quality variables (electrical conductivity, temperature, pH, DO and ammonia) on the Wolverhampton arm of the River Tame, UK. 10 out of 15 turbidity events considered, coincided with peaks in ammonia, due to overflowing in sewage or waste water treatment works. Sediment fingerprinting can be used to demonstrate the source of suspended sediment. Work by Carter et al. (2003), provides an insight into the sources of sediment within the catchment of the River Aire and its main tributary the River Calder. Within the upper part of the River Aire's catchment, a significant amount of sediment comes from channel bank erosion. However within the urbanised lower reaches, large quantities come from road dust (Carter et al., 2003). The effect of urbanisation on stream quality is scale dependent. Work by Klein (1979), looked into the degree of stream quality impairment and extent of catchment urbanisation. Results indicate that ecological degradation is first noticed at 12% urbanisation; however it doesn't become severe until imperviousness reaches 30%. More recently work by Wang et al. (2001) has provided further evidence to support this idea, as their results suggest that catchment impervious cover between 8-12% represented a threshold value where small changes in urbanisation resulted in major changes in stream degradation.

Although a lot of the literature cited is based in the United States, the principles associated with the effects of urban development on catchment hydrology apply more globally. Many parallels can also be drawn between the hydrological, climatic and geomorphic conditions between these studies and UK sites like Red House Gill.

2.2 Sediment Budget Approach

Traditionally geomorphologists have used reductionist approaches to research river catchments through the analysis of individual processes (Swanson et al., 1982). However, this approach is unsatisfactory when considering complex natural

systems such as Red House Gill because of the highly interconnected nature of the geomorphic system. As such, a system science approach using the conceptual framework of a sediment budget will be employed here.

Sediment budgets are quantitative statements expressing the rates of production, transport and discharge of eroded material within a catchment system (Dietrich et al., 1982, Reid and Dunne, 1996). These models have been constructed for a variety of spatial scales ranging from small agricultural catchments (Walling et al., 2002) to large river watersheds (Meade, 1982). This integrated approach draws links between terrestrial and aquatic systems helping develop management strategies. However, relatively few studies have taken place using a sediment budget approach to investigate the effects of urban development on erosion, especially within the UK. Reconnaissance field visits have provided an initial assessment of key erosion and transport processes at Red House Gill, resulting in the drafting of an initial sediment budget framework (Figure 2.1). The conceptual model emphasises the linkages between the Red House Gill hillslopes and channel which eventually discharges into the River Wear. Within the catchment, hillslope processes including bank erosion, landslides and soil creep are widespread in delivering fine sediment to the stream. Sheet wash and tree throw also occur within the catchment. However, initial field visits suggest that these processes don't contribute large quantities of sediment. Once delivered to the channel, material can be divided into bedload, suspended load and dissolved load, which flows into the River Wear. During high flow events, slack water sediments from the River Wear are deposited into the Red House Gill catchment within the lower stream channel.

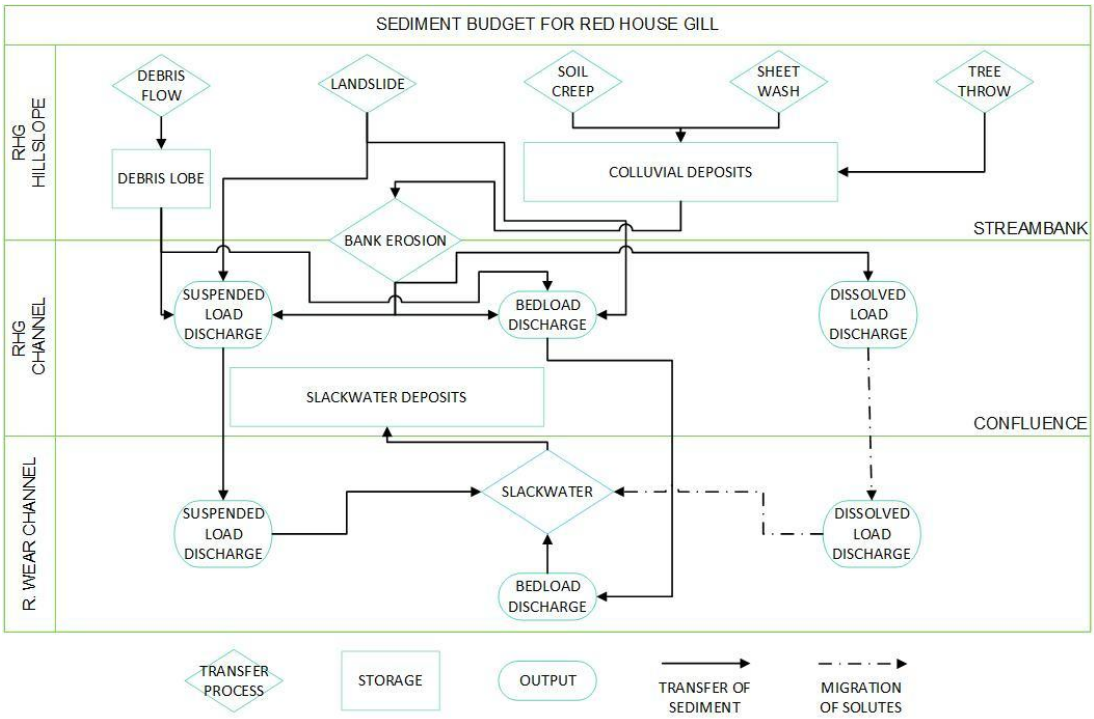

Figure 2.1-Initial sediment budget for Red House Gill demonstrating the main processes occurring within the catchment hillslopes, channel and River Wear.

2.3 Hillslope Processes

The Red House Gill catchment contains a large area of wooded hillslopes (~20%), where the three streams converge. Within this area, trees and understorey vegetation play an important role in controlling local geomorphic processes, helping to create a 'geoecosystem' (Pawlik, 2013). Vegetation on hillslopes modifies soil moisture through intercepting rain but it also has the ability to alter drop size distribution, intensity and areal distribution, which significantly alters erosive power and therefore rain splash erosion (Goudie et al., 1981). The reduction in soil moisture along with intertwining roots helps increase slope stability and therefore reduce the risk of mass movement (Rickli and Graf, 2009). Above ground biomass creates micro-tographical features, which inhibit overland flow due to an increase in hydraulic roughness and therefore reduces soil erosion (Parsons et al., 1992). However, vegetation can also increase soil transport. Tree throw upheaves not only a root ball but also any attached sediment and is therefore an important soil transport agent in some forested hillslopes (Dietrich et al., 1982). The hillslope processes occurring in Red House Gill appear to be dominated by soil creep,

landsliding and bank erosion as outlined in the sediment budget shown in Figure 2.1.

2.3.1 Soil Creep

Soil creep is the slowest form of mass movement caused by a variety of processes moving regolith downslope under the influence of gravity. These processes typically include: mass flows of debris under continuous shear caused by soil weight, displacement of soil caused by expansion and contraction from wetting and drying along with freeze-thaw action and weathering (Dietrich et al., 1982). As these processes are more dominant near the soil surface, the rate of soil creep is typically greater at the top of the soil column, rapidly decreasing with depth (Kirkby, 1967). Soil creep plays an important role in sediment delivery within small basins, due to its high frequency albeit low magnitude of soil movement (Osterkamp and Toy, 1997). In large catchments, soil creep also plays a significant role in the development of landslide hazards as the downslope movement of material fills existing landslide scars, creating soil wedges. As the wedge is formed, the probability of landslide failure increases, suggesting that landslide frequency is related to rates of soil creep (Dietrich and Dunne, 1978). More recent work by Yamada (1999) demonstrates the importance of soil creep as a hollow infilling process before slope failure occurs.

The rate of soil creep varies due to a range of spatial and temporal factors. Research by Jahn (1989), looked at the effects of different altitudinal and ecological zones on soil creep. Results demonstrated that soil creep rates in lowland pastures were 2-3 mm yr^{-1}, although this tripled for higher altitudes. The results also indicate that no soil creep was observed over a 12 year period in a mature forest. A review of previous literature has been compiled by Saunders and Young (1983) demonstrating the variability of soil creep rates depending on climate. Within temperate maritime climates, soil creep ranges between 0.5-2.0 mm yr^{-1}, whereas in temperate continental climates, the rate is far higher ranging between 2-15 mm yr^{-1}, within the upper 20-25 cm of soil. The authors suggest this is due to more severe freeze thaw action within temperate continental climates. Although it has been suggested that soil moisture content within the summer months is the most important factor controlling soil creep with freeze thaw activity contributing very small amounts of transport (Yamada, 1999).

Measuring soil creep is difficult (Reid and Dunne, 1996). Dietrich et al. (1982) has suggested the difficulty surrounding creep measurements has restricted

quantification and therefore its use within sediment budgets for forested catchments. An exception is a study in a forested catchment in Luxembourg, where sediment traps were used to quantify superficial (seasonal) soil creep. The results suggest that soil creep was responsible for just 0.8% of bank derived sediment into a stream channel (Duijsings, 1987). A nylon mesh was attached to the soil trap, limiting the effects of splash erosion although it is unlikely that these effects would have been completely removed. Nelson and Booth (2002) calculated the volume of sediment derived from creep using an average rate based on the work by Saunders and Young (1983). Soil creep was only calculated for hill slopes immediately adjacent to the channel, suggesting that soil creep was responsible for 3% of total sediment yield. However, this technique assumes a constant rate of soil creep across the area giving rise to potential errors within the study and doesn't reveal prominent areas of soil creep.

2.3.2 Landslides

Mass wasting or slope movement is an important geomorphological process delivering sediment to river channels (Reid and Dunne, 1996). Slope movement occurs when shear stress (the main mechanism causing downslope movement of materials or the external force) exceeds the shear resistance of the material (the main mechanism resisting movement or the internal force) (Terzaghi, 1950).

Previous research conducted by Duijsings (1987) found that landslides within a forested catchment typically occurred after periods of prolonged rainfall or snowmelt. Within this sediment budget, landslides accounted for 14% of sediment delivered by the hillslopes. Heavy rain and snowfall cause landslides by temporarily raising the water table to a shallower depth, increasing soil saturation and therefore pore water pressure. The increase in pore pressure, slightly forces the grains apart, reducing inter-grain friction, cohesion, shear strength and resisting forces (Walker and Shiels, 2013). However Rickli and Graf (2009) mapped 500 shallow landslides which were less than 2 m deep after heavy rainfall events in Switzerland, finding that shallow landslides were less frequent in forest than in open land. Research has demonstrated that landslides can produce up to 50% of the available sediment in a catchment (Nelson and Booth, 2002). However the authors caution that in their study the process of landsliding was only evaluated on 5% of tributary streams and then extrapolated to other stream channels which weren't field checked. This could result in a significant amount of uncertainty in the results.

2.3.3 Bank Erosion

River banks are an important store and source of material in a sediment budget. Sediment source fingerprinting conducted by Walling and Collins (2005) in British rivers reveals that river banks on average supply between 5 and 15% of suspended sediment. In high flow events however, this increased up to 40%. River bank erosion and collapse occurs as a result of two main processes: fluvial and sub-aerial. Fluvial processes occur as turbulent, high velocity water attacks the river bank through corrasion (Hooke, 1979). River bank erosion can lead to collapse. This often occurs as the lower non-cohesive part of the river bank is easily eroded leaving the cohesive top part of the bank to collapse. A large portion of research has focussed on the timing of river bank failure as Twidale (1964) suggests that slumped debris is often found at the foot of channel banks and therefore must have collapsed during the receding limb of a high flow event otherwise it would have been washed away. A reason for this has been suggested; the high velocity water supports the river bank but as the water level recedes, the cohesive layer which now has a high pore water pressure collapses into the river channel (Lawler et al., 1999). This process therefore has important implications on the timing of sediment release into streams.

Sub aerial erosion typically includes freeze-thaw and desiccation processes. However, their influence on erosion divides the literature. Sub aerial processes are typically thought as ‘preparatory’ instead of ‘erosive’ as they help weaken the bank (Hooke, 1979; Duijsings, 1987). This has been reflected by the recent work of Henshaw et al. (2013). Their results suggest that the influence of sub aerial processes is small especially when compared to fluvial erosion processes. Contrary to this, a modelling study by Lawler (1995) suggests that sub aerial and fluvial processes dominate in different parts of the river. In the upper reaches, sub aerial processes dominate due to limited stream power whereas in the lower stream reaches with high stream power, fluvial processes dominate. The results of the model were later empirically supported by fieldwork (Lawler et al., 1999). Just as the spatial distribution of erosion processes is important, so is frequency. Couper and Maddock (2001), investigated different erosive processes operating on the River Arrow, Warwickshire, finding that sub aerial processes operate more frequently than fluvial as the study period was characterised by a lack of high flow events. Duijsings (1987) reported that temporal variations in stream bank erosion were dominated by

the magnitude of discharge and to a lesser extent, freeze thaw. During his two year study, bank erosion contributed 43% of total suspended sediment (Duijsings, 1987).

2.4 Monitoring Hillslope Processes

Soil creep, landslides and bank erosion require different monitoring methods. Dendrogeomorphology, encompassing traditional tree coring and investigations surrounding tree deformation has a long history of being used to look at rapid mass movements (Alestro, 1971) but it can also be used to investigate soil creep and historic slope instability (Mills, 1984, Denneler and Schweingruber, 1993, Pawlik et al., 2013). This part of the research will help inform research objective three and five (Table 1.1). Contemporary erosion by landslides and bank collapse occurs frequently and the use of laser scanning for monitoring these processes has undergone rapid developments within the last few years and is now routinely used (Jaboyedoff et al., 2012). This part of the research will help inform research objective two and five (Table 1.1).

2.4.1 Dendrochronology in Geomorphology

Dendrochronology methods are widely used in geomorphology (Stoffel and Bollschweiler, 2008). The majority of trees produce annual growth rings which can be used to date historical geomorphological processes, by the development of reaction wood (Alestro, 1971) (Figure 4.5). In order to regain stability after being tilted, trees produce reaction wood; gymnosperms produce compression wood on the downhill side of the tree whereas angiosperms produce tension wood on the uphill side of the tree (Speer, 2010). Initially dating reaction wood focused on dating historical events including debris flows (Hupp and Sigafoos, 1982, Osterkamp and Hupp, 1987). More recent dendrochronological methods have been used to spatially reconstruct landslide patterns. Bollschweiler et al. (2008), coupled tree ring analysis with a 1:1000 scale geomorphic map, allowing the spatial pattern of several debris flows to be distinguished. However, the use of dendrochronology to look at the effects of soil creep is rarely used (Denneler and Schweingruber, 1993, Pawlik et al., 2013).

Sharpe (1938) suggested that soil creep causes trees to deform, creating a curve at the base of the tree (Figure 2.2). The curve is created through a combination of processes: the roots grow downward into bedrock or into deeper soil horizons

where soil creep doesn't occur, while the superficial layer of soil affected by creep presses the upper part of the roots and base of the tree while growing vertically. However, as pointed out by Parizek and Woodruff (1957) slow continuous movement of the tree through soil creep wouldn't create a curve at the base, instead it would create a sweeping curve throughout the length of the tree (Figure 2.3). Phipps (1974) agrees with Parizek and Woodruff (1957) suggesting that the classic curved tree shape attributed to soil creep by Sharpe (1938) would only occur where environmental conditions were much different when the tree was a sapling. Instead they suggest three possible causes: (1) a sudden slump of material causing the curve before the tree continues to grow vertically straight; (2) extreme environmental event including flooding, wind or snow build up causing the tree to curve downslope; and (3) change in sunlight conditions causing the young sapling to curve in phototrophic response (Parizek and Woodruff, 1957, Sharpe, 1938). More recently, Harker (1996) created a mathematical model predicting the curvature of trees under constant rates of soil creep, his results for a seven year old tree are similar to the sweeping curve previously proposed. Taking into account the high seasonal variability in rates of soil creep, this model was then validated over a two year period in Mount Rainer National Park, USA. This has important implications for Red House Gill, as the majority of trees are similar to the classic shape proposed by Sharpe (1938) (Figure 2.2), instead of the sweeping curved proposed. However, both soil creep and more rapid mass movements highlight soil instability within Red House Gill and therefore the importance of measuring tree deformation.

Figure 2.2-Classic curved tree proposed by Sharpe (1938), taken from Red House Gill on an initial site visit. The tree has a DBH of 0.8m.

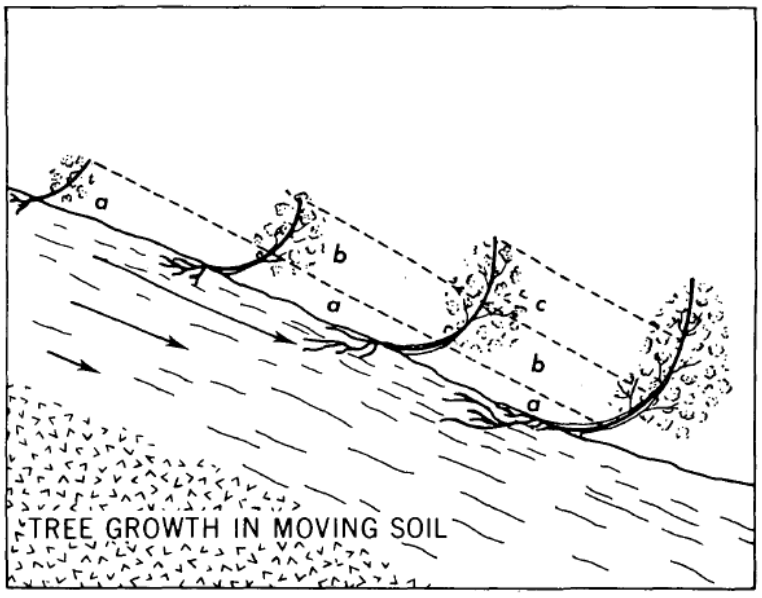

Figure 2.3-Temporal sequence indicating the effect of continuously moving soil creep on tree trunks (Parizek and Woodruff, 1957, p.65).

Three previous studies have used increment cores to gather information about the presence of reaction wood in relation to soil creep. Denneler and Schweingruber (1993), looked at the effects of soil creep in two separate locations in Gams situated in the Swiss Rhine valley. They collected cores from 36 different trees, located in two separate areas, one which was deemed stable and the other unstable. The trees ranged from 64-146 years old, providing a good temporal record. The results demonstrate the episodic nature of soil creep, with epochs of increased and decreased activity being revealed by the presence of reaction wood. Both sites showed a marked decrease in the presence of reaction wood within the 1940s which correlates to a period of low precipitation. The direction of reaction wood growth was also taken, demonstrating that on unstable slopes, reaction wood was almost entirely occurring directly downhill, whereas on the stable slope, it was offset to the east. This reveals the highly variable nature of soil creep movements. Wistuba et al. (2011) cored 52 trees within the Carpathian Mountains, developing an eccentricity index for reaction wood growth throughout time. The eccentricity index allowed the authors to distinguish between shallow slope movements (soil creep) from relatively deep seated movements (landslides). A more recent study was undertaken in the Stolowe Mountains, south west Poland, where 24 trees were sampled (Pawlik et al., 2013). The trees ranged from 48-92 years old, with reaction wood having developed in 15 trees. The results demonstrated that the development of reaction wood and therefore soil creep is generally connected with wet years; however during the wet period 1979-1981, very few trees developed reaction wood. The trees also didn't produce a clear spatial pattern of soil creep.

In addition to research using tree cores to look at soil creep, two studies have also measured the angle at the base of curved trees. Mills (1984), collected measurements for 30 curved trees at seven different locations within Giles County, Virginia. His results, demonstrated that trees on steep boulder streams were tilted more than those with comparable slopes on side slopes and suggested the difference could be caused by differences in individual tree species. His results, also demonstrated no significant correlation between angles at the base of the tree caused by soil creep and tree age. It has therefore been suggested, that the curve at the base of the trees must have developed when the trees were saplings due to a sudden mass movement and therefore agrees with previous work by Parizek and Woodruff (1957). More recent research has been undertaken by Winchester et al. (2006) in Maccu Picchu, Peru, with their results suggesting that trees exhibit a more

pronounced curve on steeper slopes, although it appears that no formal correlation analysis occurred.

In this research, the effects of soil creep on trees will be studied in two ways, providing information on the spatial and temporal patterns of slope instability and therefore fine sediment delivery. Firstly, tree cores will be taken to look at episodes of soil creep throughout time. Secondly, the angle at the base of the curved trees, known from now on as basal trunk angle, will be measured as a proxy for the spatial pattern of soil creep in the Red House Gill catchment.

2.4.2 Terrestrial Laser Scanning

The use of remote sensing techniques for landslide monitoring is undergoing rapid development (Jaboyedoff et al., 2012). Laser scanning is capable of providing high accuracy and high resolution point clouds of landslide faces which can be used for a range of purposes including: hazard assessment, modelling and monitoring. As part of this research, terrestrial laser scanning is used to monitor the volume of sediment being eroded from a slope within Red House Gill, which is representative of others within the catchment. These data have been collected for comparison with static photography of erosion sites. Point clouds can be ground filtered and interpolated to produce a Digital Elevation Model (DEM). DEMs of difference (DoD) are then produced, by subtracting two DEMs from different temporal epochs, revealing the volume of sediment having been eroded. This technique has previously been used to monitor the volume of sediment being eroded from a debris slide as part of a sediment budget in the French Alps (Theule et al., 2009).

2.5 Measuring Suspended Sediment

A variety of techniques have been developed to sample suspended sediment at a range of different temporal and spatial scales (Wren et al., 2000). These sampling techniques are generally divided into direct and indirect measurements, both of which are being employed at Red House Gill to help answer research objective one and five (Table 1.1).

2.5.1 Water sampling

Direct collection of river water provides a sample of suspended sediment at a single point in time and space (Gao, 2008). However as concentrations vary both spatially and temporally, a large number of water samples are required to build a

representative picture of suspended sediment within fluvial environments (Walling, 1977, Johnson, 1992). Automatic water samplers use a pump to draw water up from the river before the sample distribution system diverts water into sequential bottles (ISCO, 2004). Typically these samplers can collect between 24 and 48 samples with a range of different water volumes (350-3700ml) depending upon the specific system (Hicks and Gomez, 2003, ISCO, 2004). Sampling can be triggered by a range of threshold values including: stage, flow and turbidity (ISCO, 2004). Within this research, the automatic sampler has been used to constrain results generated from a turbidity probe.

2.5.2 Turbidity measurements

Turbidity describes the amount of light intensity which is attenuated by particles within the water. Using a turbidity sensor is therefore an indirect method, as it uses turbidity as a surrogate for suspended sediment concentration (Wren et al., 2000, Gao, 2008). Turbidity offers high temporal resolution data which is almost continuously recorded using a data logger making this method advantageous over automatic water samplers which contain a limited number of bottles. However, turbidity measurements can be just as problematic. Research has shown that turbidity varies linearly with homogenous sized sediment concentrations (Gippel, 1995); although the natural environment produces an array of different particle sizes. Ludwig and Hanes (1990) demonstrated that suspended sediment concentration measured with a turbidity probe can increase tenfold when compared to readings for the same concentration with different particle sizes. Typically finer particles produce higher values of turbidity (Ludwig and Hanes, 1990). In addition to particle size problems, turbidity is also affected by a range of materials that attenuate light including algae, tree branches and non-organic matter while at high particle concentrations saturation can occur (Wren et al., 2000). Despite the limitations, if carefully deployed and calibrated using sediment samples collected from the monitored stream, turbidity can provide a high resolution proxy for suspended sediment concentration. This outweighs the limitations that might apply (Gippel, 1995), which is why it is being used within this study.

2.5.3 Sediment Rating Curves

It is often necessary to predict suspended sediment concentration when sampling programmes provide insufficient data to determine a continuous record (Walling, 1977), this technique has been used within Red House Gill. This generally involves

the use of interpolation and extrapolation techniques. While interpolation techniques assume that the instantaneous sample concentration is representative of the inter-sample period, extrapolation techniques involve the development of a rating relationship between discharge and suspended sediment at any given point (Phillips et al., 1999). The success of an extrapolation technique is dependent upon a good sampling programme where suspended sediment concentrations are sampled across the full range of flow conditions (Ferguson, 1986) . There are many different ways to calculate a sediment rating curve, however most curves are based on a power function (Asselman, 2000, Walling, 1977), where suspended sediment concentration (C) is related to discharge (Q) by two empirically derived parameters (a and b):

$$C = aQ^b$$

Equation 2.2

Using a power function to generate suspended sediment rating curves is logical as it agrees with natural rules for example when discharge is zero, so should suspended sediment. There are two main approaches to obtain values for *a* and *b:* non-linear least squares regression and ordinary least squares regression. Although solving the power function using non-linear least squares regression is sometimes inappropriate as homoscedasticity isn't met, as suspended sediment concentration varies more at higher discharges (Asselman, 2000). Therefore, it is more common to use ordinary least squares linear regression in log space:

$$logC = \log a + b \log Q + log\varepsilon$$

Equation 2.3

A range of studies have used log transformed least squares regression to estimate suspended sediment. Walling and Webb (1981), used this method to calculate suspended sediment concentrations for the River Creedy, Devon, over a seven year period. The rating curve underestimated sediment load between 83-23%. Fenn et al. (1985) report similar results with loads being underestimated by 79% within a proglacial stream in Valais, Switzerland. Although more recent work by Sadeghi et al. (2008) using least squares regression overestimated sediment concentration. In order to correct for this underestimation / overestimation generated by scatter surrounding the regression line, a couple of correction factors (CF) have been generated. Ferguson (1986) has suggested the following parametric correction:

$$CF = \exp(2.65\, S^2)$$

Equation 2.4

Where S^2 is the mean square error of the log transformed regression. This correction factor aims to reduce scatter around the regression. However the scatter is natural depending on sediment supply which varies due to season, antecedent conditions in the river basin and differences in sediment supply at the beginning and end of a high flow event. Another correction factor called the Smearing Estimate has been developed by Duan (1983). This correction factor is for non-parametric data and has been most widely used on small samples (Helsel and Hirsch, 2002). Walling and Webb (1988) provide a good review of the uncertainties and benefits of using correction factors. For this they analysed continuous records of suspended sediment and discharge from three rivers in Devon, UK. Actual loads were then compared to those estimated using an ordinary least squares regression and those corrected using the above factors. Their results suggest neither the standard regression nor regression involving the correction factors were able to provide reliable estimates. They suggest it is because the bias associated with logarithmic transformation is not the prime cause of inaccuracy in rating curve estimates and therefore other issues not dealt with by the correction factors are important. These issues are: substantial scatter, seasonal differences, hysteretic and exhaustion effects. Walling (1977) computed annual and seasonal rating curves, demonstrating that annual curves overestimated loads by 280% compared to only 30% for seasonal curves.

Although non-linear least squares regression is infrequently used, it is important to note that Asselman (2000) compared non-linear least squares regression and ordinary least squares regression. His results, demonstrated that ordinary least squares regression tended to underestimate results, even when a correction factor is used, with better estimates being obtained when using non-linear least squares regression.

2.5.4 Time Integrated Mass Samplers (TIMS)

The methods discussed in Section 2.5.1-2.5.3 can be used to determine instantaneous suspended sediment concentrations. However unless sampling is of very high frequency they cannot be easily used to directly estimate longer term sediment loads (except through rating curve approach). Time integrated samplers have the potential to overcome this problem, as they have the ability to collect bulk

suspended sediment samples. It has been suggested by Nelson and Benedict (1950) that a successful time integrated device should be: isokinetic, pointed into the flow, moveable, suitable for transport, streamlined, rugged, simple to construct and inexpensive.

In light of this Phillips et al. (2000) have designed a sampler made from easily available materials (Figure 2.5). The Time Integrated Mass-flux sampler (TIMS) is installed perpendicular to the water flow at approximately 60% of the mean water depth using steel stanchions driven into the stream bed. Once submerged, water enters via the 4mm inlet tube before entering the expansion chamber. Within the expansion chamber, flow velocity reduces by a factor of 600 relative to the ambient flow, inducing sedimentation of the suspended particles as water continues to flow towards the outlet tube. Funnels placed over the inlet tube help streamline the sampler altering the ambient flow by no more than 20% (Phillips et al., 2000), while allowing water to leave without hindrance, thereby reducing sampling bias which affects other methods (Fox and Papanicolaou, 2007).

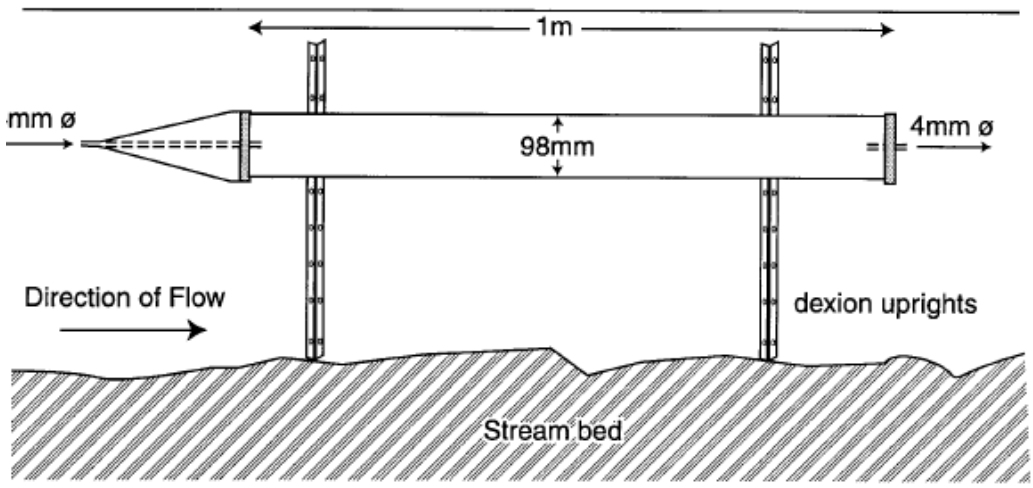

Figure 2.4-Cross section of the time integrated mass sampler (TIMS) proposed by Phillips et al. (2000).

TIMS have undergone a range of laboratory and field testing for validation. Laboratory tests reveal the sampler is effective at retaining sediment under a range of ambient velocities (0.3-0.6 m s^{-1}). Although, the fraction of retained suspended sediment is coarser than the ambient inflowing sediment, suggesting the device isn't isokinetic (Phillips et al., 2000). However, the occurrence of fine sediment flocs in the natural environment is likely to increase sampling efficiency within the field

(Woodward and Walling, 2007). Within field tests, Phillips et al. (2000) found that the stored suspended sediment was statistically representative of the ambient flow which ranged between 1.6-5.3 µm. Russell et al. (2001), compared sediment samples from TIMS and manually collected grab samples during storm events from a small catchment in Leicestershire. Results suggest that the TIMS produce a geochemically representative sample of fine suspended sediment. Hatfield and Maher (2008), found a significant correlation between sediment samples from TIMS and maximum recorded discharge. For 99.9% significance level, R^2 values of 0.97 and 0.89 were achieved from the River Derwent and Newlands Beck near Bassenthwaite Lake, UK. Although the results were achieved from only six samples, the results suggest that high rainfall and river discharge results in higher levels of suspended sediment. Schindler Wildhaber et al. (2012) compared both turbidity and TIMS for collecting information regarding suspended sediment concentration and load. Their results suggest a better correlation occurs between TIMS samples and suspended load compared to turbidity and suspended sediment concentration. Perks et al. (2013) used a network of 39 TIMS to monitor fine suspended sediment within the River Esk Catchment, results demonstrate that suspended sediment was underestimated between 66-99% compared to reference samples. However, the authors highlight their use when capturing spatial patterns and temporal variability of sediment flux across catchments. Within Red House Gill, TIMS will be used to look at the spatial (relative) variability of suspended sediment from the two urban and one rural stream.

2.6 Summary

Catchment urbanisation has the potential to produce a cascade of negative hydrological changes. High intensity urban run-off can be erosive, therefore increasing suspended sediment concentrations. Increasing suspended sediment concentrations have negative biological and chemical effects. Within Red House Gill, the highly erosive run-off from the upper part of the catchment is being combined with a range of hillslope processes delivering sediment to the streams. Due to the complex relationship between spatial and temporal characteristics of hillslope processes and suspended sediment dynamics, a range of research methods are going to be used to characterise these processes so that an overall sediment budget for the catchment can be constructed.

3 Site Description

3.1 Overview

The Red House Gill catchment provides an excellent opportunity to monitor fine sediment supply, transfer and delivery in relation to urbanisation. This is because the catchment has undergone extensive urbanisation, converting natural and agricultural land into houses and local services creating a peri-urban environment. Extensive areas of bankside erosion occur throughout the Red House Gill woodland and this erosion could be further compounded due to additional planned developments within the catchment. The aim of this chapter is to describe the physical setting of Red House Gill (Sections 3.2-3.6); discuss the historical and potential future developments within the catchment and their effects on hydrology and ecology (Section 3.7-3.9); and summarise the management programmes currently in operation around the local area (Section 3.10).

3.2 Location

Red House Gill is a small tributary of the River Wear in Brasside, County Durham (E 428240, N 546479). The catchment area was defined in ArcGIS using a 5 m resolution DEM and is outlined in Figure 3.1. The catchment is approximately 2.5 km^2, draining a small sub-catchment of the River Wear. The catchment consists of three tributary streams arranged in a simple dendritic pattern. For the purpose of this research, the streams have been labelled East, Middle and West. The three streams display very different characteristics which have been summarised in Table 3.1. The East stream drains the biggest area (1.51 km^2) while also being the most urbanised, as 72% of the catchment contains residential dwellings. The Middle stream drains 0.73 km^2 of which 64% is urbanised, while the West stream drains the smallest area which is only 0.29 km^2 of which only 7% is urbanised.

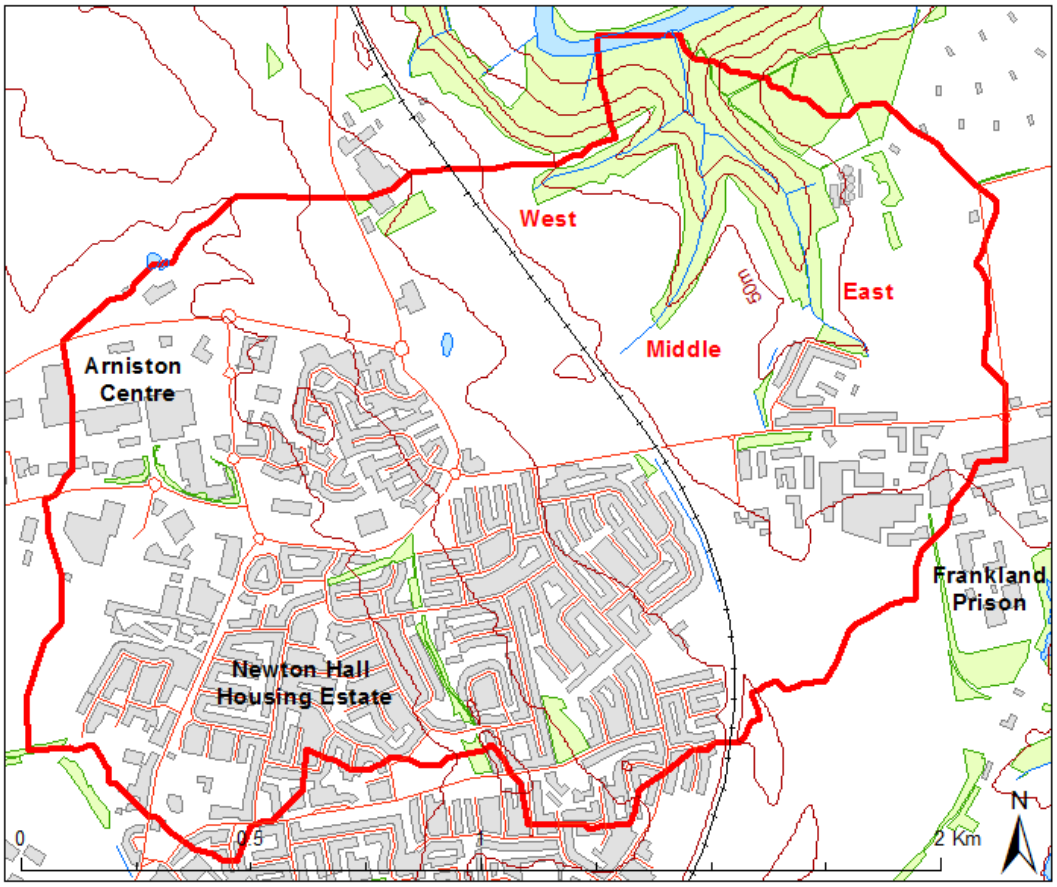

Figure 3.1-Detailed view of the Red House Gill catchment, demonstrating the high level of urbanisation and three tributaries (East, Middle and West). 10m contours have been added to provide information on catchment relief.

	East Stream	Middle Stream	West Stream
Catchment Area (km^2)	1.51	0.73	0.29
Stream Length (m)	800	570	390
Stream Source	Culvert	Culvert	Emerges from underground.
Geology	Cohesive silts and clays.	Gravel and fine sediment.	Mixture of clay, silt and fine sediment.
Hill slope Gradient (^{o})	15	22	9
Hill slope Vegetation	Highly vegetated with trees, herbs and *Impatiens glandulifera.*	Heavily vegetated, with a good mix of riparian vegetation including grasses, herbs and trees in the upper section while the lower section is dominated by trees and *Impatiens glandulifera*	Healthy mixture of trees and herbs.
Channel Morphology	Constrained, well defined in places and sinuous	Laterally incised and therefore overly wide with a low sinuosity.	Well defined, steep with step pool morphology.
Stream Gradient (^{o})	0.04	0.05	0.07
Bed Material	Dominated by fine sediment, with some sub angular gravels and cobbles in the upstream section before becoming well mixed with sub rounded gravels and cobbles in the lower section.	Unsorted with a large proportion of fine sediment along with sub rounded boulders and cobbles.	Boulders and cobbles. Fine sediment is also prevalent within deep pools.
Depositional Features	Gravel and fine sediment bars.	Gravel and fine sediment bars.	Not prevalent.
High Flows	Evidence suggests they occur regularly however, there are few signs to suggest overbank flooding occurs.	Trash lines suggest they occur often.	Not common.
Bank Undercutting	Some evidence, in the upper and middle part of the stream.	Hydraulic scour is extensive.	Not common.
Tree Throw	5 occurrences next to the stream.	7 occurrences next to the stream.	4 occurrences next to the stream.
Mass Wasting	Slab failure and debris flows have previously occurred. Soil creep is occurring.	Predominately slab failure and debris flows. Ground water seepage is also common. Soil creep is occurring.	No evidence for fast moving failures. Soil creep is occurring.

Table 3.1-Comparison of the East, Middle and West streams. Information has been attained from field walks, GIS and Moggride (2010).

3.3 Topography and Relief

Red House Gill joins the River Wear in its lower reaches, where it displays many characteristics of a large lowland river including: low channel gradients, wide flood plains and lateral erosion. The Red House Gill catchment has a varied relief (Figure 3.2). The upper portion of the catchment characterised by urban developments is relatively flat lying 97 m above sea level. However, the flat urban plateau ends with an escarpment down into Red House Wood. The culverts for the East and Middle streams along with the underground source for the West stream is at the top of the woodland. The woodland displays typical steep stream morphology, with deeply incised valleys which fall down to almost sea level at the confluence of the River Wear. Table 3.1, shows information on hillslope and channel gradients for all three streams. The East, Middle and West stream valleys have side slope gradients of 15^0, 22^0 and 9^0 respectively, which can be seen in Figure 3.3. These gradients are highly representative of the steep V shaped valleys which comprise the catchment. Steep slopes are a more significant source of sediment compared to shallower slopes as the rate of geomorphic processes tend to increase with slope gradient. Therefore, the hillslopes surrounding the Middle stream should naturally deliver more sediment compared to the East and West hillslopes. Figure 3.3 also demonstrates the longitudinal profiles for all three streams from the source. The East stream is the longest; however the West stream has the steepest gradient at 0.07^0 and step pool morphology.

Considering the combined effects of valley geometry, channel slope and catchment area (Table 3.1), the three sub catchments of Red House Gill will have different geomorphic and fluvial regimes. The West stream occupies the smallest catchment area and has the smallest hillslope gradients. Due to the small drainage area and shallow gradients, the West stream is unlikely to produce highly erosive flows compared to the East and Middle streams. However, the East and Middle streams have much larger drainage areas and therefore greater potential flow combined with steeper hillslope gradients. Hence during flood events, the stream power of these streams will be very high resulting in channel scour and slope undercutting which in turn will cause instability of the steep slopes.

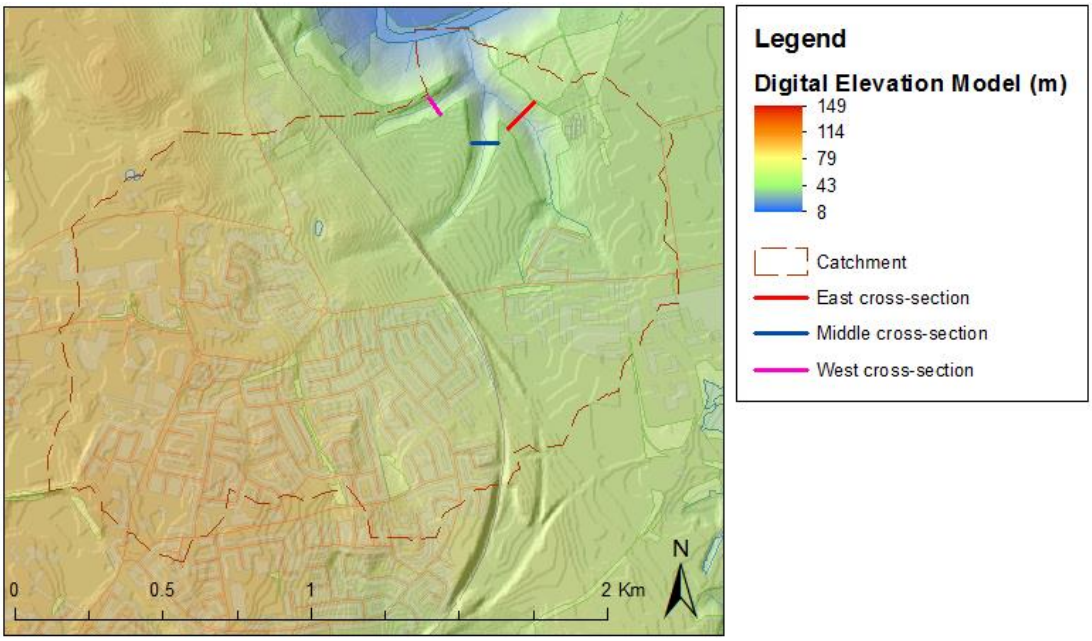

Figure 3.2-Relief of Red House Gill displayed using a 5m DEM and hillslope shade model. The location of the East, Middle and West cross-sections has also been noted.

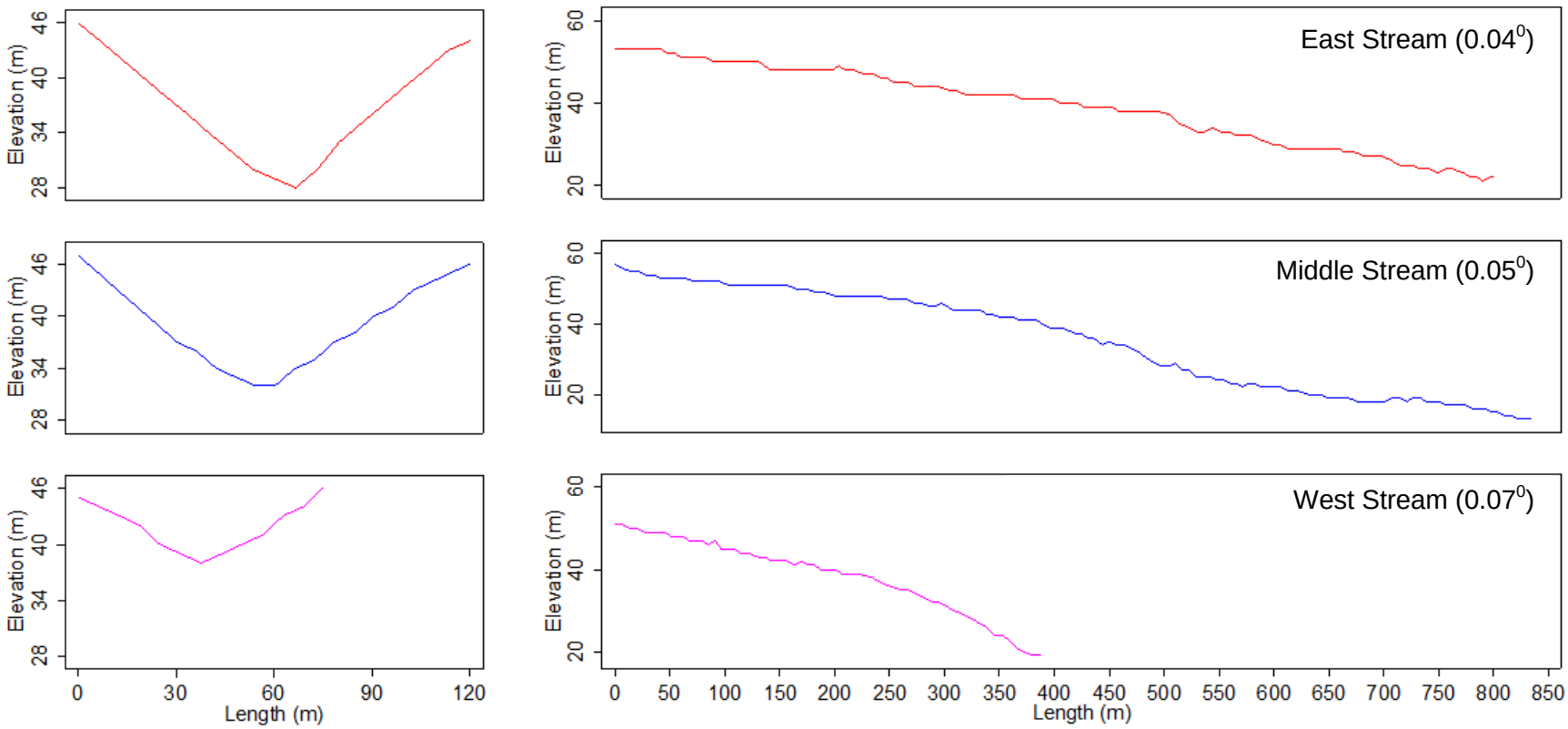

Figure 3.3-Cross-sectional and longitudinal profiles for the East, Middle and West streams within Red House Gill.

3.4 Geology

Geology plays an important role in how catchments respond to rainfall events. Red House Gill is underlain by Pennine Middle Coal Measures (PMCM) (Figure 3.4). This type of bedrock was formed during the Westphalian epoch of the Carboniferous period approximately 316-306 million years ago. Predominately sedimentary in origin these rocks contain a mixture of mudstone, sandstone, siltstone and coal seams (Lawrence et al., 2004). Due to the presence of coal these rocks are economically significant and prompted early development within the catchment through the opening of Framwellgate Moor Colliery.

In County Durham, superficial deposits are primarily from the last Devensian cold stage, which ended approximately 11,500 years ago. There is very little evidence to suggest deposits have been preserved from earlier glacial and interglacial stages within the Quaternary (Lawrence et al., 2004). The Red House Gill catchment is mainly composed of Devensian glaciofluvial deposits and till (Figure 3.4). Glaciofluvial deposits are primarily composed of sand and gravel, having been deposited by glacial melt water. Whereas till is deposited directly by the glacier, with the content varying between clay, sand, gravel and boulders. Superficial deposits provide the main source of inorganic materials for soil development resulting in soils that are heavy, poorly drained gleys with pockets of light soils connected with glacial sands and gravels (Lawrence et al., 2004).

A British Geological Survey (BGS) borehole within Red House Wood, drilled to a depth of 70m reveals information based on bedrock and superficial geology (Figure 3.5). The borehole reveals that the superficial deposits are roughly 30m thick, divided into distinct layers of sand, clay or a mixture of both (loamy sand and loamy clay) which range in thickness from 0.5-0.8 m. These layers of sand and clay are likely to increase landslide susceptibility due to differences in vertical hydraulic conductivity. The bedrock geology is dominated by grey post and stone, which refers to grey sandstone and grey shale, with a few distinct layers of coal at 49m and 68m. There is no distinct difference between the deposits in each of the three sub-catchments.

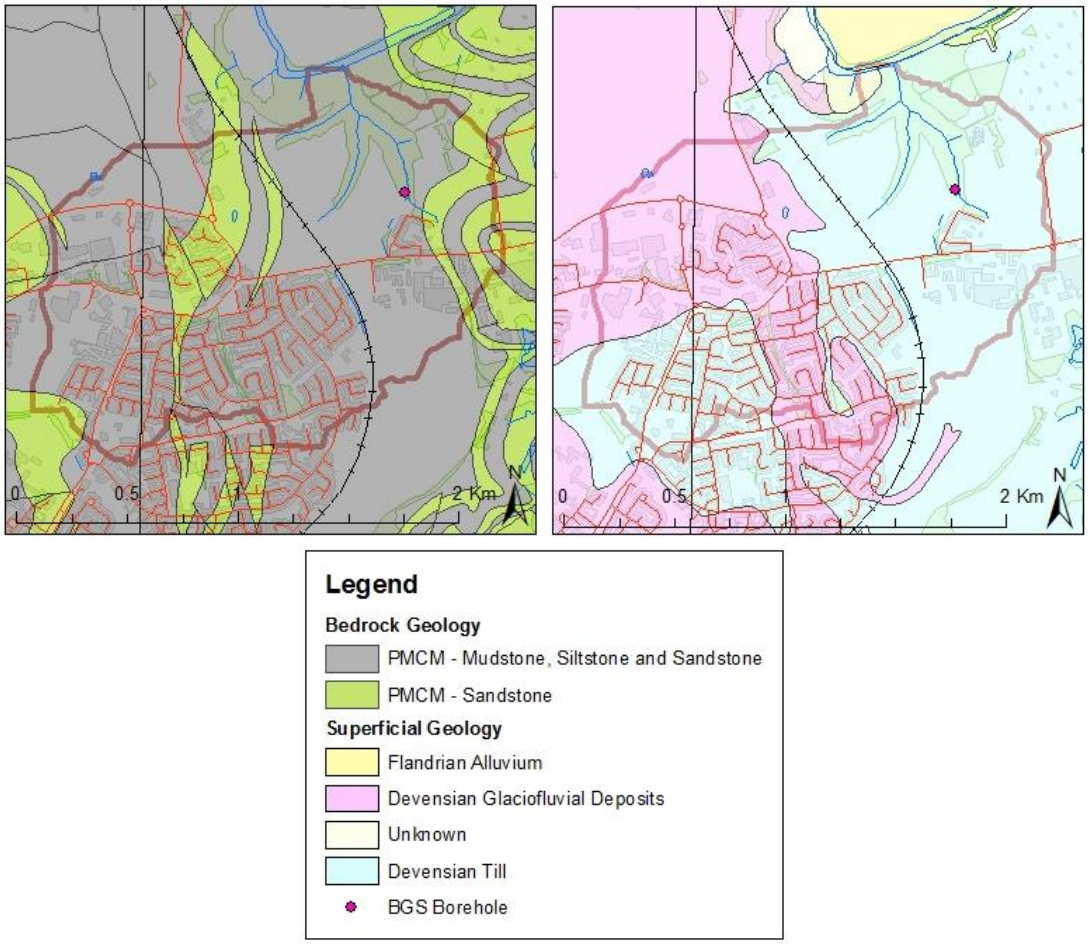

Figure 3.4 -A) Bedrock geology of Red House Gill. B) Superficial geology of the Red House Gill catchment (Edina, 2013). The catchment boundary is on both maps.

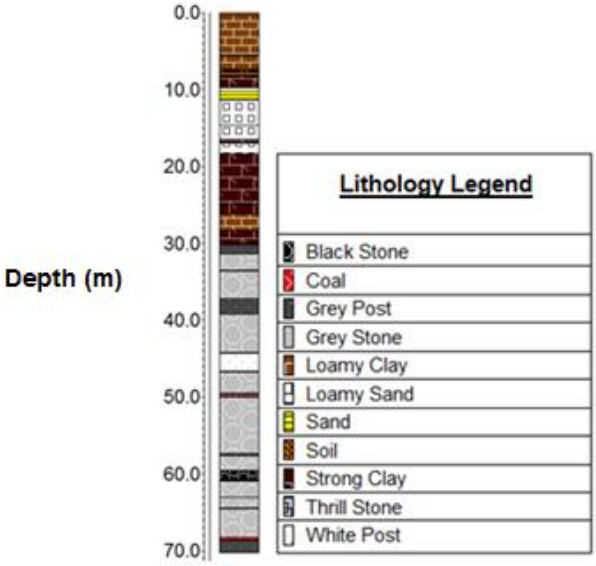

Figure 3.5-Strip log for the Red House Gill bore, demonstrating the distinct layers.

3.5 Climate

The closest weather station to Red House Gill is the Durham University Observatory, which is 4.9 km south west of the site. Using records from 1850, the mean annual precipitation in Durham is 652.4 mm. The wettest months are August, October and November receiving 67.8 mm, 64.1 mm and 63.4 mm of rainfall respectively (Durham, 2013). The mean annual temperature is 9.2^{o}C, ranging from 3.8^{o}C in January to 15.6^{o}C in July (Durham, 2013).

Although the Pennines cast a rain shadow over Durham, it still receives bursts of intense rainfall, which vary depending on season. In the winter months, the North of England is dominated by cold dry continental air masses, whereas in the summer months its controlled by warm moist maritime air masses which have a greater capacity to generate intense storms (MetOffice, 2013).

3.6 Woodland

The source of all three streams is visible at the top of Red House Gill wood before they converge downstream within the wooded area (Figure 3.1). The woodland is dominated by deciduous trees especially Ash and Sycamore which both have open airy canopies. These open canopies help encourage understorey vegetation growth. Table 3.1 provides more information about vegetation which occupies the stream banks. The Middle stream is the most heavily vegetated, with a wide mix of riparian vegetation including grasses, herbs and the invasive species *Impatiens glandulifera.* The East and West streams are both well vegetated although not to the same degree as the Middle stream. Figure 3.6 demonstrates that even in the earliest Ordnance Survey maps, Red House wood had already been developed and has therefore provided continuous woodland since before 1861. The woodland has therefore undergone several phases of succession with pioneer species helping the establishment of hardwood trees like Ash and Sycamore which are prevalent.

3.7 Land Use Change

Catchment urbanisation often results in a flashy drainage regime which has the potential to increase erosion often leading to elevated suspended sediment yields (Jacobson, 2011). Historic Ordnance Survey maps demonstrate that over the past 150 years, the character of the Red House Gill catchment has changed significantly with an enormous increase in urbanisation (Figure 3.6). In 1861, the catchment was

predominately agricultural with only a few small areas of impervious industrial land cover including Framwellgate Moor Colliery. By 1923, the North Eastern Railway had been built through the catchment along with a small cottage. By 1951, Framwellgate Moor Colliery had closed down having been replaced by numerous buildings while very little other development occurred. By 1962 only a few extra houses had been built, meaning the catchment was still predominately agricultural. However, by 1979 the Newton Hall housing estate had been developed. Further developments occurred in the 1980's with the demand for local services increasing, resulting in an out of town retail park (Arniston Centre) being built. Over this period, the percentage of urbanisation increased from 2.6% to 53.8% within the catchment (Figure 3.7). This level of urbanisation is well above the 15% impervious cover threshold where stream quality impairment is observed and is also above the 30% impervious cover threshold where severe ecological degradation occurs according to work by Klein (1979) in Maryland, USA.

The extent of urbanisation within the catchment is planned to increase further (Council, 2013). A green belt review has already been undertaken, with a site North of Red House Gill earmarked for development (Figure 3.6). If the development goes ahead, 30% of the site will be within the Red House Gill catchment, increasing urban land cover to 64.7%. Planning proposals put forward have already suggested the use of sustainable urban drainage (SUDS) to help control run-off rates (Council, 2013).

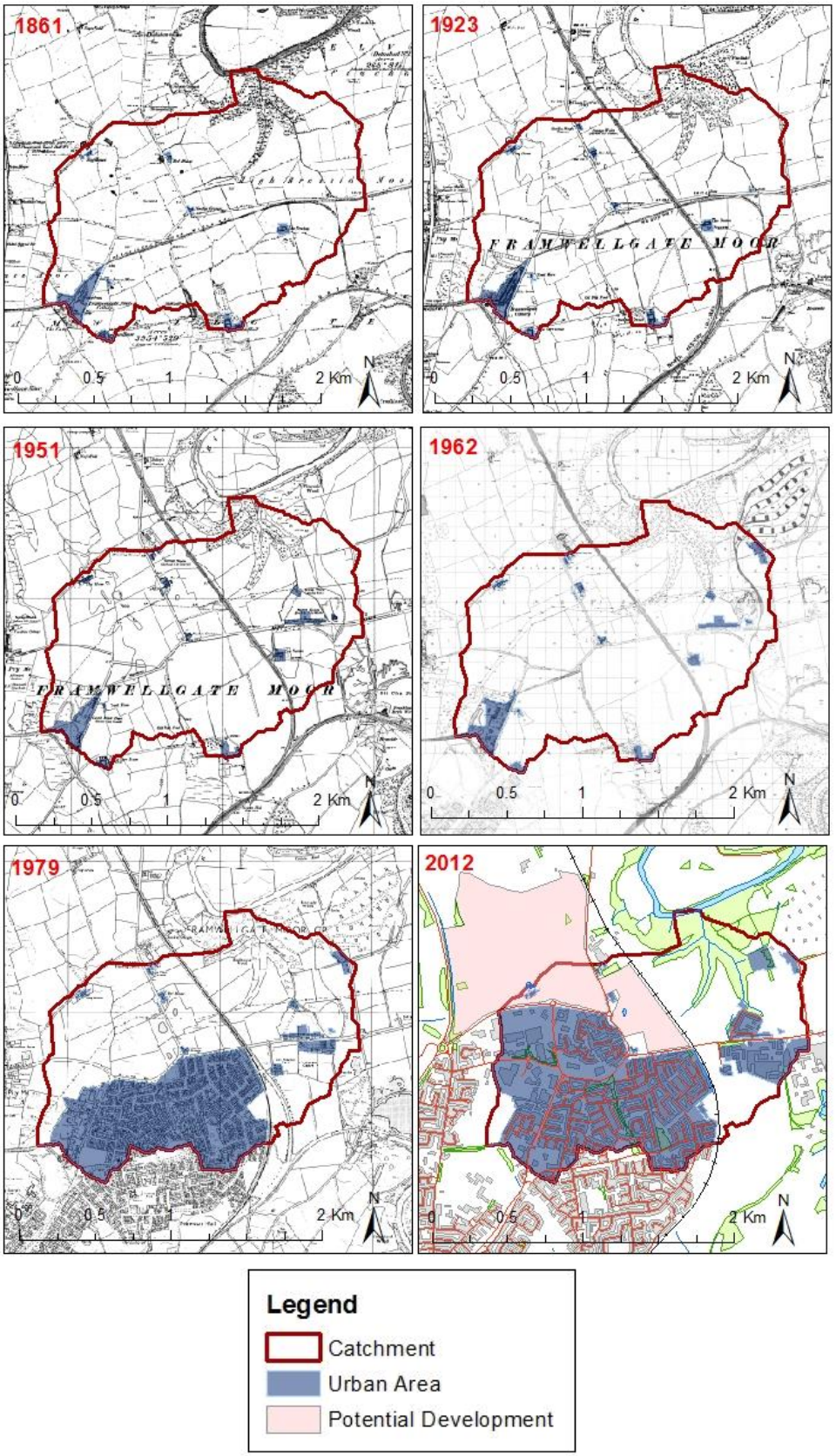

Figure 3.6-Ordnance Survey maps showing changes in land cover over time

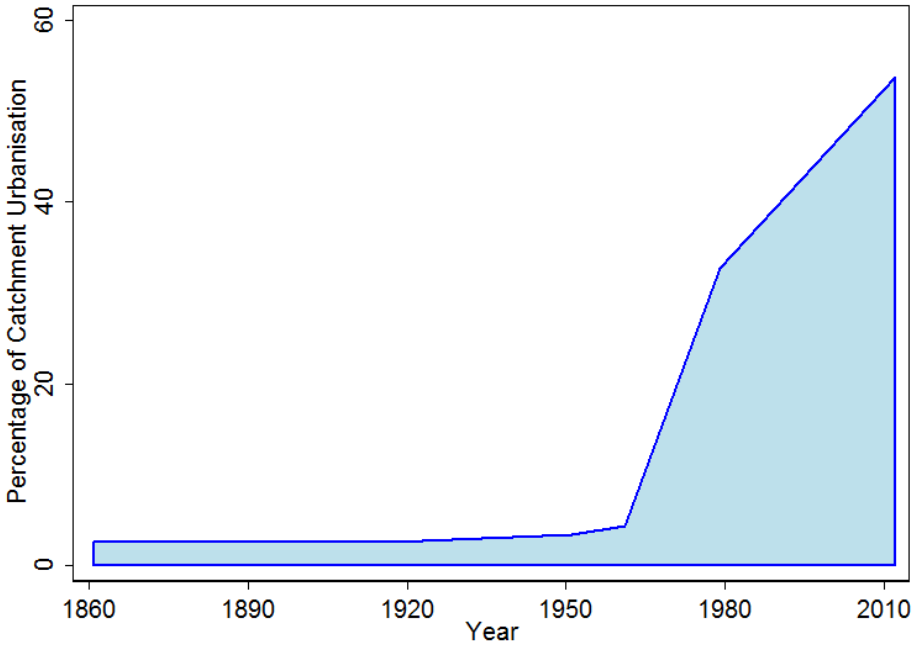

Figure 3.7-Graph showing the increase in urbanisation within the Red House Gill catchment over the past 150 years.

3.8 Hydrology

Along with urban developments, surface water drainage was also put in place. Figure 3.8, shows that surface water drains from the Newton Hall housing estate, Frankland Prison and the Arniston Centre to outfall numbers 3803, 6901 and 0906 which discharges into Red House Gill at the top of the East and Middle streams. Due to the surface water drainage the majority of drainage within the catchment is underground and therefore the sub-catchments for individual streams cannot be calculated accurately using topography. Table 3.1, suggests the size of each sub-catchment based on topography, however based on the information from Figure 3.7, it is possible that the Middle stream drains a larger area than the East stream. Consequently the Middle stream will have a greater potential flow and erosive power.

Given the recent concerns regarding high flows and resulting erosion, the Environment Agency commissioned a modelling study, looking at surface water run-off rates from the Arniston Centre (JBA, 2012). Flow discharge, velocity, depth and rainfall were monitored for ten weeks starting in February 2012 and used to verify

the hydraulic model created using InfoWorks-CS. The results demonstrated a good match between observed and modelled discharge and therefore the model was used to calculate discharge and water volume for 5, 30 and 100 year storm events with varying durations before looking at the effects of proposed urban development. Table 3.2, provides details for peak flow discharges for a 5 and 100 year storm event, which suggests there is a critical threshold for storm duration between 30-60 minutes after which discharge starts to decrease. The results suggest that the Arniston Centre outfall has the highest peak flow discharge followed by Newton Hall. In terms of urban development, no future developments considered within the study increase flow discharges into Red House Gill as they are either serviced by another outfall or will have a negligible effect. However it was recommended that any future development should consider sustainable urban drainage systems (JBA, 2012). Although the effects of the proposed development outlined in Section 3.7 weren't fully modelled as the only proposed development at the time of the modelling study was a bypass. Therefore, the proposed development could have more than a negligible effect on Red House Gill.

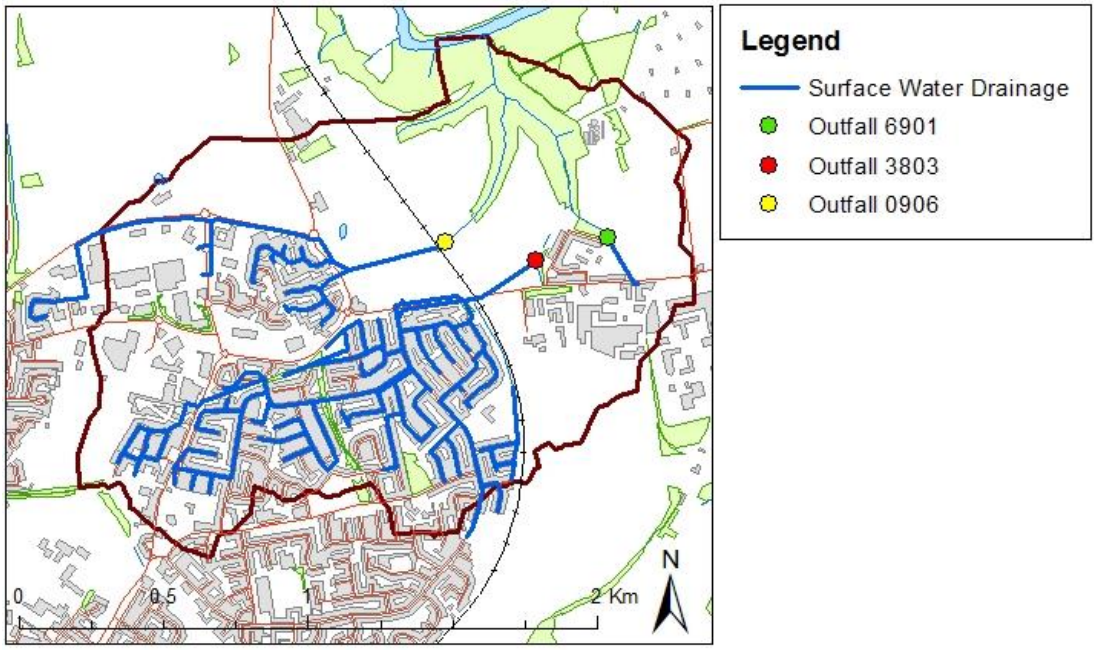

Figure 3.8-Surface water infrastructure patterns in Red House Gill. Surface water from the Arniston Centre, Newton Hall housing estate and Frankland prison drains through this system to outfalls at the head of the East and Middle streams

Storm Duration (mins)	Peak Flow Discharge ($m^3 s^{-1}$)					
	Outfall 0906 (Arniston Centre)		Outfall 3803 (Newton Hall)		Outfall 6901 (Frankland Prison)	
	5yr	100yr	5yr	100yr	5yr	100yr
30	1.55	1.84	1.22	1.63	0.33	0.45
60	1.46	1.77	1.07	1.47	0.23	0.43
120	1.08	1.61	0.90	1.22	0.15	0.29
360	0.50	0.97	0.45	0.85	0.07	0.13
720	0.30	0.57	0.27	0.51	0.04	0.08

Table 3.2-Modelled peak flow from the JBA study at all three outfalls.

3.9 Ecological Importance

The River Wear catchment in East Durham has a long history of coal mining, although the industry has all but ceased production, the effects are still evident in water quality (EA, 2008). Under the EC Water Framework Directive, the River Wear achieves a 'good' chemical status however it only achieves a 'moderate' ecological status despite this it's diverse fluvial habitat. The river is home to a range of fish including brown trout, grayling, salmon and most recently lamprey. Lampreys are rare fish, which are extremely selective about their spawning sites, choosing gravel reeds with only the highest water quality, which is why they are protected through the UK Biodiversity Action Plan and the EC Habitats Directive. Lampreys have previously spawned in the River Wear by Chester Le Street, which is only a few miles downstream of Red House Gill (BBC, 2009).

Concerns are increasingly growing about the effect of urban development on Red House Gill and how urban discharge is funnelled into the River Wear. The East stream under the EC Water Framework Directive has a 'moderate' ecological and chemical status (Moggridge, 2010). The Environment Agency has previously assessed the confluence between Red House Gill and the River Wear grading it as: chemistry (very good), biology (good), nitrates (moderate) and phosphates (high) (Moggridge, 2010). The results for chemistry and biology are excellent, suggesting that the confluence is a natural ecosystem, only just short of being an unpolluted river (Moggridge, 2010). However, the results for nitrates and phosphates are high, suggesting that Red House Gill is already being affected by the current levels of urban development. New development could now further compound the problem.

Red House Wood provides habitat for a range of indigenous mammals such as mink, badger and deer. Figure 3.9, demonstrates the difference in suspended sediment concentration between discharge from Red House Gill and the River Wear. As the image demonstrates, the River Wear is clear, whereas murky water from Red House Gill enters the river by the gravel bar. This picture clearly highlights differences in suspended sediment concentrations.

Figure 3.9-The confluence between the River Wear and Red House Gill. The red arrow indicates the flow direction of the River Wear, while the blue arrow demonstrates the flow from Red House Gill (Source: Lloyd Atkinson).

3.10 Management

Given the increase in urban development within the Red House Gill catchment, there is increasing concern from local fisherman about the effects of eroded fine sediment in the River Wear. Currently there are two key management programmes in operation which should help deal with this problem:

- The River Wear Salmon Action Plan (SAP) - Aims to help improve the survival of salmon populations by improving the quality of the River Wear. In the 2008 report, remedial work at Red House Gill was seen as a priority to

help reduce the amount of fine sediment being delivered to the River Wear (EA, 2008).

- Between March 2011 and December 2013, DEFRA were piloting a catchment project in the lower River Wear in the context of the EC Water Framework Directive. The project provided an opportunity for the Environment Agency to work with local community stakeholders and organisations to protect the river. As part of the project the Environment Agency wanted to see a range of improvements: better education on the effects of harmful waste in surface water drainage, working together to manage river bank erosion, cleaner waterways for everyone to use recreationally, increased fish populations for anglers and more green space to access water (EA, 2011).

Both of these management projects show a clear commitment to ecological improvement for the River Wear catchment which encompasses Red House Gill. The Salmon Action Plan has the sole purpose of protecting salmon breeding habitats whereas the River Wear catchment project uses a more holistic approach educating local stakeholders about the benefit of riverine environments. Both of these projects will benefit Red House Gill but the long term result will be dependent on the interplay of these management projects with the potential effects of increased urbanisation.

3.11 Summary

The Red House Gill catchment is situated on the outskirts of Durham city centre and can be considered peri-urban due to the mix of natural, agricultural and urbanised areas. Over the past 150 years, the catchment has undergone extensive urbanisation, with urban cover increasing from 2.6% to 53% which is well above thresholds for ecological degradation. The geology and geomorphology of the lower catchment predispose the area to erosion due to the readily available sources of erodible sediment and the steep side slopes and stream courses. Concerns are now growing about the effects of urbanisation and increasing storm discharge resulting in severe erosion which increases suspended sediment concentration within the River Wear. Due to this, the River Wear Salmon Action Plan (SAP) has already identified Red House Gill as an area of interest, making remedial work within the catchment a priority

4 Methodology

4.1 Overview

Given the spatial and temporal controls on hillslope sediment delivery and fluvial suspended sediment transfer, a range of methods have been applied to answer the research questions outlined in Chapter 1. Chapter 2 provided a rationale for these methods which will now be discussed in greater detail. The aim of this chapter is therefore to firstly describe how data was collected in the field (Section 4.2) before explaining the laboratory processes and initial processing used to analyse the collected samples and data (Section 4.3).

4.2 Data Collection

4.2.1 Main Monitoring Station

A central monitoring station was set up in Red House Gill, 15 m below the confluence of the East and West streams (Figure 4.1). This site was chosen as it would provide information on suspended sediment from both of the urbanised streams; while the steep river banks ensured that during high flows water would not spread laterally, creating a relatively stable gauging section over a large range of flows. The main site was installed on the 8th March 2013 and consisted of the following equipment:

- Automatic Water Sampler - ISCO 6712 Water Sampler
- Turbidity Sensor – McVan Analite 395 Turbidity Probe
- Stage Recorder- Druck PDCR 1830 Pressure Transducer
- Data Logger- Campbell Scientific CR10X data logger powered by a 12V battery / solar panel charger

4.2.2 Turbidity

In order to continuously measure suspended sediment, a McVan Analite 395 nephlometric turbidity probe was installed at the main monitoring station. This sensor works by illuminating the water using a near infrared (0.86 µm) photodiode light and then measuring the amount of scattering at an angle of 90^0 towards the incident light. The sensor therefore records turbidity in 15 minute intervals within the range of 0-1000 NTU, with a precision of +/-1%. This probe was specifically chosen because it is ideal for monitoring suspended sediment in fast, cold running water

where sediment is likely to build up, as it has an integrated wiper, which wipes every two hours removing built up sediment and algae. Data from the automatic water sampler has been used to constrain results from the turbidity probe.

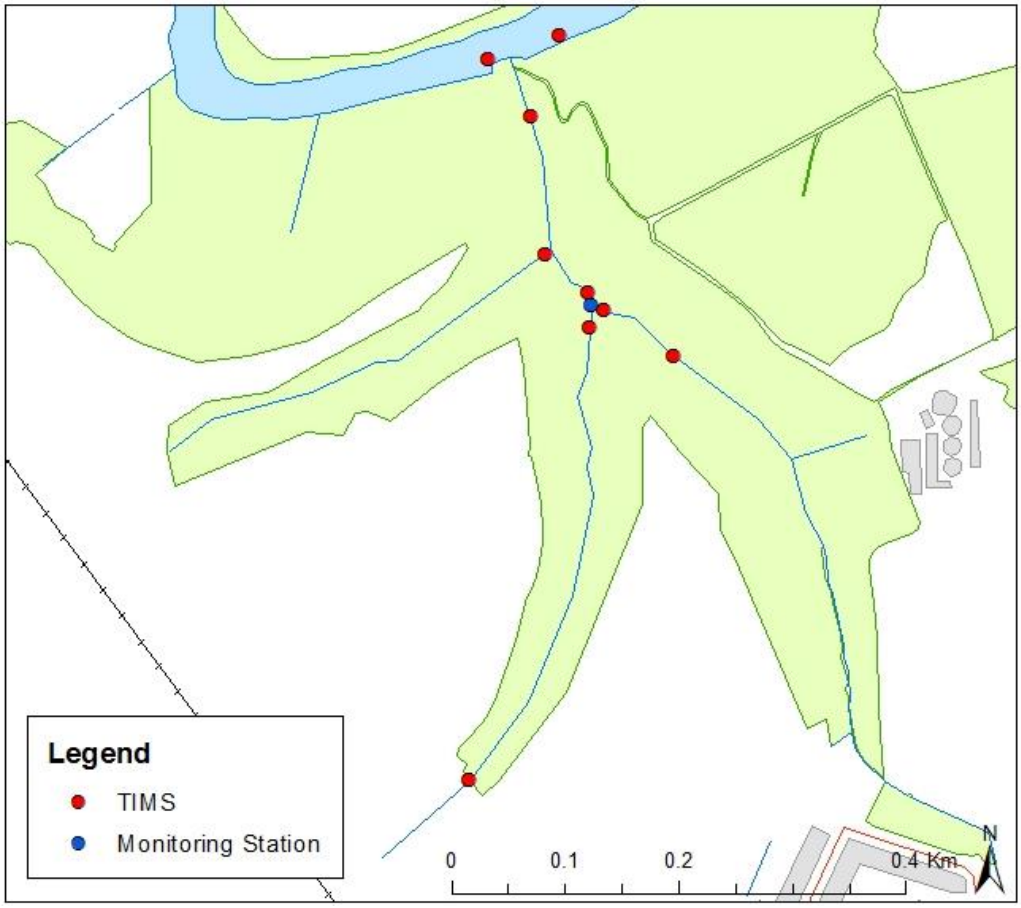

Figure 4.1-Location of the main monitoring station and TIMs within the Red House Gill.

4.2.3 Time Integrated Mass Samplers (TIMS)

To characterise fine sediment delivery within the Red House Gill catchment a network of nine TIMS was installed (Figure 4.1). Sampling locations were selected for a variety of reasons but predominately, to provide information on the movement of fine sediment from the three streams into the main trunk stream and into the River Wear. The TIMS within the River Wear were placed to compare the amount of fine sediment upstream and downstream of the Red House Gill confluence.

The TIMS were installed on three separate days between April and June 2013. Initially only a network of 6 TIMS were going to be installed however; it was decided to extend the network to 9 to provide more information. To install the TIMS, metal

stanchions were hammered into the middle of the stream bed. The samplers were then attached by threading heavy duty cable ties through the stanchion eyelets. Care was taken to ensure the inlet and outlet tube of TIMS sampler was parallel to the stream flow. The TIMS were secured approximately 0.1 m above the stream bed. After installation was complete, a two week sampling frequency was adopted as this provided sufficient time to accumulate a bulk sample (~0.3-2000 g). During data collection, the TIMS were removed from the metal stanchions and emptied into a 5 litre plastic container. If there was suspended sediment stuck in the sampler, it was rinsed with stream water, shaken and poured into the container.

Although TIMS are economical, easy to construct and maintain; sampling was interrupted on several occasions due to high flows. On the 6th August 2013, 15th October 2013 and 29th October 2013, water levels in the River Wear were high and as a result it was considered too dangerous to empty the TIMS. This has created some varying deployment lengths. Floating debris, especially leaves in the autumn months also caused problems blocking the inlet tube which would affect sampling efficiencies.

4.2.4 Tree Shape and Dendrochronology

As part of this research, two methods have been used to look at soil creep processes occurring within the Red House Gill woodland. Traditional dendrochronology has been used to look at the temporal characteristics of soil creep while a novel approach looking at basal trunk angle has been developed to assess the spatial characteristics of soil creep. Data for this part of the research was collected between August and November 2013.

4.2.4.1 Tree Shape

In order to look at the spatial pattern of soil creep, the angle at the base of curved trees was characterised using three length measurements. As part of this, information was collected for 340 healthy trees throughout the woodland (Figure 4.2). As all the trees within the woodland could not be measured, sampling focused on collecting data which demonstrated how soil creep changed in the vicinity of the main stream channels with additional observations in areas of woodland where creep was assumed to be minimal (for example, on flat summit crests).

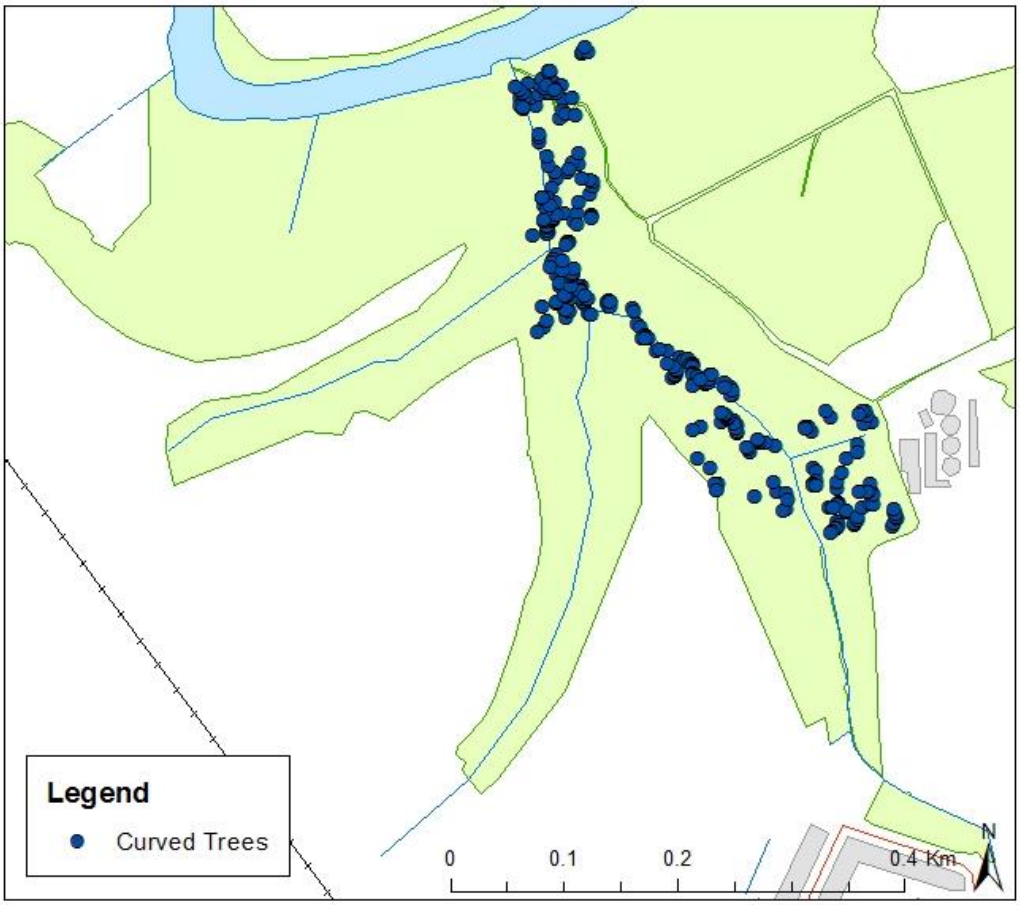

Figure 4.2-Spatial distribution of all 340 trees sampled as part of the research into tree curvature.

Observations for each tree were collated using a bespoke field record sheet. A range of information was collected while in the field:

- Identifier- Every sampled tree was given a unique number, which was temporarily marked on the tree. This ensured no tree was sampled twice, and provided an identifier for location which was recorded during the winter using a Magellan Explorist 610 GPS receiver when the leaf canopy was absent.
- Aspect- Using a compass, the direction the tree curved towards was noted. This will provide information on the direction soil creep is occurring in.
- Species – The species of every tree was recorded. Within the field an identification sheet designed by The Woodlands Trust was used to help identify tree species (The Woodland Trust, 2013). This information will be used to help calculate tree age.

- Diameter at Breast Height (DBH) – Tree trunk diameter was measured using a field tape at 1.3 m above the ground. This measurement was made on the upslope side of the tree. This information along with species has been collected to help approximate tree age. Only trees with a diameter at breast height greater than 0.2 m were included in the research, as the aim is to look at long term rates of soil creep, therefore older trees were preferentially selected.
- Plumb height, base length and trunk height – These three length measurements were collected using a survey tape to characterise the angle at the base of the tree (Figure 4.3).

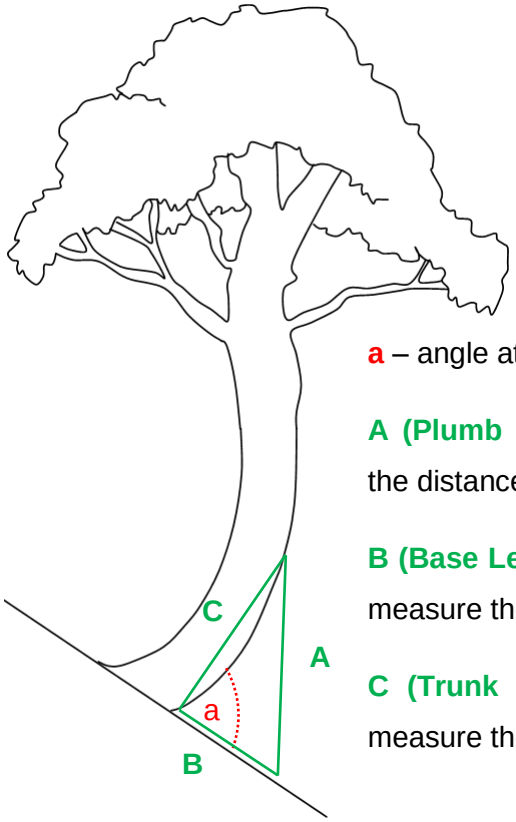

a – angle at the base of the tree and ground.

A (Plumb Height) – using a plumb line, measure the distance from where the tree starts to straighten.

B (Base Length) – from the base of the plumb line, measure the distance to the base of the tree.

C (Trunk Height) – from the base of the tree, measure the distance to the top of the plumb line.

Figure 4.3-The three measurements (plumb height, base length and trunk height) collected to calculate the angle at the base of curved trees.

4.2.4.2 Dendrochronology

Annual growth rings provide a wealth of information due to the development of reaction wood which can be analysed to look at soil creep (Denneler and Schweingruber, 1993, Pawlik et al., 2013). For the soil creep analysis, a small area (~20 m^2) of woodland was selected near the East stream (Figure 4.4). The section

of woodland did not show any obvious signs of historic rapid mass movement and therefore appeared to represent soil creep across the broader landscape of the woodland (Table 4.1). At the sampling site, a total of 8 trees were sampled (6 Ash trees and 2 Sycamore trees), all of which had been previously included in the basal trunk angle analysis. It was decided to only core Ash and Sycamore trees, as these trees accounted for 80.2% of all trees surveyed. Using an increment corer, one core was taken on the upslope side of the tree and one on the downslope side, in the middle of the curved stem (Figure 4.5). This produced a total of 16 tree cores. Figure 4.5, demonstrates the difference in ring width, as the upslope side of the tree has produced tension wood, ensuring stability.

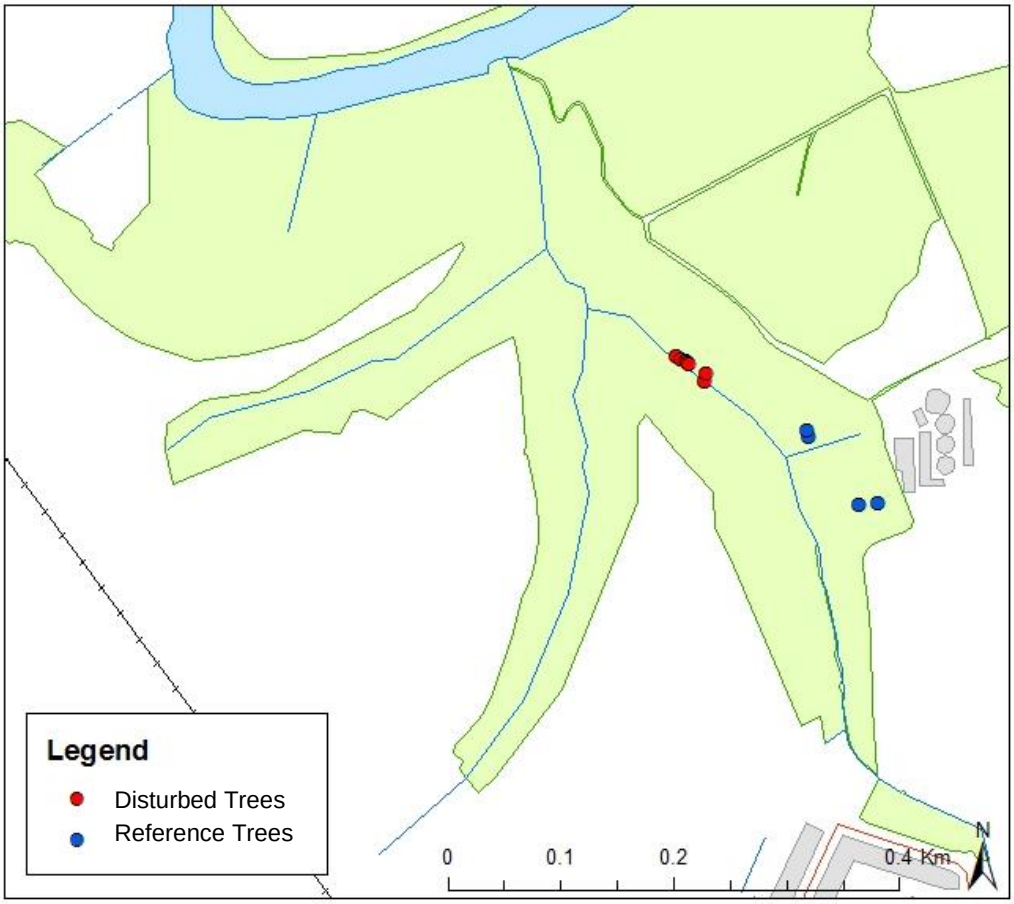

Figure 4.4-The location of the cored trees in a steep area of woodland and the location of the reference trees at the top of the hillslope.

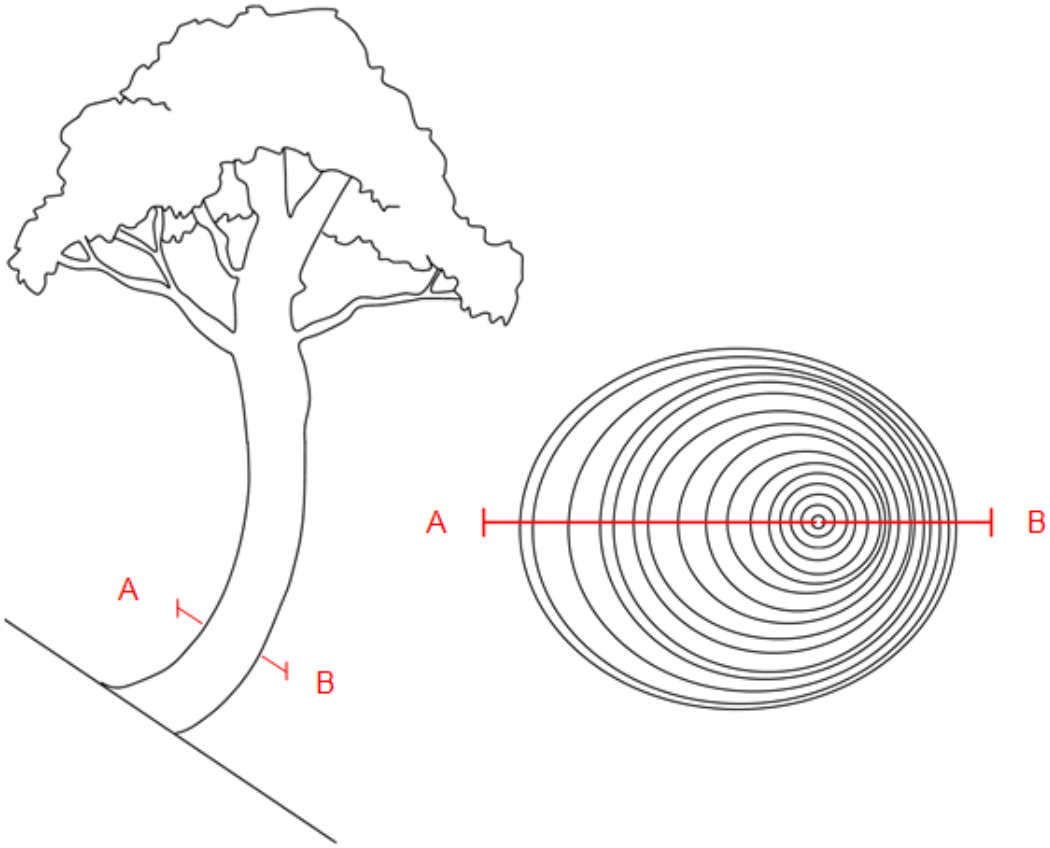

Figure 4.5-A) The location of the upslope (A) and downslope (B) cores. B) Cross-section of a curved angiosperm, demonstrating increased tree ring width due to the creation of reaction wood.

In addition to sampling trees with clear curved deformities, reference trees were also sampled from undisturbed ground at the top of the Red House Gill hillslope, where local slope was minimal (~8^{o}) (Figure 4.4). Table 4.1, compares the area of woodland for the disturbed and reference trees. Given the stable location it was assumed soil creep at the site was virtually nil. It was important to select reference trees from a stable area within the woodland to create a reference chronology which would separate any climate signals from soil creep. One core perpendicular to the slope direction was collected for every reference tree, as it provides better cross-dating results compared to collecting tree cores parallel to the slope (Owczarek, 2013). In total 4 reference trees were sampled (2 Ash and 2 Sycamore) providing a total of 4 tree cores.

	General Site Conditions	Proximity to the East Stream (m)	Slope Angle (^{0})
Disturbed Trees	Steep section of hillslope close to the stream bank. Likely to have high rates of soil creep.	1-10	14-26
Reference Trees	Flat area of land at the top or on a terraced section of hillslope	50-80	5-8

Table 4.1-Different site characteristics for dendrochronology

4.2.5 Geomorphic Mapping

To characterise the full extent of erosion across the catchment, geomorphic features were mapped. This was done by walking down all the streams, logging important features on both sides of the bank using a Magellan Explorist handheld GPS. A range of features were mapped over two days in October 2013: landslides, bank collapse, bank erosion, tree throw and zones of water seepage. These features were mapped as they were deemed important for catchment connectivity, moving fine suspended sediment from the hill slopes to the streams. Features which were less than ~2 m in length were excluded from the mapping. A small section (~50 m) of the East stream wasn't mapped due to a large landslide creating steep banks and a large amount of debris making it inaccessible.

4.2.6 Static Photography

To provide a record of geomorphic processes occurring across a range of erosion sites in Red House Gill, static photography was undertaken. Static photography was chosen as a method because it is quick, simple and easy to repeat. Within Red House Gill, 10 locations were chosen along the stream courses (Figure 4.6). The specific locations were chosen because they displayed a range of different characteristic geomorphic features for example: mass movement, bank collapse, seepage and material deposition. Survey pegs were placed in the ground, ensuring every repeat photo was taken from the same location. Photos were taken every two weeks between the 25th June 2013 and 12th November using a Nikon D70s fitted with an 18-70 mm (f3.5) Nikkor lens used in landscape mode. The landscape mode was selected to ensure a small aperture producing a photo with extended depth of field. This generally makes features from the foreground to horizon in focus

(Stafford, 2005). While in the field on the 23 July 2013, a camera malfunction meant no photos were recorded.

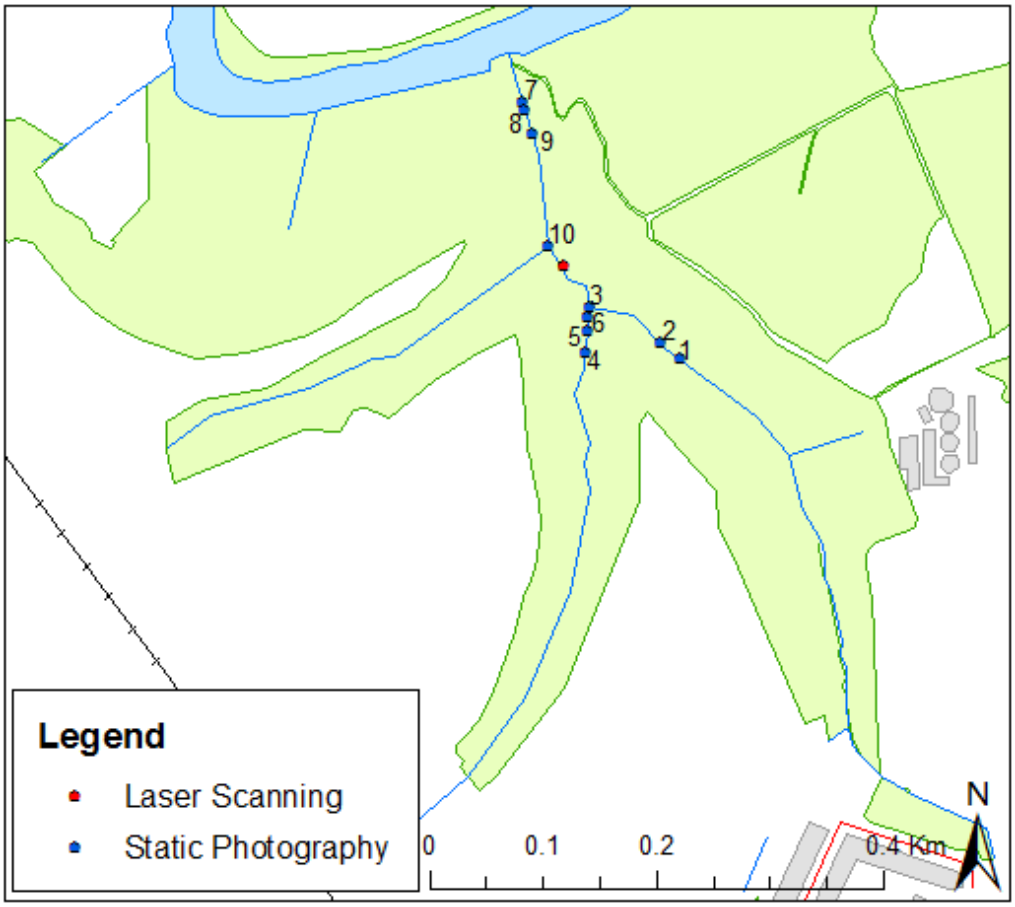

Figure 4.6-static photography locations and laser scanning location.

4.2.7 Terrestrial Laser Scanning

In this study a Riegl VZ-1000 terrestrial laser scanner, fitted with a Nikon D700 digital camera was used to collect 3D repeat spatial datasets of a landslide surface to look at the volume of material being delivered into the Red House Gill stream. This was done to provide a high resolution dataset to compliment the geomorphic mapping and repeat photography. The scanner utilises a near infrared laser capable of measuring at a range of 1400 m, with a scanning accuracy of 8 mm (Riegl, 2013). The scanner can create a 3D point cloud, where every point has an individual *XYZ* co-ordinate.

A landslide / eroding bank site slightly downstream of the East and Middle stream confluence was monitored (Figure 4.6). This site was chosen as it was characteristic of many of the direct connections between the hillslopes and stream channels that

occur in the Red House Gill catchment. Any material eroded from this site will go directly into the stream and contribute to the suspended sediment load. Due to the presence of trees, it was necessary to create three scanning locations (L1, L2, L3), to remove any 'shadow effect' (Bitelli et al., 2005). The shadow effect is caused, when vegetation or other objects are scanned, leaving the area immediately behind the object occluded. To ensure all three scans linked together, 6 target locations were set up, which could be seen from every scanning location.

Monitoring started on the 11th June 2013. The first repeat survey took place after a high rainfall event on the 16th August 2013. However, the third repeat survey occurred on the 4th October 2013, which was 6 weeks later, the same time period between the first and second scan. More frequent scanning was not possible due to the limited availability of the scanner.

4.3 Laboratory Analysis and Initial Processing

4.3.1 Suspended Sediment Concentration

Suspended sediment concentrations were calculated for samples collected using the auto-sampler following a vacuum filtration method. The volume of water collected was recorded before samples were filtered through Whatman GF/C 47 mm glass microfiber filter papers (retain particles > 1.2 µm) and then weighed. The samples were then placed in an oven at 105^0C for 24 hours then stored in desiccators to cool overnight before being reweighed. Suspended sediment concentration was calculated in mg l^{-1} by:

$$SSC = (W_2 - W_1)/V$$

Equation 3.1

W_1 – Wet weight
W_2 – Dry weight
V – Volume of water collected

4.3.2 TIMS Processing

The dry sediment weight of samples obtained from the TIMS samplers was calculated. Bulk samples were decanted into 8 litre plastic settling containers which were covered up and left until the sediment settled out (anywhere between two days and one week). Excess water was then siphoned off and measured using a

measuring cylinder. The siphoned off water was filtered using the above method (Section 4.3.1).

Sediment left within the container was poured into weighed glass beakers which were placed in the oven to dry out at 35^{o}C. This is a lower than standard temperature to ensure that geochemical properties of the sediment were not destroyed. The beaker containing the sample was then reweighed and the total dry sediment mass was calculated by adding the dry weight of the sediment to the sediment mass calculated from the concentration recorded in the excess water.

4.3.3 Calculating Flow and Suspended Sediment Concentration

The raw stage and turbidity measurements have been converted into discharge and suspended sediment concentration. Discharge was calculated from stage values using the slope area method developed by McMahon et al. (2001):

$$Q = \frac{1}{n} A\, R_3^2 S_2^1$$

Equation 3.2

Where:

A = Average Cross-section area of flow
R = Hydraulic radius
S = Water surface slope
n = Mannings coefficient

This method was chosen because of the short duration of the record and limited site access meaning recorded stage values could not be verified by direct stream gauging and an extensive water sampling program. Figure 4.7 shows the stage discharge relationship which was applied to the entire time series to estimate discharge.

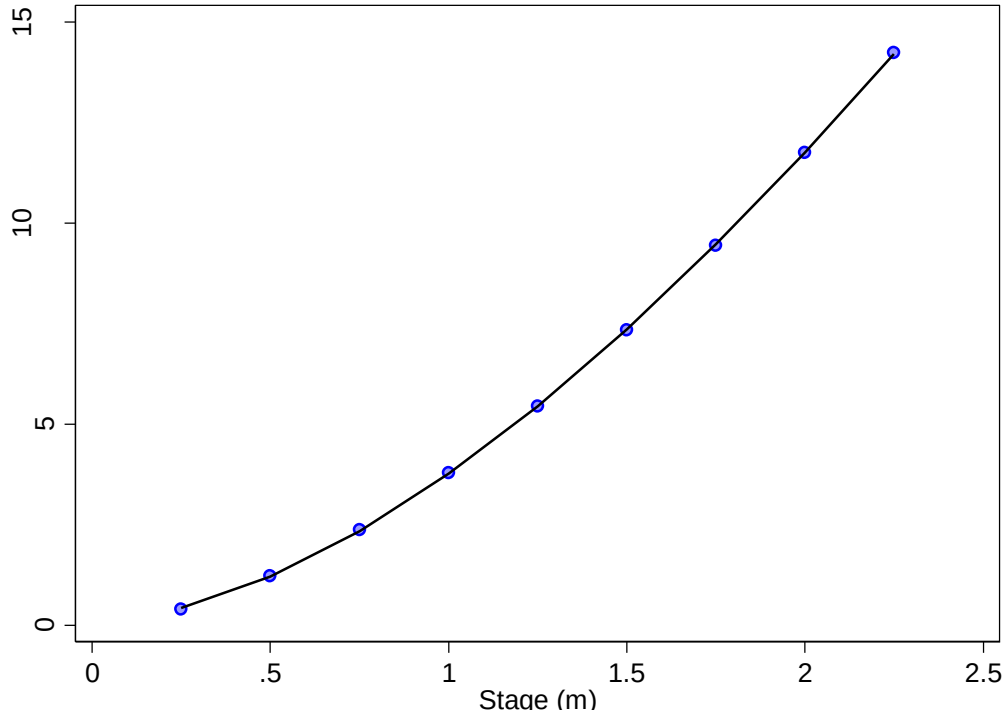

Figure 4.7-Stage discharge curve estimated for the Red House Gill gauging station.

In the field, the turbidity probe housing was occasionally blocked by sedimentation or covered by leaves so a complete time series does not exist. Therefore a rating relationship between discharge (Q) and SSC was developed. Figure 4.8 shows the relationship between discharge and SSC. A mean regional calibration relationship based on Perks (2013) was then used to calculate suspended sediment concentration (SSC); where SSC = 1.02 NTU, resulting in the final rating relationship where SSC = 1513.96*Q (R^2= 0.381). This relationship should be regarded as preliminary as the turbidity probe is only rated to 1000 NTU which is approximately 1020 mg l^{-1}. For concentrations greater than ~ 1000 mg l^{-1} and for flows in excess of ~1.0 m^3 s^{-1}, higher concentrations have been extrapolated from the linear relationship shown in Figure 4.8. This results in predicted concentrations in the range of 2000-6000 mg l^{-1} for the major flood events. Although direct sampling of suspended sediment was limited to a few isolated events, the highest concentrations measured on the falling limb of flood peaks sampled on 28th April and 24th May 2013 ranged from 1000-4000 mg l^{-1}, suggesting that the calibration relationship yields results which are plausible and provides a useful initial approximation for constructing the preliminary budget.

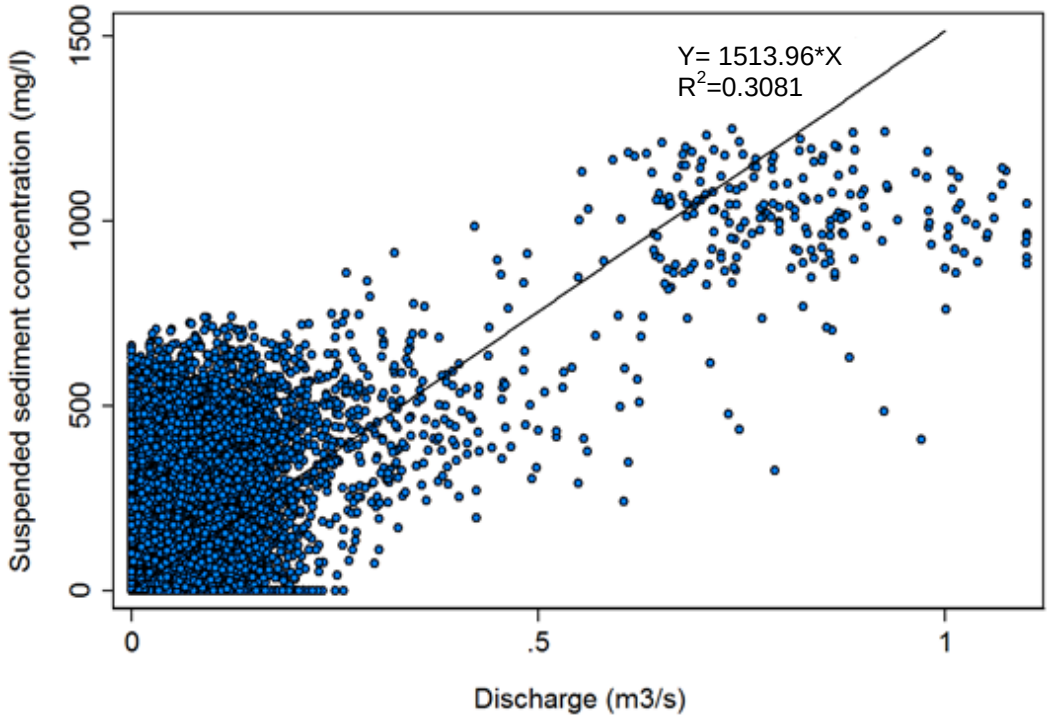

Figure 4.8-The rating relationship developed between discharge and SSC

4.3.4 Dendrochronology

Tree ring width was measured for all upslope and downslope tree cores using the following procedure:

1. The tree cores were removed from field packaging and allowed to air dry for one week prior to analysis. This ensures that the core is free of excess moisture and therefore won't crack during analysis.
2. Wooden mounts were labelled with tree core information (tree number, species and if the core was upslope or downslope).
3. The dried cores are glued on the right mount with water soluble glue, ensuring the core can be easily removed by soaking in water.
4. The cores were inspected by eye and with a 3X magnifying glass, checking for growth disturbances and the clarity of annual growth rings.
5. Annual growth rings were measured perpendicular to the current ring boundary using a digital calliper with an accuracy of 0.01 mm.

4.3.4.1 Tree Core Enhancement

On occasion tree cores are removed from the increment borer dirty, twisted or broken. This is often the result of a dirty or blunt increment corer and therefore it is

important to ensure the increment corer is clean and sharp prior to use (Speer, 2010). However, a range of techniques have been used to enhance tree ring boundaries helping to solve this problem after collection (Maeglin, 1979). Several of these techniques were trialled on tree cores from Red House Gill, before data collection occurred.

- Sanding – Sanding with progressively finer sand paper to help remove striations and dirt.
- Sulphuric Acid – placing the core in sulphuric acid for a couple of seconds before rinsing with cold water.
- Glycerine – brushing the core two or three times with glycerine at 30-40 minute intervals.
- Sodium Hydroxide – leaving overnight in a 10% solution of sodium hydroxide.

The results of this trial are shown in Figure 4.9. All the enhancement techniques worked, however it was decided if a tree core failed the visual inspection, it would be enhanced using sulphuric acid as it was the quickest and easiest technique.

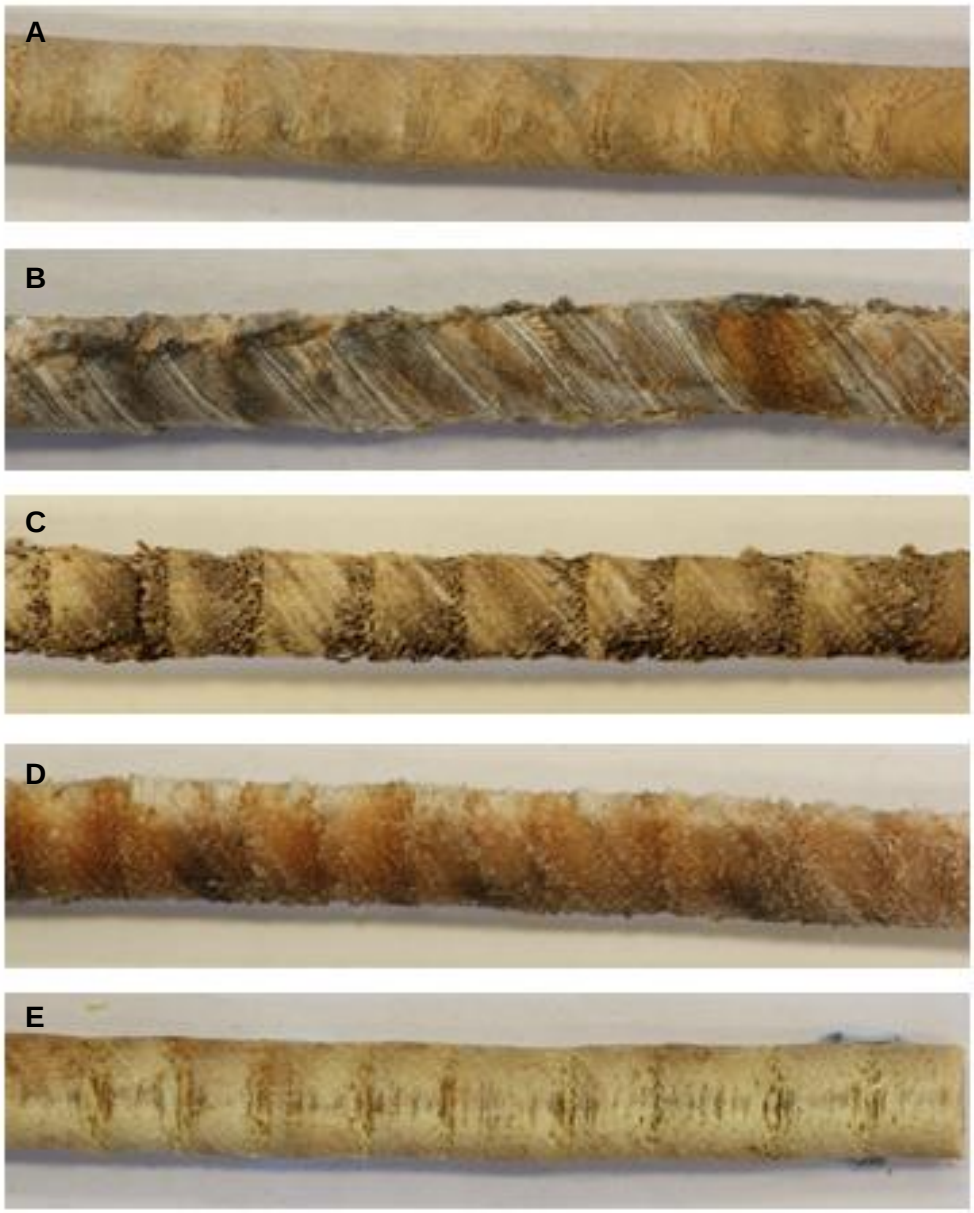

Figure 4.9- A) A clean tree core taken with a well maintained increment borer. B) A dirty, twisted tree core. C) Tree core after being enhanced with sulphuric acid. D) Tree core after being enhanced with glycerine. E) Tree core after being enhanced with sodium hydroxide. The cores were taken with a 5 mm increment borer.

4.3.5 Terrestrial Laser Scanning

The data have been processed following the steps in Appendix A. Initially the data for all three scan positions for each month were registered together using coarse registration in Riegl RiSCAN. As L2 is directly in front of the main slope face, this scan position was used as a reference position for every month, therefore laser data

from L1 and L3, where aligned with L2. The standard deviation of residuals (error) can be seen in Table 4.2. Although, the error for each month was low (~0.03 m), the scans were not adequately aligned and therefore multi-station adjustment was used. Error from the multi-station adjustment is shown in Table 4.3. After registration, the three scans for each month were combined into one point cloud, with data outside the landslide face deleted. Data for all three months were then co-registered first using coarse registration and then multi-station adjustment to improve alignment and reduce error (Table 4.3).

	L2 and L1	L2 and L3	MSA
11th June	0.0351	0.0085	0.0101
16th August	0.0120	0.0183	0.0092
4th October	0.0223	0.0118	0.0061

Table 4.2-Registration error (m) for individual scans within each month.

	August and June	August and October	MSA
Error (m)	0.0371	0.0292	0.0151

Table 4.3-Registration (m) when registering all three months together.

Sithole and Vosselman (2004), compared ground filtering algorithms demonstrating that different algorithms can have a significant effect on the resultant model. As a result of this research two different ground filtering algorithms were used to assess their effectiveness at removing vegetation. The built in vegetation algorithm in Riegl RiSCAN was used along with creating a specific macro in TerraScan. The exact parameters used can be seen in Appendix B. Both filters required large amounts of manual editing however it is hypothesised based on viewing the surface model of the respective ground models that TerraScan predominately had type 1 errors (ground points falsely removed from the ground model), whereas RiSCAN predominately had type 2 errors (points mistaken for the ground are included in the ground model). The final point cloud for each month contained a similar number of points. In the point cloud filtered using RiSCAN, there was a point density of 968 points per m^2, whereas the point cloud filtered using TerraScan had a point density of 952 points per m^2. The laser points were well distributed on the landslide slope, with a small area of microtopography near the top, which had a slightly higher point density for both datasets. The LAS files were exported and rasterised in ENVI with a resolution of 0.02 m.

4.4 Summary

Results from the main monitoring station just below the confluence of the East and Middle streams, along with the network of TIMS will provide information on the spatial and temporal variability of suspended sediment throughout the catchment. While the geomorphic mapping and static photography will be used to look at the frequency and magnitude of bank erosion along the streams. Terrestrial laser scanning will also be used to look at erosion, although it will only provide information on the feasibility in a steep wooded catchment. To provide information on historical bank instability and soil creep, information on tree shape and tree rings have been used. Data from all of these methods will then be combined to create the final geomorphic map outlining the connections between fine sediment sources and pathways. Figure 4.10, provides an overview of the spatial and temporal limits of research methods being used within this research. Over the course of this research, static photography and terrestrial laser scanning will be used to help characterise erosion processes occurring within the catchment and will be combined with suspended sediment data. The turbidity probe will provide information on a small spatial and temporal scale; however the network of TIMS will provide information on a larger catchment scale. While dendrochronology and information collected about basal trunk angle aims to provide information historically over a catchment scale.

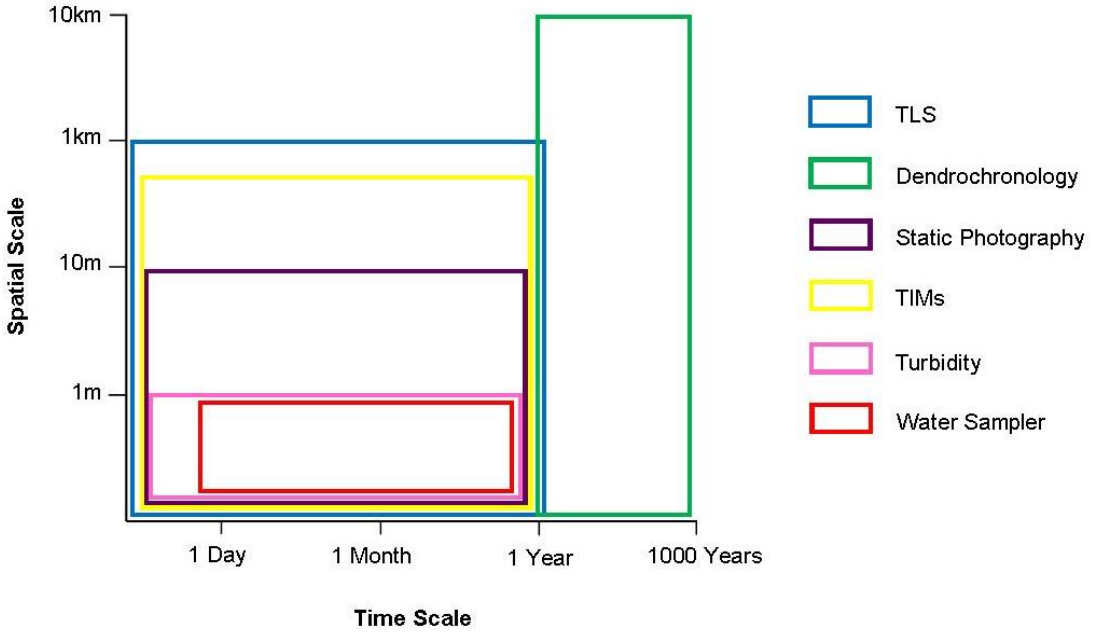

Figure 4.10- The spatial and temporal limits of research methods used within this research

5 Contemporary Sediment Transfer

This chapter will be divided into three main sections. Section one, displays and analyses the results from geomorphic mapping, static photography and terrestrial laser scanning to help identify key hotspots of bank instability supplying fine suspended sediment into the Red House Gill streams (Section 5.1). The second section then uses data acquired from the suspended sediment monitoring and network of TIMS to produce a picture of fine sediment movement through the catchment (Section 5.2). Then the last section draws together the preceding parts, characterising key periods of enhanced fine sediment delivery (Section 5.3).

5.1 Sources of Fine Sediment

To assess the impact of high flow events on bank erosion, geomorphic mapping, static photography and terrestrial laser scanning have been used to document erosion processes and estimate the volume of material supplied to the Red House Gill streams. This section is divided into three parts, initially presenting a geomorphic map of the catchment (Section 5.1.1), before discussing results from the static photography (Section 5.1.2) and the terrestrial laser scanning (Section 5.1.3).

5.1.1 Geomorphic Mapping

Geomorphic features such as landsliding and bank erosion which lead to bank collapse are important controls on the supply of suspended sediment to the stream. Based on reconnaissance field walks an inventory of key features was determined before all attributes were mapped in October 2013. Figure 5.1 shows the results from geomorphic mapping within the lower Red House Gill catchment. Within the catchment, most landslides are deep seated translational failures; however there are some examples of rotational failures. Bank erosion occurs in areas where channel scour at the base of the banks results in erosion. Although less effective at transporting sediment to the stream channel, bank erosion leads to bank collapse. Bank collapses within the catchment are normally small failures, connected directly to the stream channel. These sediment sources are located throughout the catchment occurring on all three tributary streams. However their distribution varies spatially (Figure 5.1). On the East and Middle stream, the head of the stream is dominated by bank collapse, followed by landslides and then bank erosion within

the lower reaches. However on the West stream, bank collapse is the most prominent feature in the lower reaches.

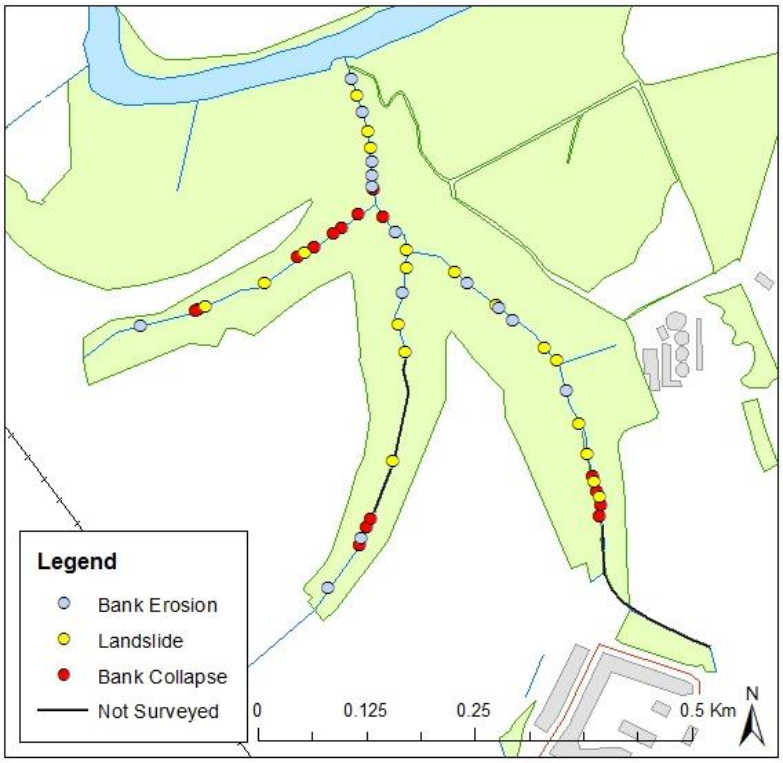

Figure 5.1-Results from the geomorphic mapping carried out across all streams

5.1.2 Static Photography

At Red House Gill, static photography has been taken fortnightly starting on the 25th June 2013 over a five month monitoring period gathering information on the fine sediment supply due to lateral bank erosion. As part of this, 10 sites were selected throughout the woodland where erosion would directly feed into the streams, increasing fine sediment supply (Figure 4.6). Table 5.1 provides an overview of all sites. As the table shows, two sites were selected on the East Stream, three on the Middle stream and five on the trunk (one before the West confluence and four downstream of the West confluence). Initial field walks along the streams demonstrated that the main erosion processes are bank undercutting leading to bank collapse, landsliding, and a mixture of both processes. As a result it was important to use sites which characterised these processes, consequently five landslide faces, three areas of bank undercutting and collapse and two areas of mixed mass wasting were selected. Approximate dimensions for every site have also been calculated using a reference scale which was included in the baseline

photo for every site. The biggest site is location two, which is a landslide face approximately 20 m long and 8 m high, compared to the smallest site, which is an area of bank erosion which is approximately 3 m long and 1 m high. Table 5.1 also details geology type demonstrating clay is the most prevalent material which corresponds with the BGS borehole located within the Red House Gill woodland (Section 3.4). Details of the main erosion processes are discussed with reference to sites four and ten which are representative of the larger group of 10 sites.

Location	Stream	Length (m)	Height (m)	Depth (m)	Feature Type	Geology
1	East	9	6	1	Mass Wasting	Loosely consolidated topsoil mixed with small pebbles.
2	East	20	8	0.5	Landslide Face	Two well defined layers. Well drained sand on top of poorly drained clay.
3	Confluence of the East and Middle stream	8	10	1	Landslide Face	Gley soil mixed with pebbles. No distinct layers can be seen.
4	Middle	15	10	1	Landslide Face	Well drained sand is underlain by clay.
5	Middle	20	4	1	Mass Wasting	Loamy Clay with a small section of clay.
6	Middle	10	10	1.5	Landslide Face	Loamy clay on top of clay containing less sand and silt.
7	Trunk	15	6	1	Landslide Face	Loamy clay mixed with small pebbles.
8	Trunk	10	2	0.5	Bank Undercutting and Erosion	Clay mixed with pebbles which are a variety of sizes.
9	Trunk, near the West confluence	3	1	0.5	Bank Undercutting and Erosion	Loosely consolidated top soil.
10	Trunk	3	1	0.5	Bank Undercutting and Erosion	Loamy clay with a few large boulders.
TLS	Landslide	10	10	1	Landslide Face	Loamy clay, with small areas of sand.

Table 5.1-Summary of key features for all ten static photography locations and the landslide face being monitored using terrestrial laser scanning. Information on length, height and depth have been rounded to the nearest 0.5m.

5.1.2.1 Erosion Processes – Site Four

Location four is a large landslide face directly feeding fine sediment to the Middle stream. The baseline photo which can be seen in Figure 5.2, demonstrates a range of important geomorphic features. The landslide face can be divided into distinct geologic layers; well drained sand is underlain by clay increasing landslide susceptibility due to differences in hydraulic conductivity (Figure 5.2a). The sand layer also has several drainage holes which will aid hillslope drainage (Figure 5.2e). The initial landslide has created a lobe of debris at the base, which the East stream has eroded a channel through (Figure 5.2b). Part of this debris lobe is a large tree (Figure 5.2c). During high flow events, it appears that the East stream is powerful enough to undercut the landslide face (Figure 5.2d). Vegetation colonisation on the landslide face suggests the landslide occurred several years ago; this vegetation along with vegetation at the top of the landslide face should aid stability (Figure 5.2f).

Throughout the monitoring period, four key photos demonstrate erosion processes occurring at location four (Figure 5.3). High levels of rainfall at the beginning of August generated elevated flows, with repeat photography on the 6th August demonstrating that the small area of bank undercutting identified on the baseline photo has completely collapsed. The tree has also been completely removed, demonstrating the scale of undercutting along the landslide face. The next significant change occurred during the middle of September, when undercutting eroded away a large section of clay (~1 x 1 x 0.5 m). A smaller section of clay (0.5 x 0.2 x 0.2 m) was eroded by the 1st October, however by the end of October; the whole landslide area has been eroded into a flatter surface. Minimal erosion has occurred at the top of the landslide face presumably due to the well-drained sandy geology and height above the stream.

Figure 5.2-Baseline photography for location four, outlining key geomorphological information -A- Distinct substrata layers. B –stream channel within in the debris lobe. C- Tree at the base of the scar. D- Stream undercutting. E – Drainage channels within the landslide face. The landslide face is 15 x 10 m.

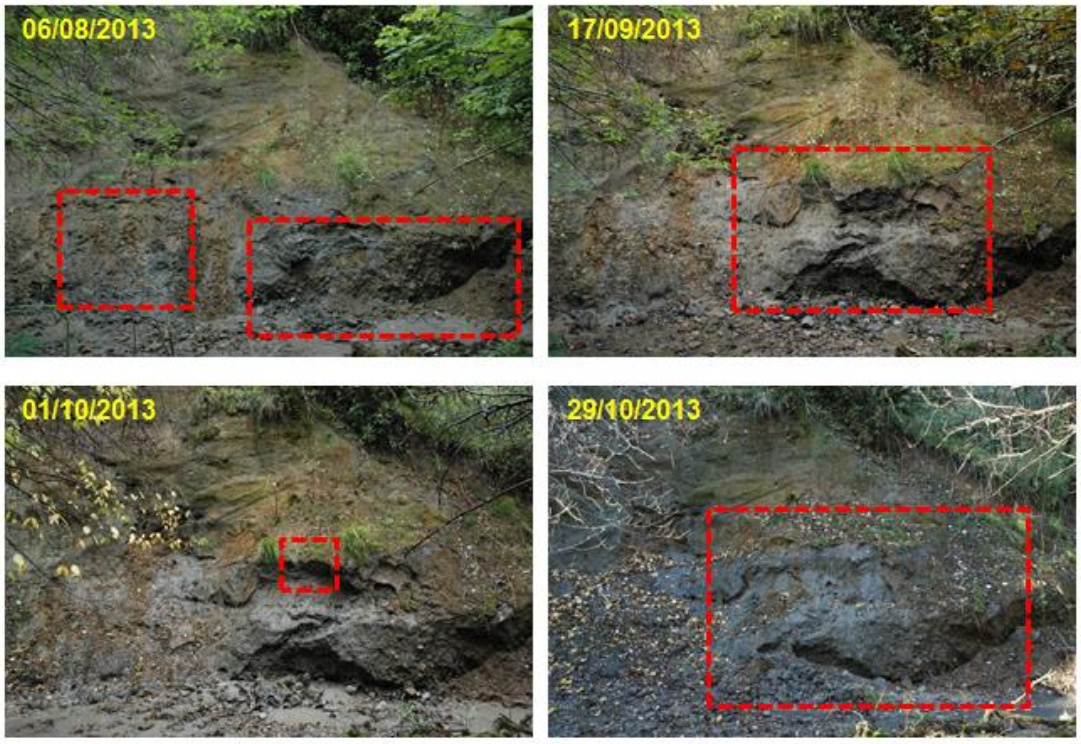

Figure 5.3-Temporal changes occurring at static photography location 4. The red boxes denote areas of change.

5.1.2.2 Erosion Processes – Site ten

Static photography location ten is an area of bank undercutting on the trunk stream, close to the confluence with the West Stream. In this reach, bank undercutting is extensive; however there are few recent signs of bank collapse. Figure 5.4 is the baseline photo of site ten taken on the 25th June 2013 when monitoring first began. As the photo demonstrates, this stretch of the river bank has been extensively undercut (Figure 5.4a) and has led to bank collapse in certain parts (Figure 5.4b). It appears that the extensive root system has helped to stabilise the bank, ensuring that bank collapse is minimal (Figure 5.4e). There is also a large debris block within the stream made of organic (tree branches) and inorganic (stones) material (Figure 5.5d) while the hillslope is filled with curved trees caused by soil creep.

Key changes that have occurred at site ten throughout the monitoring period can be seen in Figure 5.5. The first key change occurred at the beginning of August, when the photo demonstrates the high stream level compared to the baseline photo. Within the area of collapse, plants have died back and the mass appears to have slumped further into the stream. By the end of August, a large tree branch had fallen to the ground, while the area of bank collapse had extended laterally upstream, and

a small area of deposition had developed. Only minor changes occur until the middle of October. High levels of rainfall before the 15th October caused high flows which flowed over the debris block. A fortnight later, the stream is still high compared to the baseline photo and the area of bank collapse is continuing to slump further down and extend laterally upstream.

Figure 5.4-Initial photography providing a base line for change. A – Bank undercutting. B – Bank collapse. C – Debris blocking the stream. D – Root system. E – Steep forest with curved trees. The meter rule by the root system, provides information on scale.

Figure 5.5-Main changes occurring throughout the monitoring period at location ten. The red boxes denote areas of key change.

5.1.2.3 Frequency and Magnitude of Erosion

To quantify the erosion at each site, the volume of material eroded has been estimated. This has been estimated using the scale on the baseline photo and field notes written fortnightly when images were taken, to generate measurements of length, height and depth of erosion which has taken place. Due to the high error margin on calculating volume based on photographs and field notes, all values have been calculated conservatively. It is therefore believed, these values represent a minimum volume of eroded material. Figure 5.6, shows the volume of eroded material over the entire study period for each site. The graph demonstrates that the landslide face in location four has eroded the most, with ~2.8 m^3 of material being washed into the stream, increasing suspended sediment concentration. Location two, which is the largest area of erosion being monitored, has eroded the second highest with ~ 1.5 m^3 of erosion being observed. The three sites displaying bank erosion (8, 9 and 10) have eroded far less only eroding 1 m^3, 0.1 m^3 and 0.6 m^3 respectively. No erosion has been visibly observed at location 7 which is a landslide face on the trunk stream. This has presumably been caused for two reasons; firstly the stream channel is relatively flat and unconstrained, leaving the stream to flow

close to the other side of the bank. Secondly, the landslide face doesn't show any clear geologic stratification and also has a dense network of vegetation roots which aid stability.

Figure 5.7 shows the area of eroded material per collection date. As the figure shows most erosion was observed in photos taken on the 6th August, after intensive summer rainfall on the 28th July and 5th August. The volume of erosion remained low until the middle of September when erosion became continuous until the end of the monitoring period at the beginning of November.

Information regarding the frequency and magnitude of erosion has also been compiled for all ten sites throughout the monitoring period and graphically represented in Figure 5.8. Each site is represented by a separate marker, which indicates how many times visible erosion was seen in the ten photos collected for each site throughout the monitoring period along with the volume of eroded material. As the graph demonstrates there is a clear positive relationship between frequency of erosion and magnitude. Site two and four which are both landslides have demonstrated the highest frequency of erosion throughout the monitoring period, although site four on the Middle stream has eroded almost double the volume (2.8 m^3) of site two on the East stream (1.5 m^3). Site four, eroded more as the magnitude of erosion was greater on every occurrence compared to site two. However, site two and four demonstrate the cumulative nature of erosion, with high frequency of events, generating the two highest magnitudes seen throughout the ten sites. Five sites in total (sites one, five, six, eight and nine) have all undergone visible erosion in two photos, with sites five and six even eroding by the same magnitude of 0.2 m^3 throughout the monitoring period. Site seven, where no visible erosion occurred, consequently has a frequency and magnitude of zero.

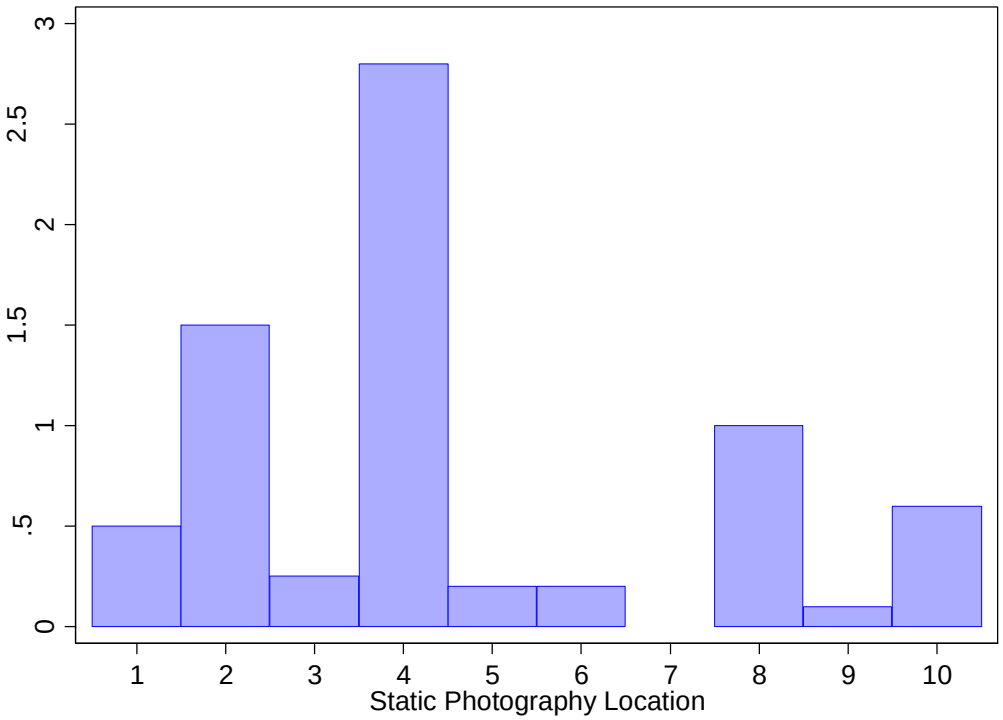

Figure 5.6-Volume of material eroded (m^3) for each site

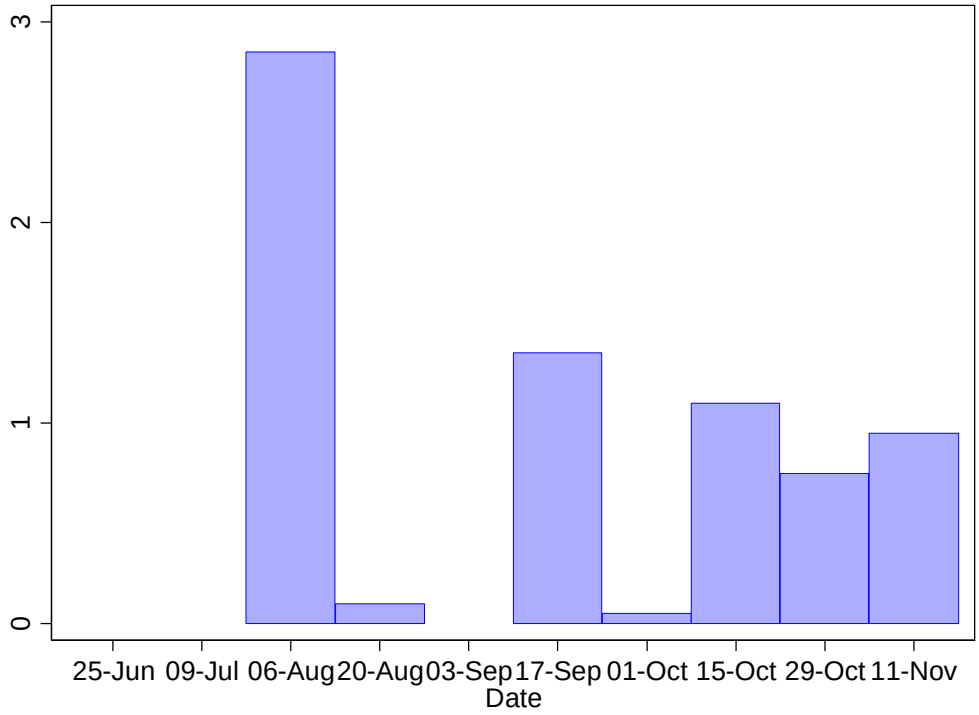

Figure 5.7-Volume of material eroded (m^3) on each static photography collection date for all sites

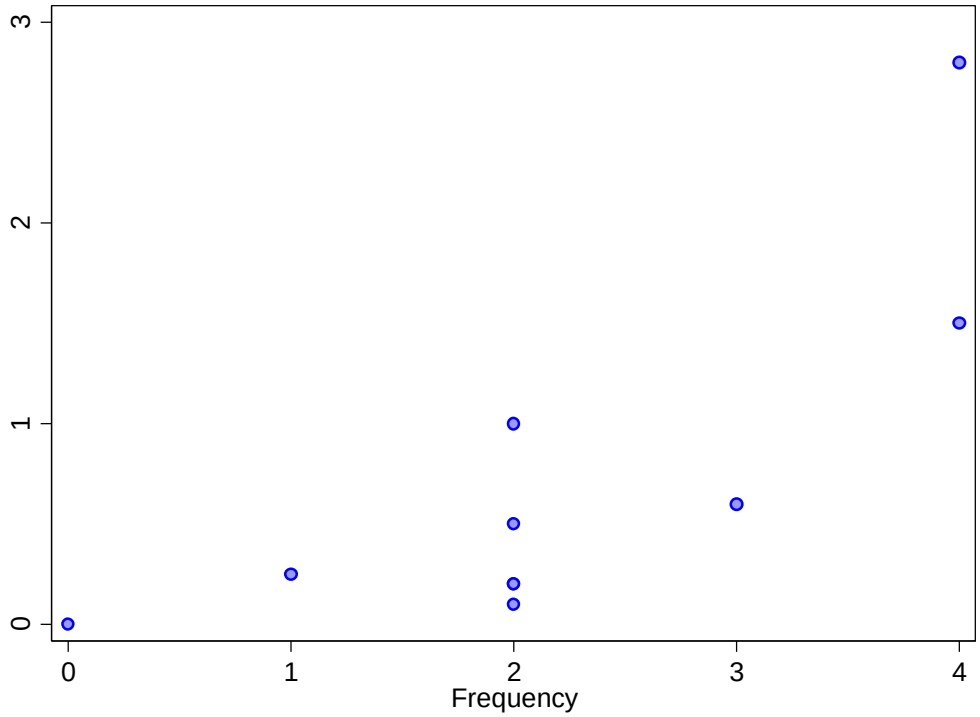

Figure 5.8-Frequency and Magnitude of change at all 10 sites. The potential maximum frequency is 10 as 10 observations were made.

5.1.3 Terrestrial Laser Scanning

Post landslide erosion can contribute as much as 33% of the total sediment loss from a landslide site (Walker and Shiels, 2013). Information gathered from initial site visits and geomorphic mapping revealed 19 landslide scars and it is therefore important to investigate the amount of erosion occurring at these sites. In order to do this, terrestrial laser scanning has been used to monitor the volumetric change (both erosion and deposition) on a landslide face approximately 40 m downstream of the East and Middle stream confluence (Figure 4.6). The failure that occurred was shallow, only 0.5 m deep and occurred over a small area 10 x 10 m. This landslide face was selected because it is a similar size to other landslides located on the East, Middle and trunk streams and therefore the processes of erosion occurring here would be similar to other sites in the catchment. As the photo in Figure 5.9 demonstrates, the landslide face is primarily composed of well mixed loamy clay and is heavily vegetated with ferns. Due to the succession of vegetation, the landslide would have occurred several years earlier.

Figure 5.9-Photo demonstrating the geology and high amount of vegetation on the monitored landslide face taken in October. The landslide face is approximately 10 m high by 10 m in length.

5.1.3.1 Volumetric Change Results

The data was then analysed in ArcGIS using raster calculator to create a DEM of Difference (DoD), which filtered out the final registration error (0.0151 m, Table 4.3). The final DoD has several areas of 'no data', where the results were below the error threshold. Figure 5.10, demonstrates the difference in elevation between June and October for the landslide face when filtered using RiSCAN. The results show that between June and August, very little change was detected (below the error threshold) although there is more erosion (red) than deposition (blue). There is an area of deposition at the base of the landslide face, presumably where material sourced from higher up the landslide face, hasn't been eroded by the trunk stream yet. At the top of the landslide face, there is an area which has under gone very little change. Figure 5.11, demonstrates the difference in elevation between June and October for the landslide face when filtered using TerraScan. There is a marked difference between results using RiSCAN and TerraScan. The results using TerraScan reveal that a lot of change is below the error threshold shown by large amounts of 'no data' gaps. However, they still agree with data processed using RiSCAN, as more change can be seen between August and October, than between June and August.

The DoD in Figure 5.10 and 5.11, can then be used to estimate the volume of eroded sediment for each time period. These results can be seen in Table 5.2. Between June-August, the volume of material eroded calculated using both RiSCAN and TerraScan is similar, as RiSCAN derives 1.175 m^3 of material has been eroded whereas TerraScan derives 1.414 m^3 of material has been eroded. This is a difference of 0.239 m^3. However, the results for August-October demonstrate a large discrepancy as RiSCAN derives 10.099 m^3 of material has been eroded and TerraScan derives that only 1.254 m^3 of material has been eroded, which is a difference of 8.845 $m^3$of material. All three months have a final registration error of 0.00151 m, however as Figure 5.11 demonstrates the results for TerraScan reveal a lot of data gaps, where the volumetric change was below this error threshold and therefore explains why higher volumetric change was recorded using RiSCAN. These results agree with previous work by Sithole and Vosselman (2004), who compared ground filtering algorithms and demonstrated that different algorithms can have a significant implication on the resulting ground model. They used a range of datasets (steep slopes, dense vegetation and highly urbanised areas) and found that most worked well in flat rural terrain but all produced errors in complex vegetated settings. More research is needed into the effects of ground filtering on volume calculations, especially in areas with a high density of vegetation that helps mask the true ground model increasing uncertainty in the derived results.

As part of the static photography, three landslides were monitored all of which are larger than the landslide face monitored using terrestrial laser scanning. The largest volume of erosion monitored through the static photography is 2.8 m^3, which is similar to the volume of eroded material suggested through TerraScan vegetation filtering method. It is therefore suggested that the static photography and TerraScan filtering method provide quasi-comparable results. However, more research is needed comparing the results of erosion from laser scanning and more established survey methods.

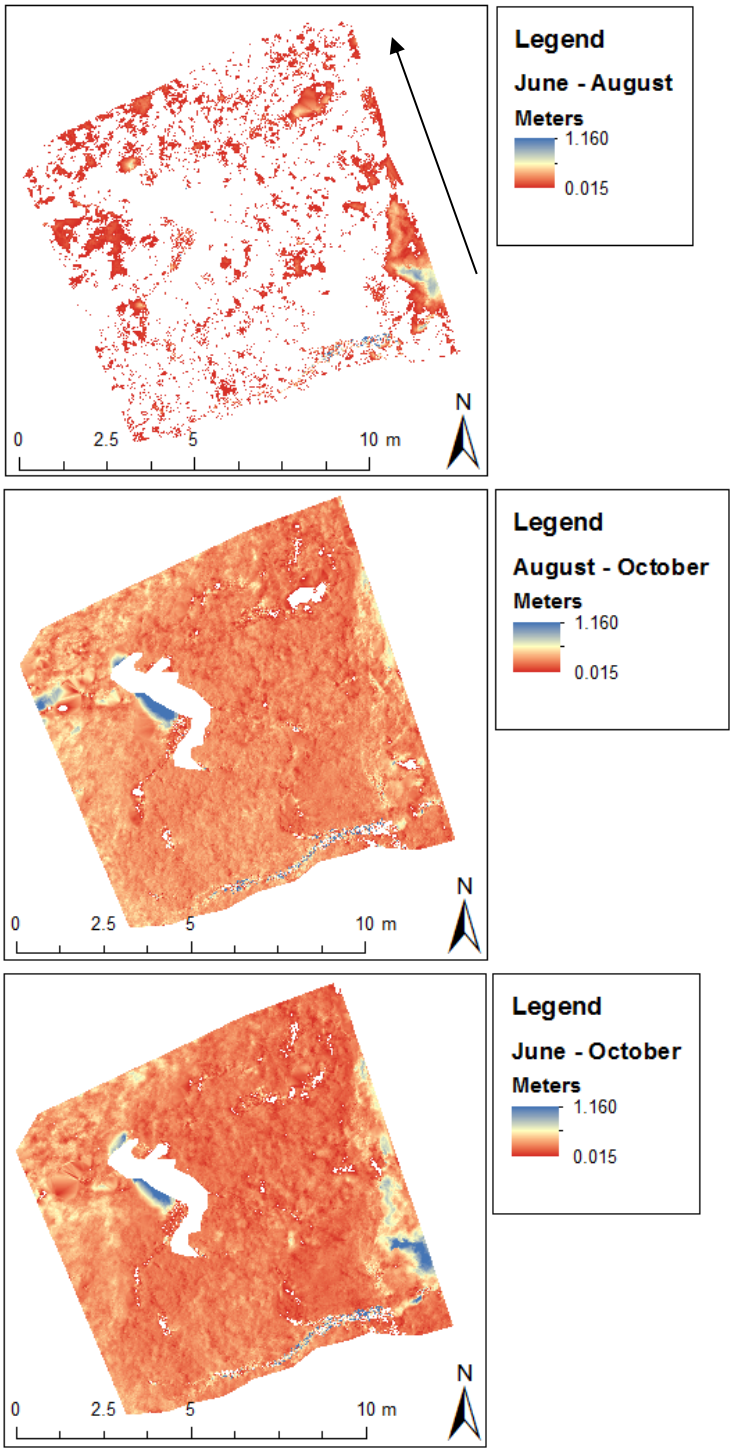

Figure 5.10-DoD for the landslide face between June and August (a), August and October (b) and the total difference between June and October (c) after using the RiSCAN vegetation filter. The black arrow denotes stream direction at the base of the landslide face.

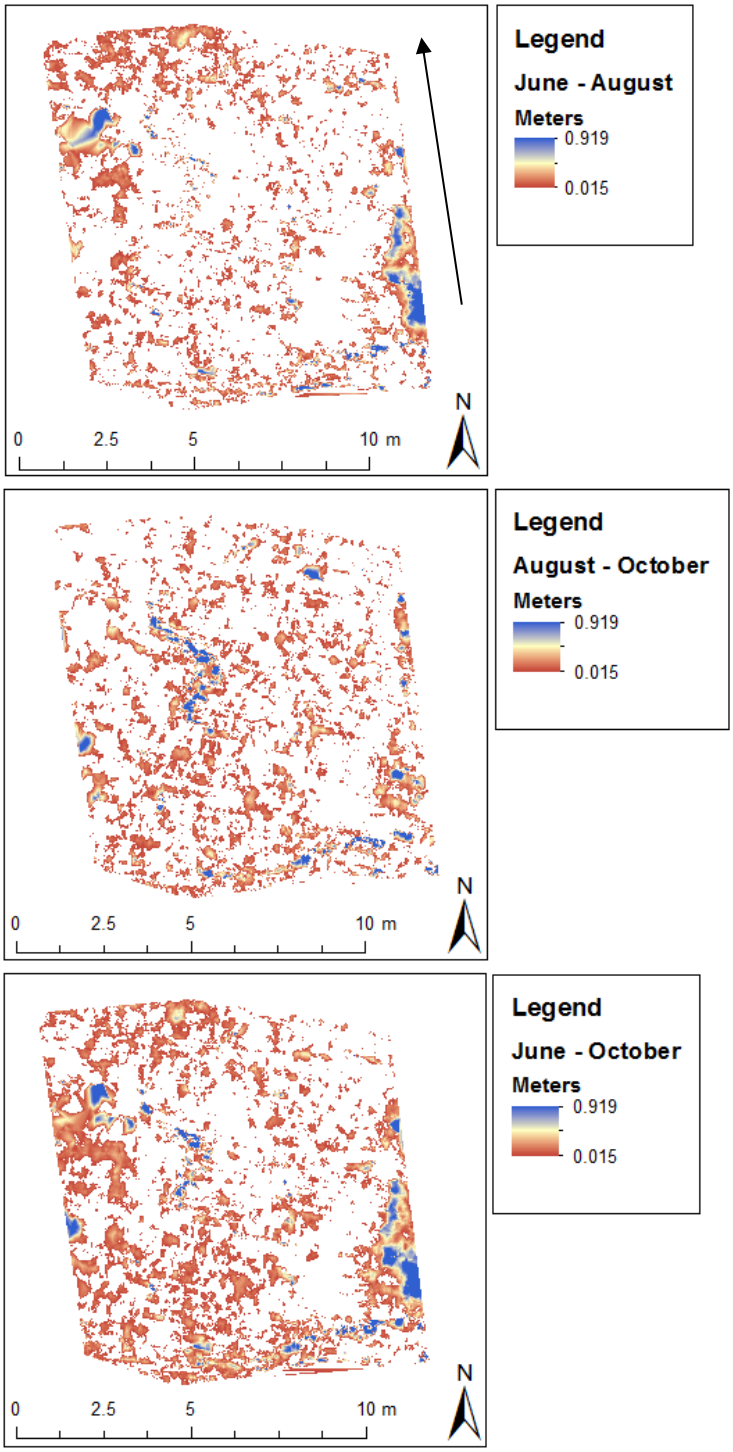

Figure 5.11-DoD for the landslide face between June and August (a), August and October (b) and the total difference between June and October (c) after using the TerraScan vegetation filter. The black arrow denotes stream direction at the base of the landslide face.

	RiSCAN ground filtering volume eroded (m^3)	TerraScan ground filtering volume eroded (m^3)
June – August	1.175	1.414
August – October	10.099	1.254
June - October	10.861	2.062

Table 5.2-Volume of eroded material calculated using the two different ground filtering techniques.

5.2 Suspended Sediment

To investigate fine suspended sediment dynamics within the Red House Gill catchment, a network of TIMS and a main monitoring station consisting of an automatic water sampler, turbidity probe and stage recorder were installed. Here results describe the time series of suspended sediment concentration generated using the turbidity probe (Section 5.2.1) and then characterise the spatial and temporal pattern of fine sediment delivery from the TIMS (Section 5.2.2).

5.2.1 Suspended Sediment Time Series

To explore the relationship between stream flow and suspended sediment the main monitoring station 15m below the confluence of the East and Middle stream was installed (Figure 4.1). After calculating discharge and SSC (Section 4.3.3), suspended sediment load of Red House Gill was then generated using Equation 5.1.

$$SSL = K \sum_{i=1}^{n} SSC_i \, Q_i$$

Equation 5.1

Where:

K = Multiplication Factor
SSC_i = Instantaneous value of SSC
Q_i = Instantaneous value of Q
n = Total number of samples

It is important to look at the whole time series to identify events, periods and conditions leading to high rates of discharge and suspended sediment concentration (large fine sediment transfer events). Figure 5.12, provides a time series of discharge recorded every five minutes and daily precipitation recorded from the Durham University Observatory between 11th April to 23rd October 2013. As the graph shows, there is a clear connection between peaks in daily precipitation and

discharge. There are four major peaks in discharge throughout the monitoring period, firstly on the 18th May 2013, 28th July 2013, 5th August 2013 and 6th September 2013 and numerous smaller peaks throughout October.

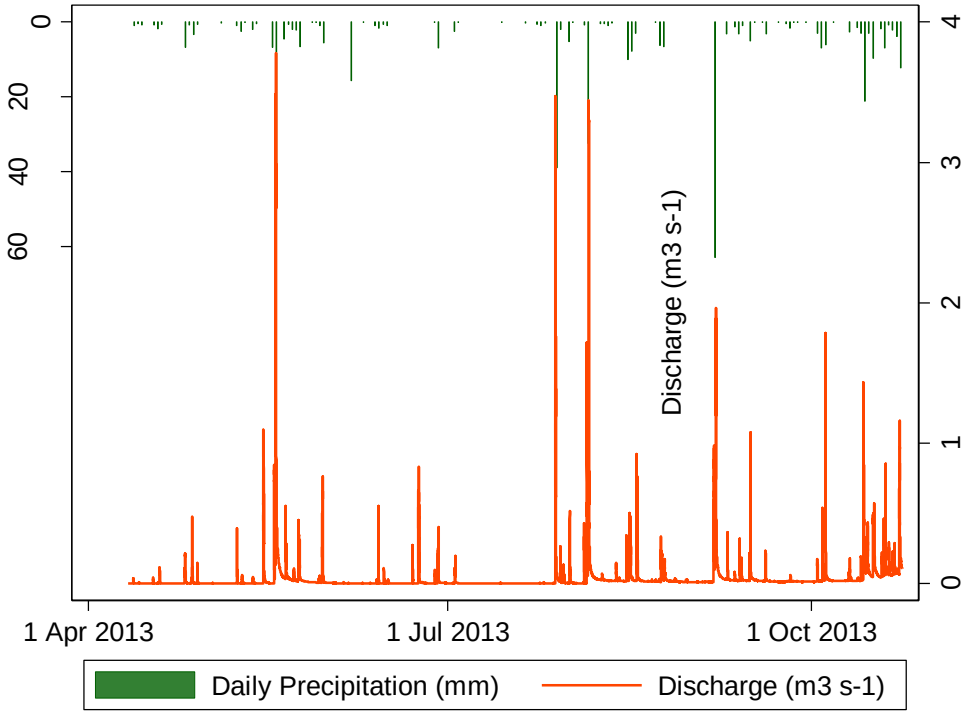

Figure 5.12-Time series of discharge from the main monitoring station in Red House Gill and daily precipitation from Durham University Observatory.

Figure 5.13, shows a detailed view of daily precipitation and resultant changes to discharge. On the 17th May 2013, there was 7 mm of rainfall, which dramatically increased to 40.8 mm on the 18th May 2013. This produced the peak in discharge, which reached 3.78 m^3 s^{-1}. Using the rating relationship, this equates to a suspended sediment concentration of 5718 mg l^{-1}. This is the highest peak in discharge and suspended sediment recorded during the monitoring period. The next peak occurs on the 28th July 2013, after 39.2 mm of rainfall (Figure 5.14). The resultant discharge is formed of three peaks, it is possible that these three peaks were caused by the East and Middle urban areas and then by run-off from the wider forested hillslopes. A week after this peak, there is another high rainfall event, with 32.8 mm of rainfall falling on the 5th August 2013 (Figure 5.15). The discharge for this event can be separated into two distinct peaks, with the second peak being much larger. It is possible, that after the rainfall event a few days earlier, the field and woodland were already saturated, therefore run-off from these areas exceed

run-off from the urban area as the land didn't need recharging. Figure 5.16, provides a detailed picture of precipitation and discharge on the 6th September 2013. On the 6th September 2013, 63 mm of rainfall was recorded which is the highest amount of daily rainfall over the monitoring period, which resulted in high levels of discharge. As the graph demonstrates, there appears to be two distinct peaks, with the first peak which is presumably from the urban area being smaller. Although this is the highest rainfall, recorded the resultant discharge only reached 1.903 $m^3 s^{-1}$ with a suspended sediment concentration of 2704 mg l^{-1}. There is a clear connection between peaks in rainfall and stream discharge and therefore suspended sediment concentration. These peaks also coincide with high levels of erosion seen within the static photography, with high levels of erosion being recorded after intense rainfall on the 5th August and 6th September (Figure 5.7).

Throughout these storm events, it is hypothesised that the East stream responds first. This is because the East stream is 72% urbanised, with a dense network of surface water drainage. As water velocity is indirectly proportional to land surface roughness, storm water run-off quickly passes smooth impervious storm drains into the wooded area of the East catchment. Due to floodplains in the lower part of the East catchment which has the ability to store sediment it is believed that the Middle catchment produces the most suspended sediment. This also agrees with results from the static photography, as sites on the Middle stream have eroded more.

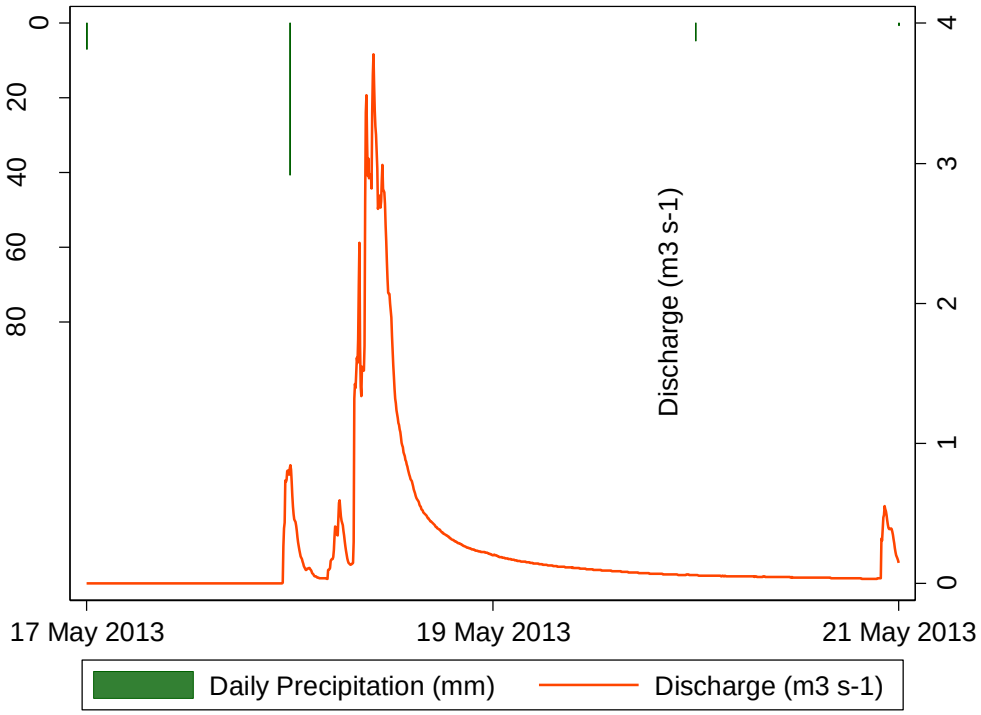

Figure 5.13-Precipitation and discharge on the 18th May 2013.

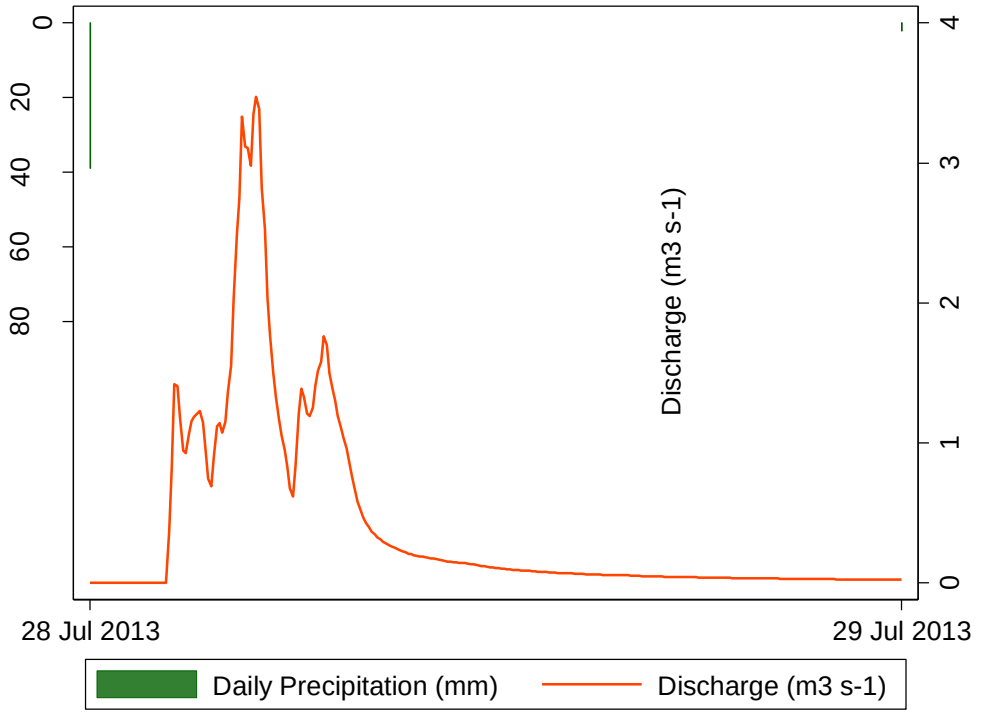

Figure 5.14-Precipitation and discharge on the 28th July 2013.

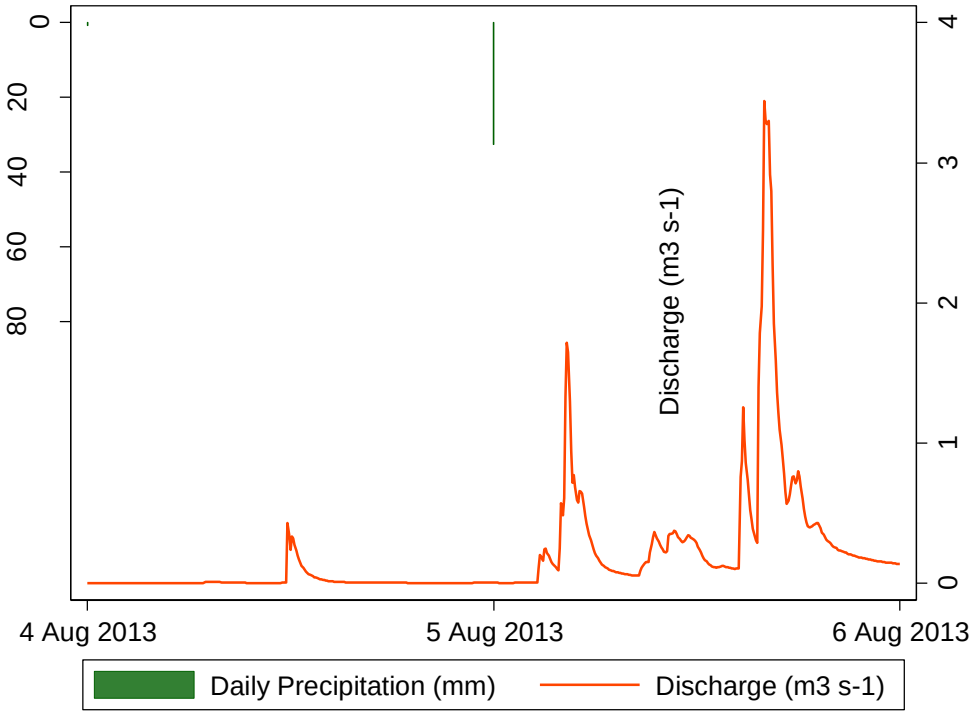

Figure 5.15-Precipitation and discharge on the 5th August 2013.

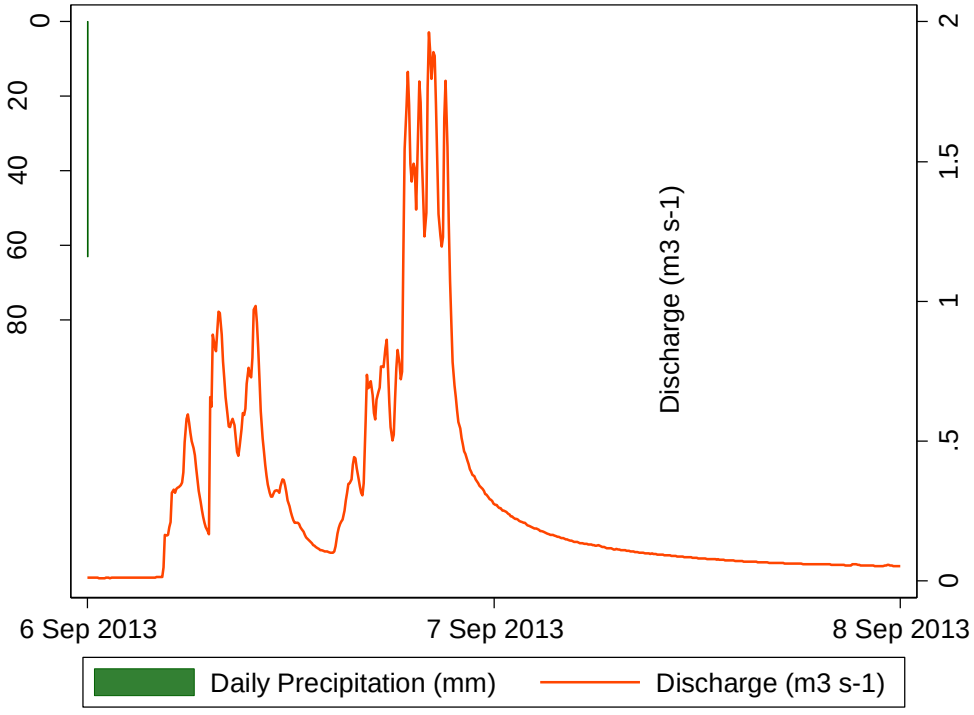

Figure 5.16-Precipitation and discharge between 6-7th September 2013

An estimated 492 t of sediment has passed through the main monitoring site during the period of monitoring. Figure 5.17, provides a time series of sediment load

passing though the Red House Gill catchment. As the graph demonstrates, suspended sediment load peaks during the four main high rainfall events on the 18th May 2013, 28th July 2013, 5th August 2013 and 6th September 2013. Table 5.3 presents the sediment load in tonnes for the four main events, along with the percentage of total sediment load, peak discharge and the approximate duration of the event. As the table shows, 80% of the total suspended load was transported in just four days which is only 2% of the monitoring time. Therefore the remaining 20% of the total sediment load was transported in 98% of the monitoring period. This agrees with previous research by Walling et al. (1992) who found that 90% of total sediment load can be transported in as little as 5% of the time. The large amounts of suspended sediment transported during storm events is consistent with the geomorphology of the system and episodic nature of sediment discharge to the River Wear. During these high discharge events, hillslope sediment sources, including landslides and bank erosion are very active and due to the steep sided geometry of the slopes connect directly to the channel. Whereas at moderate to low discharges, these sources are relatively inactive which results in less sediment supply.

Out of the four main events, the event in May, occurred over the longest time period, had the highest peak discharge and transported the most suspended sediment. However, the second longest event occurred in September over a period of seventeen hours although it had the smallest peak discharge and transported the smallest load of material. Although this event occurred because of the highest amount of daily rainfall over the monitoring period, it is possible that the peak discharge and resulting suspended sediment load is low because the rainfall was used to recharge the surrounding fields instead of causing run-off. Peak discharge for the four main events, can also be compared to the discharge modelled for the three outfalls draining into Red House Gill (Table 3.2). As discharge was measured on the trunk stream after the confluence of all three outfalls, discharge for all three outfalls needs to be summed together (Table 5.4). The modelled discharge is highly comparable to the discharge recorded as part of this research. The event in May had a peak discharge of 3.78 $m^3 s^{-1}$, which is close to the modelled discharge for a 100 year event lasting between 30-60 minutes.

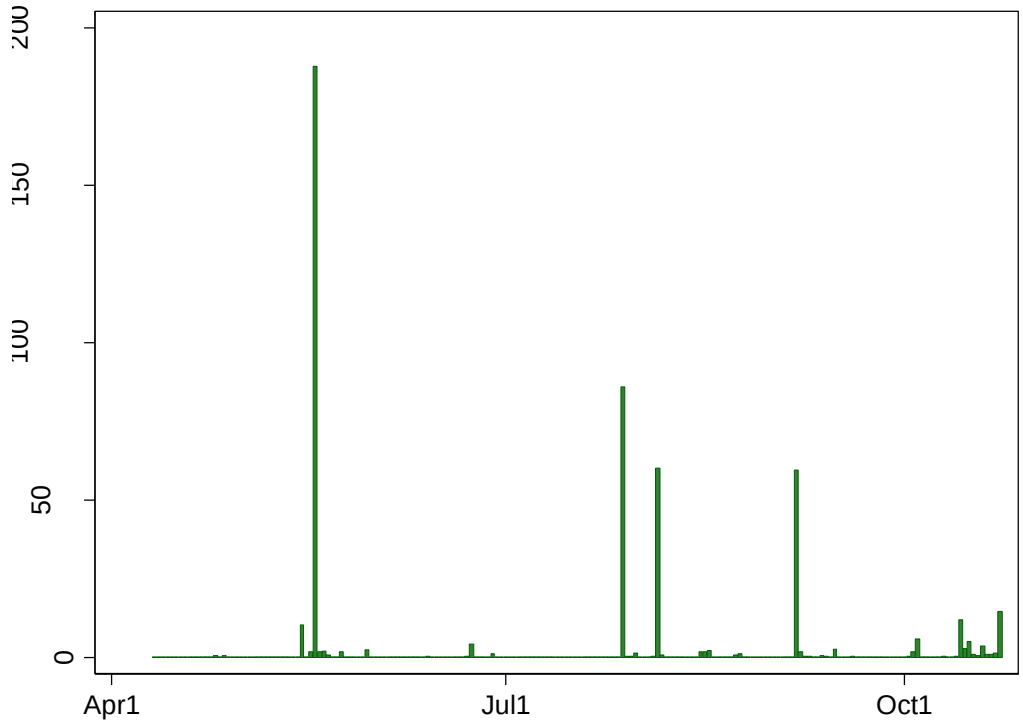

Figure 5.17-Time series of suspended sediment load throughout the monitoring period

Date	Load (t)	Percentage of Total Load	Peak Discharge ($m^3 s^{-1}$)	Approximate duration of event (h)
18th May 2013	187.77	38.12%	3.78	29
28 July 2013	85.98	17.45%	3.47	10
5th August 2013	60.10	12.20%	3.43	10
6th September 2013	59.53	12.08%	1.98	17
	Total	79.865%		

Table 5.3-Percentage load transported during high rainfall events

Duration (minutes)	**Peak Flow Discharge ($m^3 s^{-1}$)**	
	5 Year	100 Year
30	3.10	3.92
60	2.76	3.67
120	2.13	3.12
360	1.02	1.95
720	0.61	1.15

Table 5.4–Peak discharged modelled by JBA

5.2.2 TIMS

TIMS are an inexpensive and simple suspended sediment sampling device. Once installed within the stream they sample the full range of flow conditions providing a

continuous record of suspended sediment flux across the network (Figure 4.1). Suspended sediment stored in each sampler was collected fortnightly between June-November providing a five month record of sediment transfer.

5.2.2.1 Spatial Sediment Flux

Average sediment flux in grams per day (g d^{-1}) has been used to assess the spatial pattern of sediment transfer. This was calculated by dividing the dry sediment flux by the number of days the sampler was deployed during each sampling period (normally 14 days). Figure 5.18 shows the average flux for each TIMS. As the graph shows, the Middle downstream TIMS has the highest average sediment flux at 39.47 g d^{-1}. This is far higher than the Middle upstream TIMS, which has an average sediment flux of 0.70 g d^{-1}. This result suggests that the high levels of suspended sediment is not coming from the highly urbanised catchment before the culvert of the Middle stream. Instead the high level of suspended sediment must correspond to the large areas of bank collapse and landsliding present along the Middle stream, due to high flow events. The East downstream TIMS also has a higher average sediment flux of 7.96 g d^{-1} compared to 4.80 g d^{-1} for the upstream TIMS. The difference between the upstream and downstream TIMS on the East stream is far smaller compared to the Middle stream, this is possibly caused by the proximity of the two samplers as they are closer compared to the Middle stream samplers. The West sampler also has a far lower average sediment flux of 1.15 g d^{-1} compared to the downstream East and Middle stream. This is presumably due to the lower discharge which therefore doesn't create such highly erosive flows. Figure 5.18 also demonstrates that the average sediment flux of 4.17 g d^{-1} for the River Wear upstream TIMS is greater than the River Wear downstream TIMS which is only 3.36 g d^{-1}. This is presumably caused as the downstream River Wear TIMS is situated on one side of gravel bar and the current containing suspended sediment can also flow on the other side of the gravel bar, leaving the TIMS out of water. A rapid discharge from Red House Gill could therefore bypass the downstream sampler, before the River Wear rises, fully submerging the sampler. Whereas, the upstream River Wear TIMS is located within the main flow of the river and was constantly submerged, accumulating suspended sediment. As a result, it is important to compare River Wear TIMS and the downstream trunk TIMS. The downstream trunk TIMS has an average sediment flux of 8.89 g d^{-1} which is higher than both the River Wear TIMS, due to the high levels of erosion seen within the catchment. However, it is important to note that when the discharge from Red House Gill enters into the River Wear, it

undergoes massive dilution and therefore the downstream River Wear TIMS is likely to have a lower sediment flux compared to the lower trunk TIMS.

To further explore these results, a Student's t-test has been used to asses if the total dry sediment in paired TIMS locations are statistically similar. Table 5.5 shows the results. The pair-wise comparisons between: River Wear upstream and downstream, East upstream and downstream, and trunk upstream and downstream show no statistical difference in the sediment loads. However, the Middle upstream and downstream are statistically different as the t-value is 2.4833 with 10 degrees of freedom which corresponds to a P-value of 0.0324 which is smaller than 0.05. This significant difference is caused by the high amount of erosion and high rates of sediment delivery along the Middle stream. The table also shows that all the three streams are statistically different from one another. This is presumably because of the different geomorphology of the stream courses and varying catchment characteristics. For example, the West stream is the smallest in size and will therefore produce less suspended sediment, whereas the East and Middle catchments are far larger, with steeper V-shaped gullies, which have the ability to generate higher flows and therefore suspended sediment.

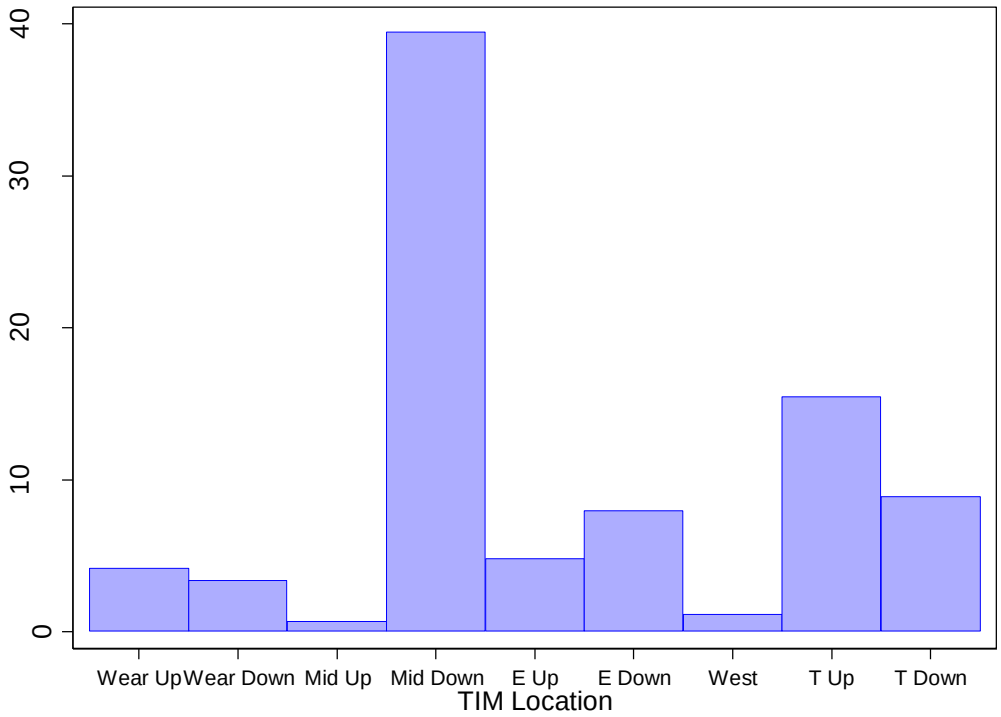

Figure 5.18-Average sediment flux (g d^{-1}) for every TIMS location within the Red House Gill catchment

	T-Value	Degrees of Freedom	P-Value	Alpha Value	Outcome
River Wear Upstream/Downstream	0.4168	9	0.6886	0.05	Statistically Similar
East Upstream/Downstream	0.7099	9	0.4958	0.05	Statistically Similar
Middle Upstream/Downstream	2.4833	10	0.0324	0.05	Statistically Different
Trunk Upstream/Downstream	1.8878	10	0.0884	0.05	Statistically Similar
East Stream/West Stream	2.9117	11	0.0141	0.05	Statistically Different
East Stream/ Middle Stream	2.4256	12	0.0320	0.05	Statistically Different
West Stream/Middle Stream	-2.7001	11	0.0207	0.05	Statistically Different

Table 5.5-Students t-test results showing a pair-wise comparison of total dry sediment recorded by the TIMS.

5.2.2.2 Temporal variability in the Flux of Sediment

To look at the temporal changes over the main monitoring period suspended sediment stored within the samplers were collected every two weeks. Figure 5.19, shows the total sediment in grams for every collection date. As the graph

demonstrates, the highest total amount of sediment collected was on the 17th September, when 3885.19 g of sediment was retained in the samplers. This corresponds to a period of high rainfall (Section 5.2.1.2). Although, interestingly this doesn't correspond to the highest level of erosion noted from the static photography. As a result, it is suggested that the erosion must have occurred along the stream banks which weren't being directly monitored as part of the static photography or sediment was derived from within channel storage. The second highest total sediment load collected was on the 6th August 2013, when 3681.86 g of sediment was retained in the samplers. This peak in sediment collected coincides with the highest peak in erosion noted by the static photography and high levels of rainfall. The lowest level of suspended sediment recorded was on the 23rd July, when only 38.82 g of sediment was collected.

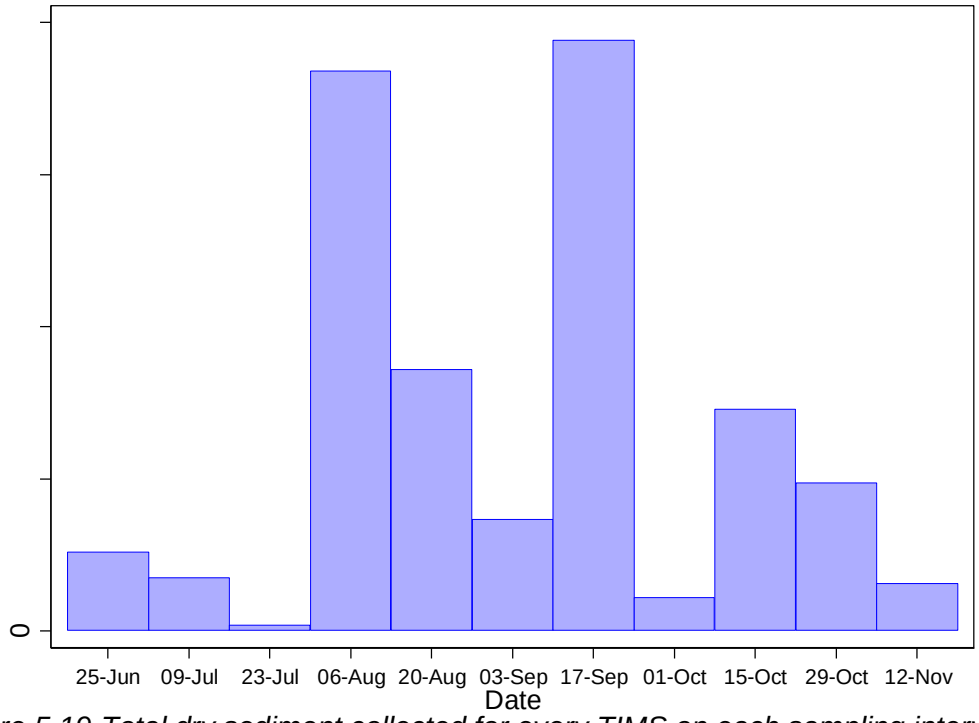

Figure 5.19-Total dry sediment collected for every TIMS on each sampling interval

In order to explore spatio-temporal sediment dynamics within the Red House Gill catchment, the total sediment collected for each individual TIMS can be mapped. Within ArcGIS, the data was grouped using Jenks Natural Breaks algorithm, where the data is grouped based on natural groupings inherent in the data. Class boundaries are identified that group similar values while maximising differences between classes. This has been done for the data collected on the 9th July 2013 and for the 17th September 2013 and can be seen in Figure 5.20. The map for the 9th

July 2013 demonstrates that both the Middle upstream and West TIMS have similar levels of total suspended sediment between 0.67-2.33 g. This is presumably because the West stream is the smallest of all three catchments and also has the shallowest V-shaped geometry which naturally won't produce much suspended sediment, while the upstream Middle TIMS, will only have received discharge from a small portion of the catchment, instead of the steep sided gill which naturally produces vast amounts of suspended sediment. Both the River Wear upstream and downstream TIMS are in the same class, along with the East upstream and downstream. Interestingly, the Middle downstream TIMS and trunk downstream TIMS are both in the same class. This pattern is different after a period of high rainfall and therefore data collected on the 17th September 2013 have also been mapped. The main difference is that the downstream River Wear TIMS captured more suspended sediment than the upstream TIMS. This is presumably because the downstream River Wear TIMS was submerged during periods of high rainfall at the beginning of September (Section 5.2.1.2). The downstream trunk stream, also records less suspended sediment compared to the Middle downstream TIMS, this is most likely due to deposition within the trunk stream channel.

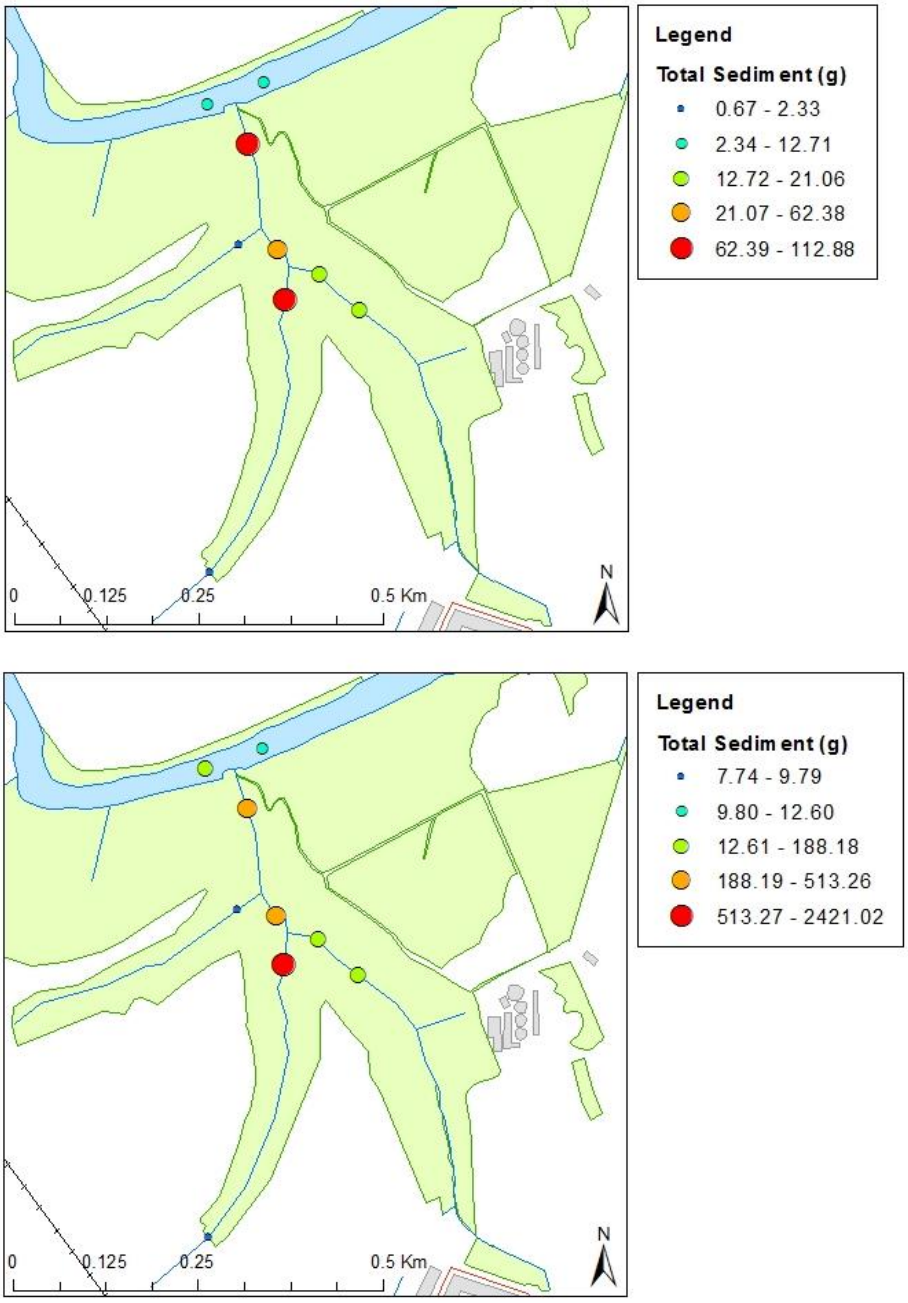

Figure 5.20-A) Total sediment in grams for each individual TIMS collected on the 9th July. B) Total sediment in grams for each individual TIMS collected on the 17th September.

5.3 Summary

This chapter demonstrates the important links between erosion monitored using static photography / terrestrial laser scanning and suspended sediment dynamics. The static photography demonstrates, that the majority of erosion occurs in the two weeks before 6th August 2013 and the two weeks before the 17th September 2013,

which agrees with high suspended sediment flux on those dates. High rainfall was recorded on the 5th August 2013 and 6th September 2013 producing peaks in discharge and suspended sediment concentration, which is within the two week period prior to high erosion recorded using the static photography and the high flux in suspended sediment recorded from the TIMS. The TIMS also demonstrate that the majority of sediment within the Red House Gill catchment comes from the Middle stream. This is probably due to the influence of the urbanised catchment, producing high, flashy discharges which have the potential for greater erosion. Results from the suspended sediment load time series, confirm that the majority of suspended sediment was transported in four key events; 80% of the total suspended load was transported in 2% of the time.

6 Dendrogeomorphology and the estimation of longer term slope instability

This chapter summarises results from methods used to investigate longer-term slope instability caused by soil creep in the Red House Gill catchment. The aim is to determine spatial and temporal patterns of soil movement on the wooded hillslopes of Red House Gill and provide an insight into historical patterns of slope instability. This chapter is divided into three sections: interpretation of the results from the basal trunk angle survey (Section 6.1), analysis of tree ring data (Section 6.2) and synthesis of the results to estimate the spatial and temporal patterns of soil movement within the Red House Gill catchment.

6.1 Tree Tilt – Basal Trunk Angle

To examine spatial and temporal patterns of soil creep throughout the woodland, information on the morphology and characteristics of 340 different trees has been gathered. This section analyses species distribution (Section 6.1.1), diameter at breast height (Section 6.1.2) and how this has been used to approximate tree age (Section 6.1.3), before calculating basal trunk angle (Section 6.1.4). This leads to an explanation of the significance of local slope (Section 6.1.5) before looking at the direction of soil creep (Section 6.1.6). The average rate of tree tilt will then be calculated and combined with aspect to provide an estimate of the direction and magnitude of soil creep within the catchment (Section 6.1.7). Section 6.1.8, builds on this information to help identify and differentiate areas of active soil instability along with stable areas. The last two sections (Sections 6.1.9 and 6.1.10) look at correlations between local slope and basal trunk angle and between tree age and basal trunk angle.

6.1.1 Species Distribution

The Red House Gill woodland consists of a range of deciduous tree species. Figure 6.1, outlines the spatial distribution of all trees surveyed. As the map demonstrates, the sampling focused on the East and trunk stream, sampling trees from the stream to the top of the hillslopes, to help gather information on the spatial pattern of soil

creep and slope instability. The 340 surveyed trees can be divided into 11 different species (Figure 6.2). Figure 6.2 shows that Ash and Sycamore trees were the most commonly surveyed accounting for 80.9% of all trees, whereas the other eleven species only account for the remaining 19.1% of those surveyed. Ash and Sycamore trees appear dominant throughout the catchment, whereas other species are clustered. For example Oak and Beech trees are clustered on the trunk stream. This species clustering is likely to be caused by preferential soil types and moisture status. Table 6.1, provides information about key characteristics and preferences for all 11 species.

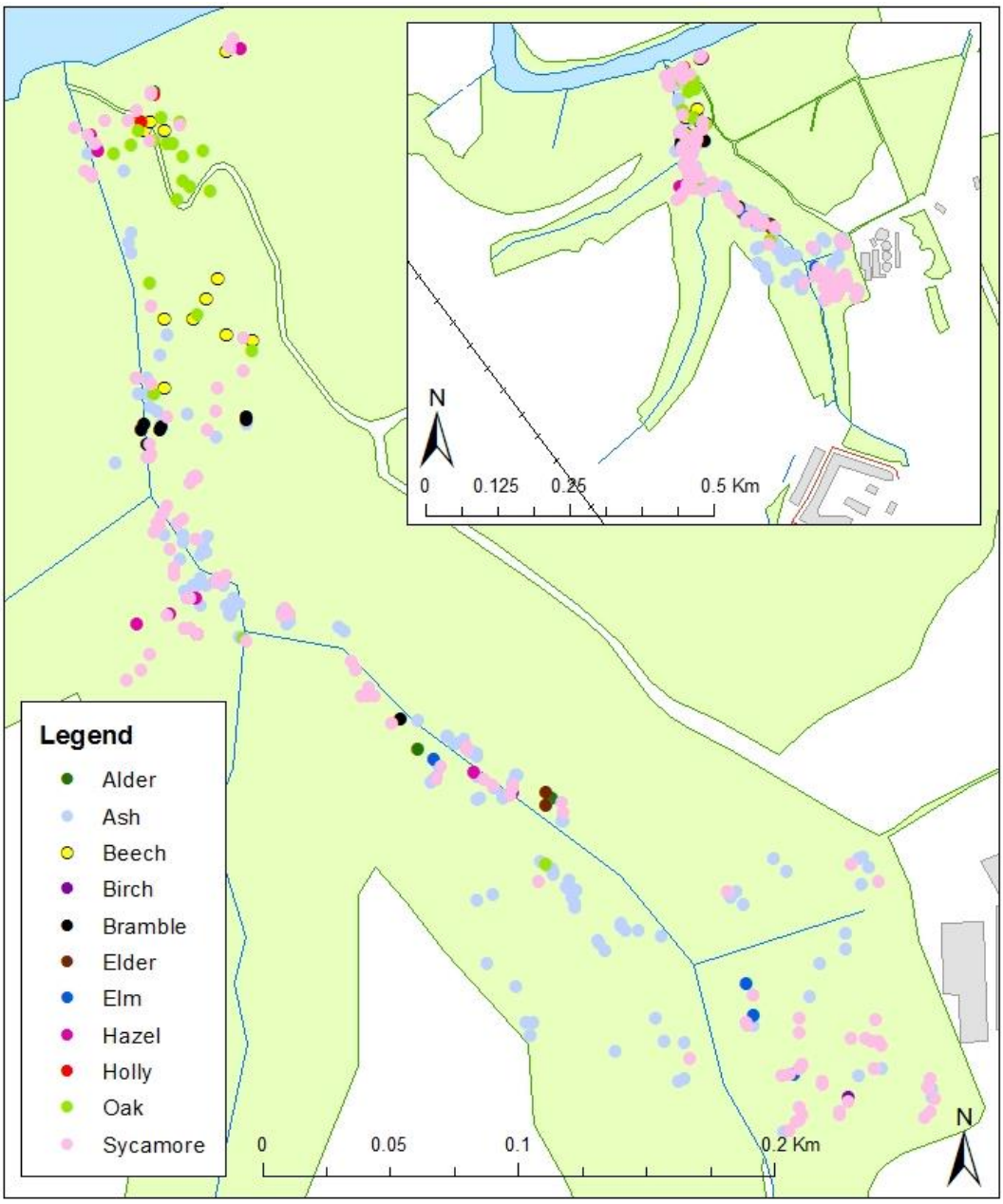

Figure 6.1-Location and species of all surveyed trees, the inset map demonstrates the location within the wider wooded area.

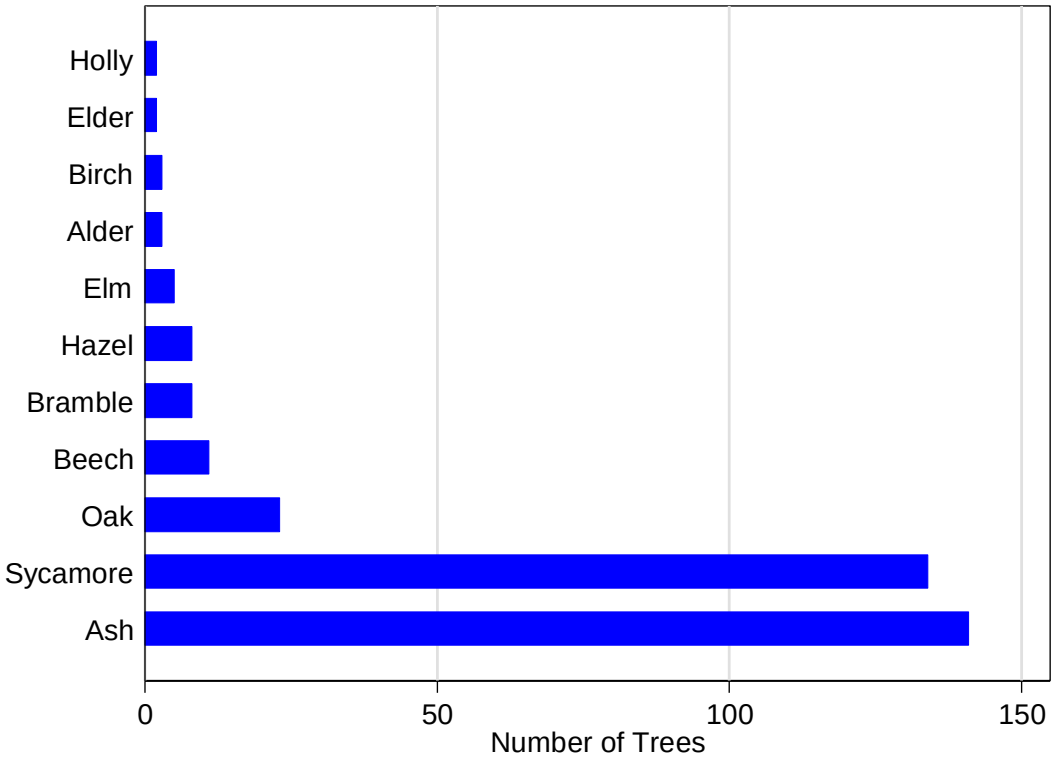

Figure 6.2- Frequency of the 11 different species surveyed in Red House Gill.

	Key Characteristics				
Tree Species	Tree Height	Canopy Spread	Soil	Moisture	pH
Ash	>12m	>8m	Chalk, Clay and Sand	Moist, but well drained	Alkaline to Neutral.
Sycamore	Typically 4-8m although can grow up to 35m.	4-8m	Chalk, Clay, Sand and Loam	Well drained, moist but well drained.	Acid, Alkaline, Neutral
Oak	>12m	>8m	Loam, Sand, Clay and Chalk	Well drained, moist but well drained	Acid, Neutral Alkaline
Beech	>12m, growing up to 40m.	4-8m	Sand, Clay, Chalk and Loam	Well drained, moist but well drained	Acid, Alkaline, Neutral
Bramble	2m	1.5-2.5m	Loam, Chalk and Clay	Well drained	Acid, Alkaline, Neutral
Hazel	<12m	>8m	Chalk, Clay, Sand and Loam	Well drained, moist but well drained	Acid, Alkaline, Neutral
Elm	>12m growing up to 30m.	>8m	Sand, Clay, Chalk and Loam	Well drained, moist but well drained	Acid, Alkaline, Neutral
Alder	>12m, often up to 25m.	4-8m	Loam and Clay	Moist to poorly drained.	Acid, Alkaline, Neutral
Birch	>12m	4-8m	Sand, Clay, Chalk and Loam	Well drained although moist.	Acid, Alkaline, Neutral
Elder	>15m	2-4m	Chalk, Clay and Sand	Well drained, moist but well drained	Acid, Alkaline, Neutral
Holly	>12m	4-8m	Sand, Clay, Chalk, Loam	Well Drained	Acid, Alkaline, Neutral

Table 6.1– Summary of key characteristics and habitat preferences for every tree surveyed.

6.1.2 Diameter at Breast Height (DBH)

DBH is a commonly used forest metric for estimating tree age. Breast height is defined as 1.3 m above the woodland floor, on the uphill side of the tree. Table 6.2, provides summary DBH statistics for every species surveyed. For all 340 trees, the mean DBH is 0.98 m, whereas the median is 0.93 m which suggests a slight positive skew. A positive skew can be seen in many species including: Ash, Sycamore, Beech, Bramble, Hazel, Elm, and Birch. However, a slight negative skew can be seen in Alder, whereas Oak is normally distributed as the mean and median are equivalent. This positive skew is largely the result of only selecting trees with a diameter at breast height greater than 0.2 m, as the aim of this research was to look at long term rates of soil creep, therefore old trees were preferentially surveyed. Beech trees have the largest statistical dispersion, with a standard deviation of 0.63 m, while Elder has the smallest standard deviation of only 0.1 m. The largest tree sampled, had a DBH of 2.36 m and is a Beech tree, whereas the smallest sampled tree is a Sycamore tree which is only 0.2 m. Figure 6.3, shows the distribution of DBH for all the surveyed trees and the three most commonly surveyed trees: Ash, Sycamore and Oak. The histogram and kernel density plot for all surveyed trees and Ash trees demonstrates the slight positive skew. Whereas the histogram and kernel density plot for Sycamore trees, suggest the data is tri-modal with peaks at 0.4, 0.9 and 1.3 m.

Tree Species	Count	Mean (m)	SD (m)	Min (m)	Quartile 25th (m)	Median (m)	75th (m)	Max (m)
All	340	0.98	0.4	0.20	0.68	0.93	1.25	2.36
Ash	145	0.94	0.32	0.35	0.71	0.89	1.09	2.01
Sycamore	130	1.07	0.45	0.20	0.73	1.08	1.40	2.32
Oak	23	0.93	0.36	0.35	0.66	0.93	1.17	1.63
Beech	11	1.07	0.63	0.36	0.70	0.87	1.45	2.36
Bramble	8	0.50	0.13	0.35	0.38	0.49	0.57	0.73
Hazel	8	0.81	0.28	0.50	0.59	0.74	1.02	1.30
Elm	5	0.62	0.15	0.45	0.56	0.61	0.62	0.87
Alder	3	1.16	0.29	0.83	0.83	1.30	1.35	1.35
Birch	3	1.04	0.30	0.75	0.75	1.02	1.34	1.34
Elder	2	0.91	0.10	0.84	0.84	0.91	0.98	0.98
Holly	2	0.72	0.29	0.52	0.52	0.72	0.93	0.93

Table 6.2– Summary statistics for diameter at breast height for every species

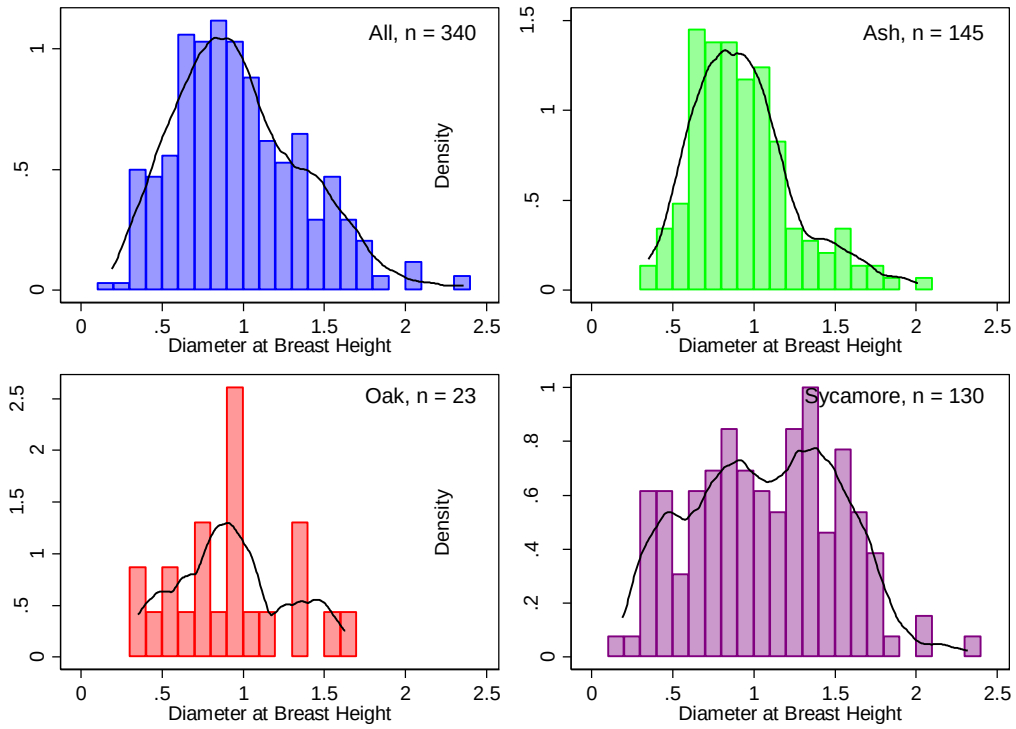

Figure 6.3– Density histograms overlaid with kernel density plots for every tree sampled, Ash trees, Oak trees and Sycamore trees

6.1.3 Tree Age

In order to look at historic rates of soil creep, tree age needs to be determined. Although absolute methods using tree coring are very effective they can often damage trees leading to infection (Maeglin, 1979). However, tree age can be estimated by comparing DBH measurements against a series of databases of calibrated tree age including: The Forestry Commission National Tree Register, Tree Register Of The British Isles (TROBI) and English Nature's Veteran Tree Initiative (White, 1998). Using these databases, The Forestry Commission has published a series of tables, outlining expected tree growth relative to DBH (White, 1998). Using the equation below, DBH can be converted into estimated tree age for a variety of common woodland species using the published data.

$$\text{Tree Age in years} = \left(\frac{(R^2\pi - BA)}{CAI}\right) + CA$$

Equation 6.1

Where:
R – Radius (cm)
BA – Basal Area (cm^2)
CAI – Current Annual Increment (cm^2)
CA – Core Age (years)

Diameter at breast height is converted into stem radius (r) before applying equation 6.1. Equation 6.1 is based on the principle that trees age through three growth stages. The first formative stage is dominated by constant tree ring width, before ring width starts to decrease in the mature stage, further declining in width for the last stage, senescence (White, 1998). Core age (CA), is when the tree changes from being in the formative to mature stage, which depends on species and local environmental conditions. Current annual increment (CAI) is the ring area during the mature stage of a trees life and basal area (BA), is a cross section of land that the tree stems occupy at their base. After selecting tree species and environmental condition, CA, CAI and BA can all be looked up in the Forestry Commission publication (White, 1998). At Red House Gill, as the area is an open woodland, the environmental condition 'Good site, open growth and sheltered' was selected.

Although the Forestry Commission provide information for a range of key species, it hasn't been possible to provide an age estimate for every species found in Red House Gill. Therefore using this technique, age has only been estimated for the following species: Ash, Beech, Holly, Oak and Sycamore. This accounts for 311 trees (94.1% of the total). Figure 6.4 shows the estimated tree age against diameter at breast height for the individual species. This graph demonstrates the vastly different growth curves for individual species found in Red House Gill.

For the six species that were unaccounted for in Figure 6.4 it was decided to use a simple curvilinear regression analysis of the data in Figure 6.4 to provide an approximate tree age for the remaining 29 trees. In Figure 6.4 the allometric relationship between DBH and tree age is strong (R^2 0.982), as such the following equation ($Y=27.206*1.483^x$) was used for the curvilinear regression. The curvilinear regression is an approximation and is therefore subject to uncertain error however, the method fulfils the underlying assumption that as girth increases, so does tree age and is conservative in that it makes no additional assumptions.

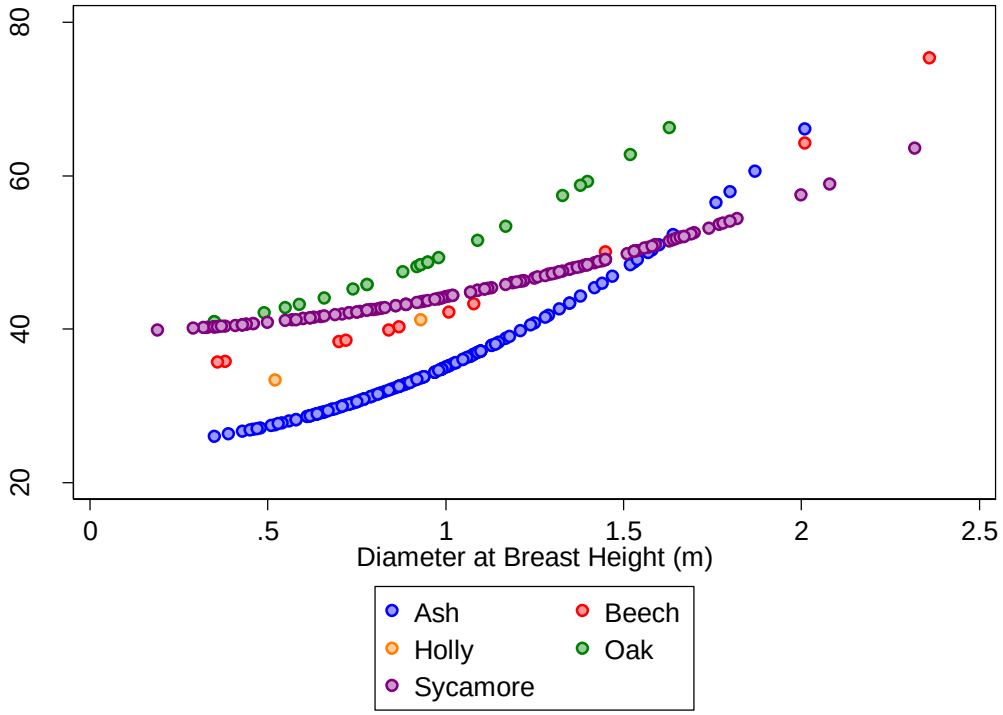

Figure 6.4– Estimated tree age for Ash, Beech, Holly, Oak and Sycamore trees based on The Forestry Commission publication.

Table 6.3, shows the age of every tree species for the minimum DBH surveyed (0.2m). The youngest age corresponds to the 6 species where curvilinear regression was used to calculate age whereas the oldest tree with the minimum DBH is Oak. Table 6.4 provides summary statistics for tree age. The average age for all trees is 40 years. The youngest tree measured is an Ash tree which is only 26 years old, whereas the oldest tree is a Beech tree which is 75 years old. The oldest tree also has the biggest DBH, measuring 2.36 m. However the youngest tree doesn't have the smallest DBH, the smallest DBH corresponds to a Sycamore tree which is 39 years old. Figure 6.5, displays the age distribution for every tree and three tree species with the highest count (Ash, Sycamore and Oak). The graph for all trees displays a prominent bi-modal distribution with peaks at 34 and 45 years. The individual graphs for Ash and Sycamore demonstrate that the bi-modal distribution is predominately caused by these species. The mean age of all the Ash trees is 34 years old whereas the mean age of all the Sycamore trees is 45 years old, which corresponds to the second peak (Table 6.4). Although these peaks can be seen in the age histogram, they cannot be seen in the distribution plot for DBH (Figure 6.3). This difference in distribution is caused by the different growth patterns of Ash and Sycamore trees which are inherent in the age calculation (White, 1998).

A t-test has also been employed to see if the age of the Ash, Sycamore and Oak trees is statistically different; the results can be seen in Table 6.5. In all circumstances, the corresponding two tailed p-value is less than the alpha value of 0.05 and therefore the age of all three species is statistically different. This result was expected as historic Ordnance Survey maps (Figure 3.5) demonstrate that woodland was established before 1861 and during this period, the woodland will have undergone succession and a range of management practices, ensuring that trees within the woodland are a variety of ages.

Species	Tree Age (DBH = 0.2m)
Ash	25.178
Beech	35.054
Holly	30.265
Oak	40.136
Sycamore	39.944
Alder, Birch, Bramble, Elder, Elm, Hazel	20.437

Table 6.3-Tree age for every species with the minimum recorded DBH (0.2m)

Tree Species	Count	Mean	SD	Min	Quartile 25th	Median	75th	Max
All	340	40.52	8.44	26.02	33.48	40.63	46.18	75.3
Ash	145	34.76	7.10	26.02	29.93	32.87	36.93	66.1
Sycamore	130	45.75	4.50	39.9	42.10	44.91	48.42	65.58
Oak	23	49.53	7.03	40.96	44.08	48.36	53.38	66.21
Beech	11	45.79	12.75	35.71	38.33	40.28	50.09	75.37
Bramble	8	33.14	1.71	31.23	31.66	33.07	34.06	36.27
Hazel	8	37.70	4.33	33.13	34.39	36.44	40.70	45.41
Elm	5	34.81	2.16	32.48	33.92	34.60	34.74	38.33
Alder	3	43.15	4.72	37.73	37.73	45.41	46.31	46.31
Birch	3	41.12	4.80	36.56	.6356	40.67	46.13	46.13
Elder	2	38.96	1.52	37.88	37.88	38.96	40.03	40.03
Holly	2	37.29	5.60	33.33	33.33	37.29	41.25	41.25

Table 6.4- Summary statistics for tree age (Forestry Cmmission and curvlinear regression) for every species.

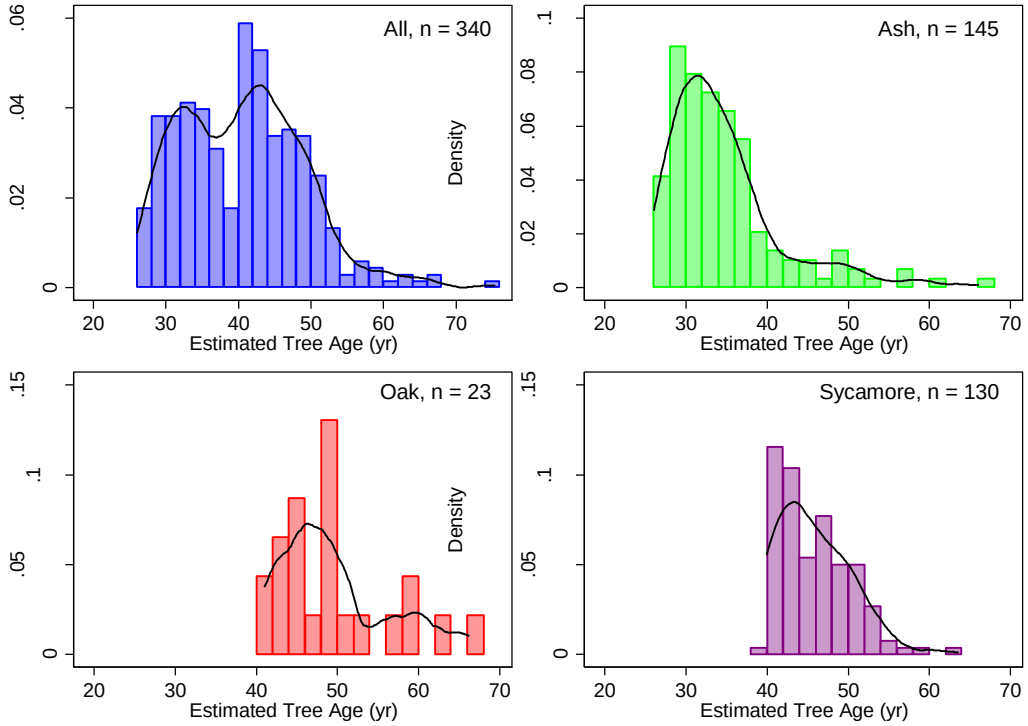

Figure 6.5- Density histograms overlaid with kernel density plots for tree age, for every tree sampled, Ash trees, Oak trees and Sycamore trees.

	T Value	Degrees of Freedom	P-Value	Alpha Value	Outcome
Ash/Sycamore	-15.1206	273	0.000	0.05	Statistically different
Ash/Oak	-9.2792	166	0.000	0.05	Statistically different
Oak/Sycamore	-3.3817	151	0.009	0.05	Statistically different

Table 6.5 Students t-test results for tree age

Along with these frequency statistics, it is important to look at the spatial pattern of tree age (Figure 6.6). It is clear from the map that older trees are generally found at the top of the hillslopes, whereas the active stream banks and steep sided slopes are lined with younger trees. There are a several exceptions to this rule, where younger trees can be seen up towards the top of the hillslope and old trees near the river bank.

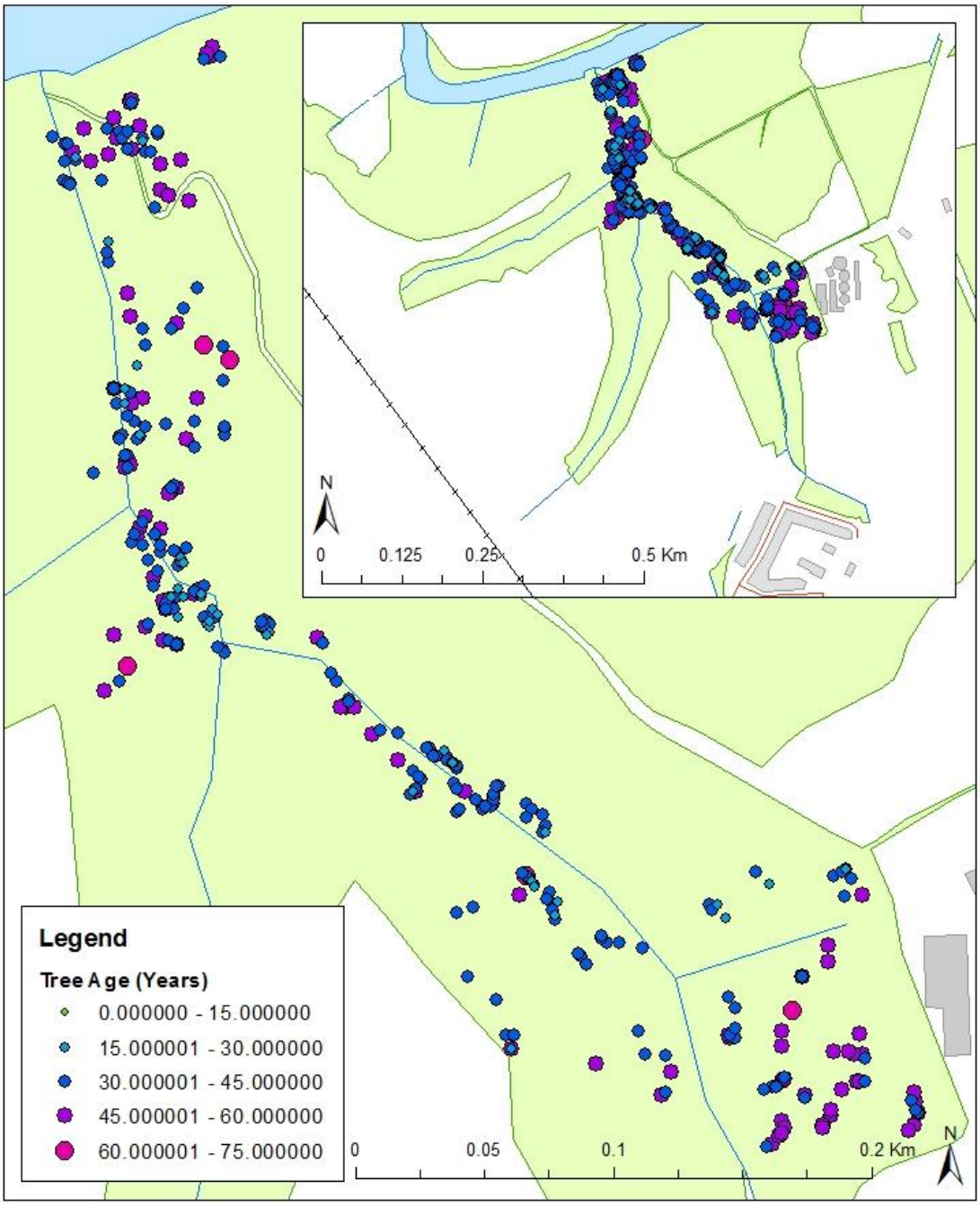

Figure 6.6-The location and age of all 340 surveyed trees

6.1.4 Basal Trunk Angle

Although the effects of soil creep on the curvature of trees growing on hillslopes is keenly debated (Parizek and Woodruff, 1957, Phipps, 1974), this research has used a novel approach to measure the angle at the base of trees (Section 4.2.4.1). Figure 6.7 shows the length measurements (A, B, C) which were recorded in the field. This creates a hypothetical triangle at the base of every curved tree. Using the three length measurements it was possible to calculate angle a, using the inverse cosine

rule.

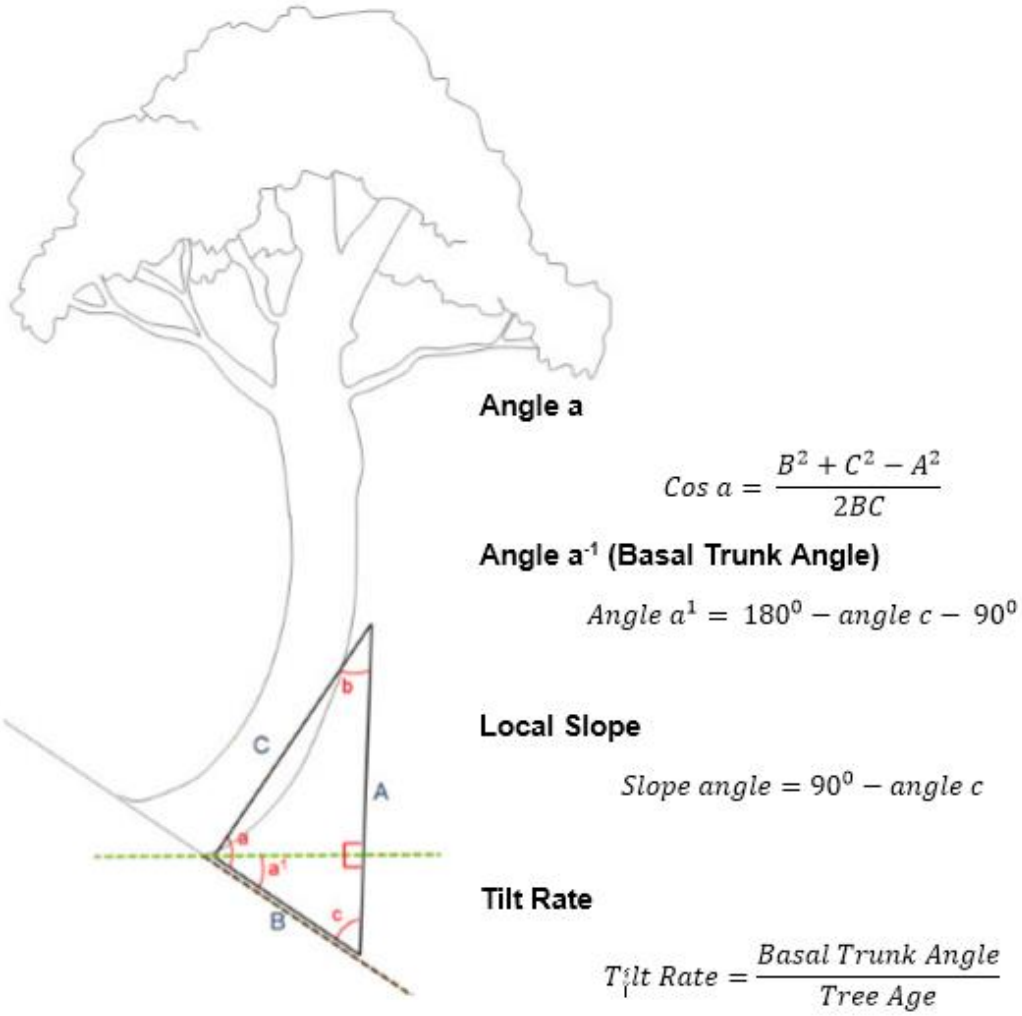

Figure 6.7-The three length measurements (A, B, C) that have been and used to gather information on tree basal trunk angle.

Clearly angle *a* as defined in Figure 6.7 could be the same on a tree curved downslope and a straight tree on flat ground. As a result, angle a needs to take into account local slope and therefore angle a^1 has been calculated, characterising the base angle taking into account slope. The equation to calculate angle a^1 can be seen in Figure 6.7. The equation works on the idea of dissecting the original triangle characterised by length measurements A, B and C into two smaller triangles by a hypothetical flat ground surface which can be seen in Figure 6.7. As length measurement A, was taken using a plumb line, flat ground will dissect this length measurement at 90^0. Using this framework angle a^1 is expected to be highly variable, ranging from small slope angles coinciding with trees growing in relatively

stable areas, to large slope angles where trees are growing on highly unstable areas for example landslides faces.

Angle a^1 has been calculated for 323 trees. For 17 trees, a full set of measurements was not determined in the field and these were omitted from the analysis. Table 6.6 shows key summary statistics for basal trunk angle (a^1) of every tree and every individual species. For every tree, the mean basal trunk angle is 74.4^0, however the standard deviation is 14.15^0 which suggests that the data are very dispersed. This is because the smallest base angle is only 7.3^0 whereas the biggest basal trunk angle is 90^0 which corresponds to a straight tree. Every species with the exception of Elm, Alder and Holly has a maximum base angle of 90^0. The distribution of base angle has been plotted using a histogram and kernel density plot for every tree and the three most commonly surveyed trees (Ash, Sycamore and Oak) (Figure 6.8). The plots are all bi-modal, displaying peaks at $70\text{-}75^0$ and 90^0. These peaks obviously represent the high number of curved trees ($70\text{-}75^0$) and the large number of straight trees (90^0) which were surveyed. Table 6.7 shows the results of t-tests used to see if the mean basal trunk angle of the three most commonly surveyed trees are similar. For all tests, the p-value is greater than the two tailed alpha value of 0.05, which demonstrates the base angle of Ash, Sycamore and Oak trees are statistically similar. This is very important as it suggests that the tree species does not influence basal trunk angle and instead implicates environmental conditions, which is assumed to be the downward movement of soil.

Tree Species	Count	Mean	SD	Min	Quartile 25th	Median	75th	Max
All	323	74.4	14.15	7.37	65.79	75.29	90.0	90.0
Ash	139	76.06	13.29	36.68	68.35	76.42	90.0	90.0
Sycamore	123	74.08	14.56	7.37	65.46	74.84	90.0	90.0
Oak	23	79.18	13.43	47.50	71.17	89.38	90.0	90.0
Beech	10	65.56	10.49	50.38	58.11	64.12	69.52	90.0
Hazel	8	66.63	14.98	43.04	54.94	69.93	75.13	90.0
Bramble	7	63.14	13.85	45.10	55.28	62.12	67.60	90.0
Elm	3	61.69	20.57	42.46	42.56	59.23	83.38	83.38
Alder	3	69.92	10.16	60.64	60.64	68.34	80.78	80.78
Birch	3	65.66	25.78	38.64	38.64	68.34	90.0	90.0
Elder	2	83.75	8.83	77.51	77.51	83.75	90.0	90.0
Holly	2	67.14	3.75	64.49	64.49	67.14	69.79	69.79

Table 6.6– Summary statistics for basal trunk angle.

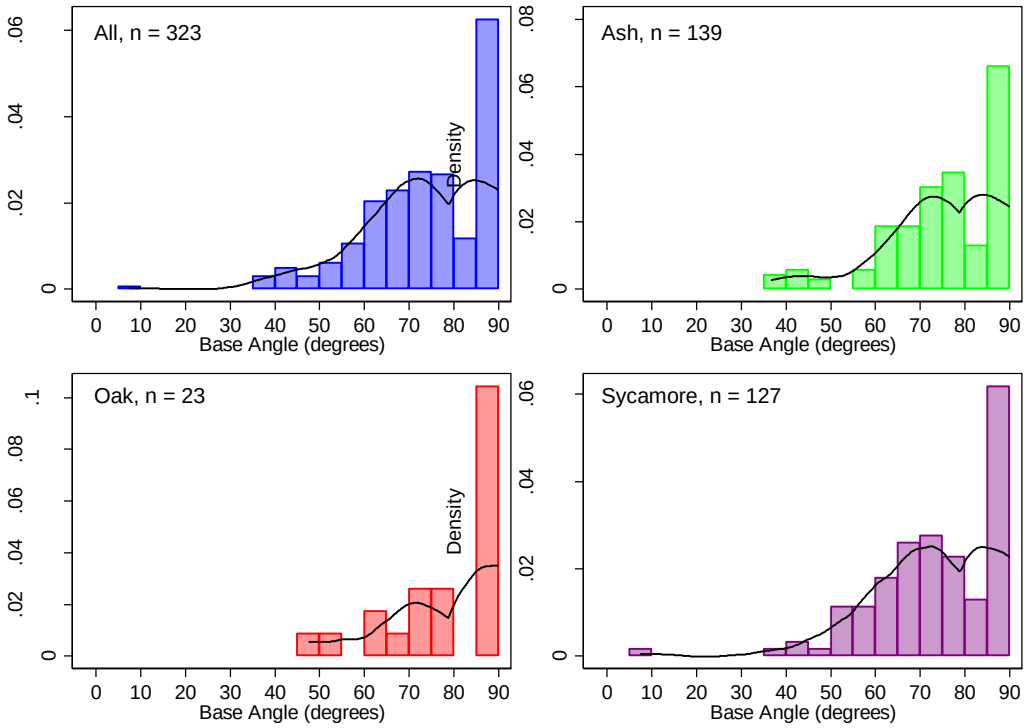

Figure 6.8-Base angle distribution for every tree, Ash trees, Sycamore trees and Oak trees.

	T Value	Degrees of Freedom	P-Value	Alpha Value	Outcome
Ash/Sycamore	1.1536	260	0.2497	0.05	Statistically Similar
Ash/Oak	-1.0422	160	0.2989	0.05	Statistically Similar
Oak/Sycamore	-1.5260	144	0.1205	0.05	Statistically Similar

Table 6.7- Students t-test results for the basal trunk angle.

The basal trunk angle has been plotted in ArcGIS (Figure 6.9). The map only includes base angles which are smaller than 90^0, as it is these trees which have been affected by soil creep as they are not straight. This map demonstrates that trees with smaller base angles are generally located near or close to the river banks whereas straighter trees are located near the top of the hillslopes. There are a few exceptions to this rule where near the top of the hillslopes on the East and Middle streams there are trees with small basal trunk angles. The most notable exception is the tree with the smallest basal trunk angle (7.3^0), which is the big red circle near the top of the hillslope on the trunk stream. These exceptions are presumably

caused by steep micro-topography, local drainage lines or trees growing on landslide scars.

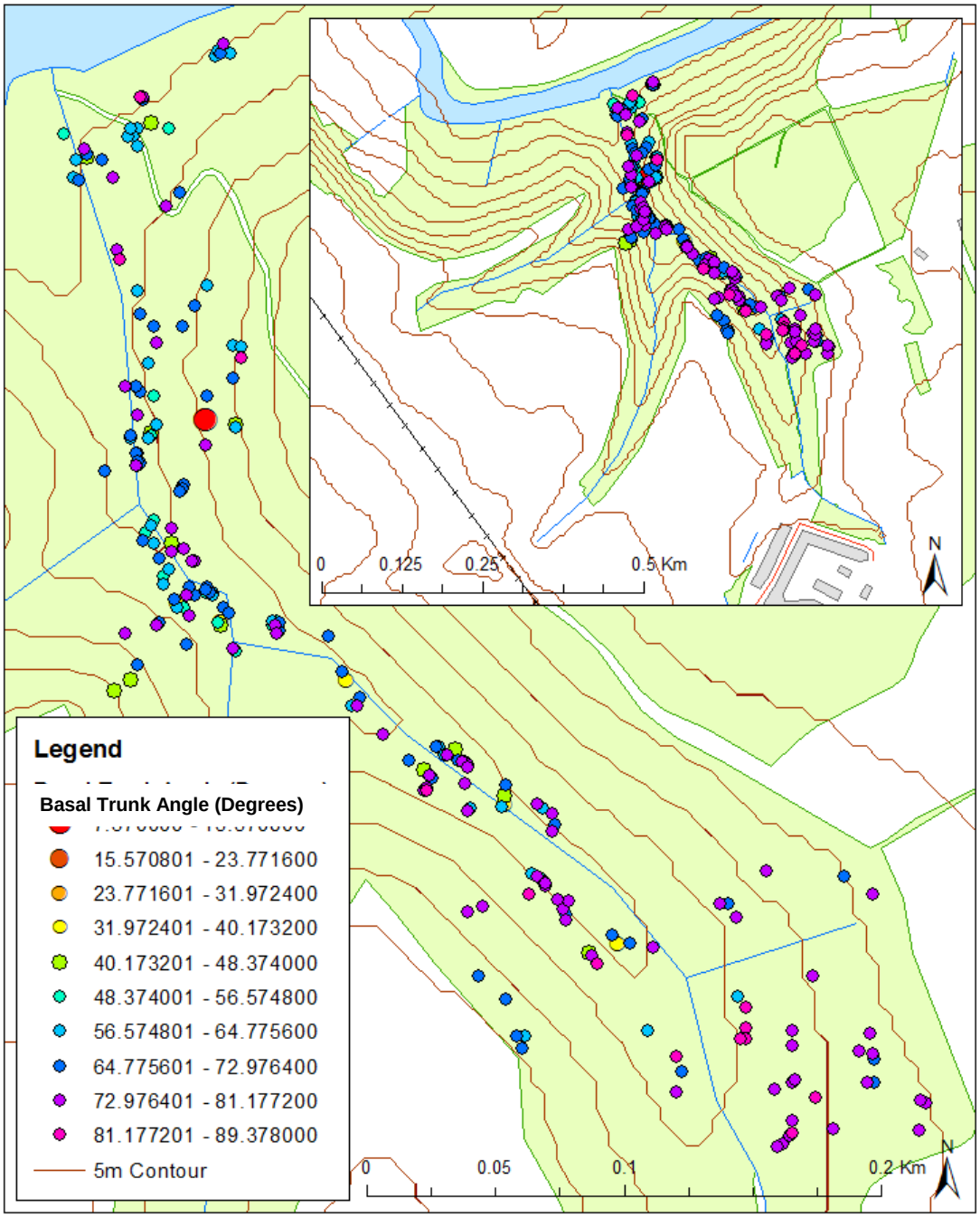

Figure 6.9– The location and basal trunk angle (which takes into account local slope) for every tree with a base angle smaller than 90^0.5m contours have been aded to demosntrate changing relief.

6.1.5 Local slope

The local slope angle has also been calculated at the base of every curved tree by subtracting angle a from angle a^1 (Figure 6.7). The field measurement of local slope,

has been compared with the proximal slope angle generated from a 5 m grid cell DEM and slope raster in ArcGIS. ArcGIS generates the angle by calculating the rate of change between every grid cell. Figure 6.10, shows the slope angles calculated by these two methods. Field measurements demonstrate that most trees are situated on a slope between 0-5^0 with the second most dominant class being 15-20^0, which results in a bi-modal distribution. The highest slope is 70^0, which coincides with steep stream banks and landslide faces. Figure 6.10, clearly demonstrates that slope angle generated by ArcGIS is very different compared to the field generated slope angle. This is because a 5 m average DEM is inadequate for characterising local slope variation as it uses averaging techniques to generate height every 5 m. The Red House Gill catchment is highly variable and topography can change hugely within 5 m, particularly in the vicinity of erosion features. Figure 6.11, is a scatter plot which further demonstrates the difference between local slope calculated using field measurements and slope calculated using ArcGIS. The graph shows a weak positive relationship; but the maximum angle generated from the DEM is < 25^0 compared to the local slope which is as great as 70^0. This may partly be explained by the tree interacting with soil moving down the slope causing a local perturbation in soil flux.

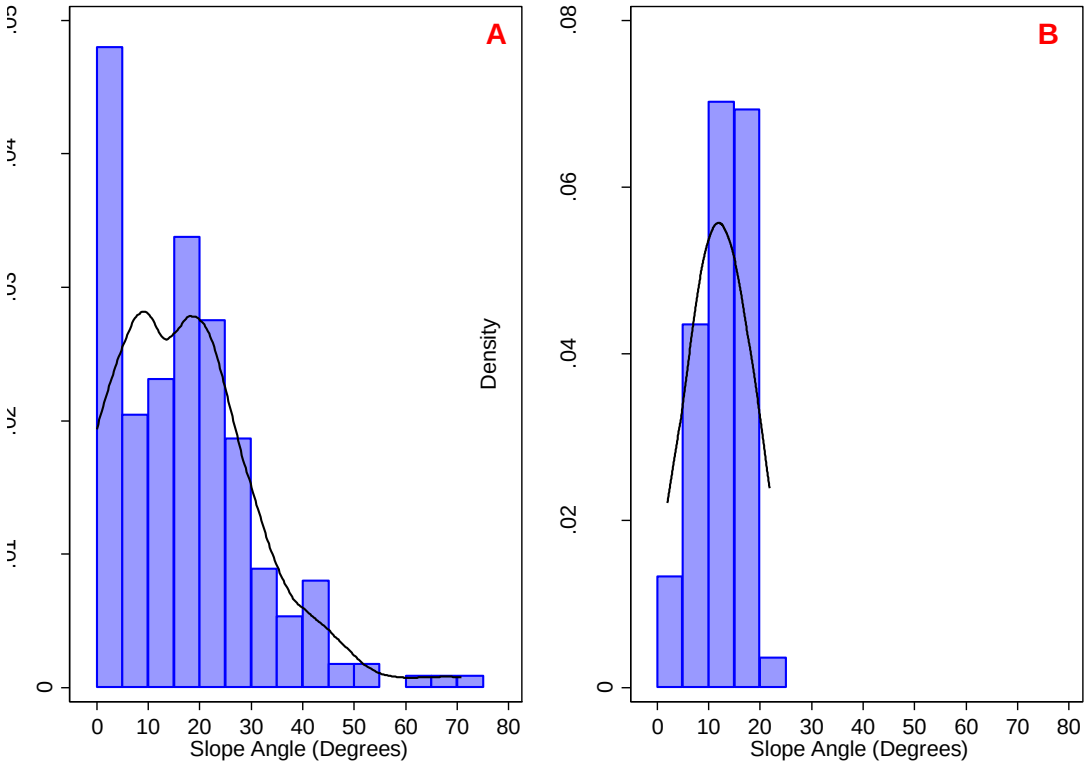

Figure 6.10 - Histogram overlaid with a kernel density plot of local slopen (A) and slope calculated in ArcGIS (B)

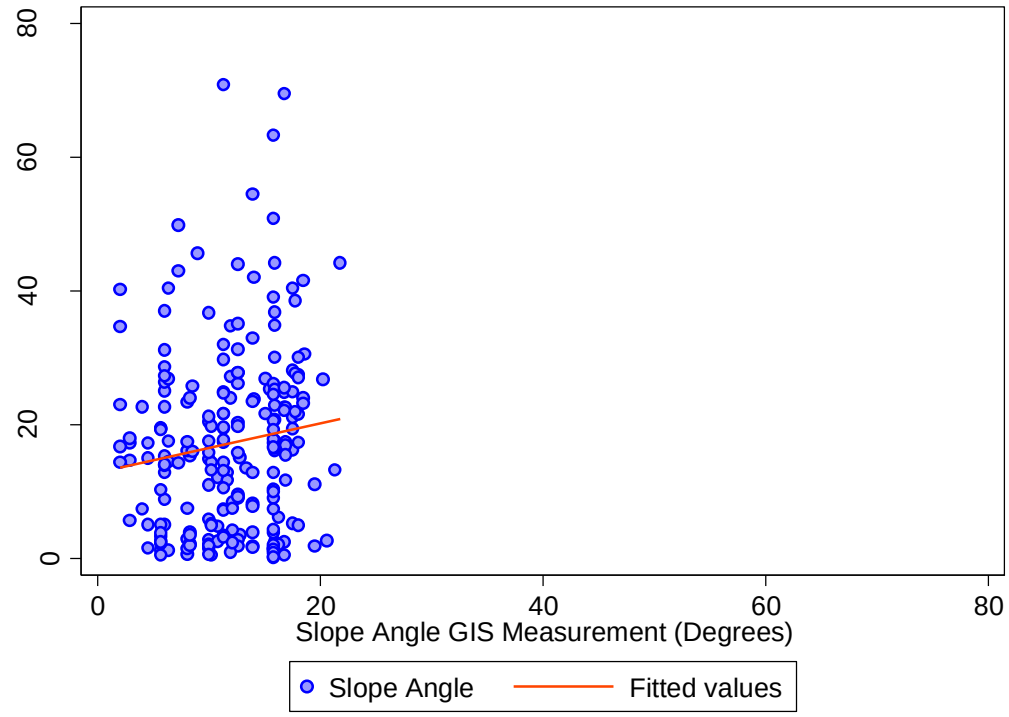

Figure 6.11-The weak positive relationship between slope calculated using field measurements and ArcGIS.

6.1.6 Significance of Slope Aspect

In the field, the aspect of every tree was recorded. Aspect is defined as the direction of tree curvature. This information is important to ascertain the direction of soil creep within the Red House Gill catchment. Figure 6.12 (A and B), are rose diagrams demonstrating the direction that every tree is curving towards on the east and west banks of all the streams. On the east bank, it appears that the majority of trees are curving in a westerly direction, as the mean direction is 250^0, which is downslope. On the West bank, the mean direction is 50.6^0 which is a north easterly direction, although there is very weak vector strength as a large number of trees are curved in other directions. Figure 6.12 (A and B) demonstrate that trees are curving in a range of directions, however it is important to determine whether this correlates with local slope as this is assumed to be the primary direction of soil creep. In ArcGIS a 5m grid cell DEM has been used to derive the downslope direction of the maximum rate of change of slope. The location of each tree has been assigned a direct downslope aspect, which is plotted in a rose diagram (Figure 6.12 C and D). For the east bank, the mean downslope direction is 264.2^0, which is similar to the tree curve aspect of 250^0.For the west bank, the mean downslope direction is 13.6^o, which is quite different to the mean tree curve aspect of 50.6^0. These results suggest that tree curvature is more closely correlated with downslope direction on the east bank than it is on the west. This result is expected as the east slopes are more steeply inclined than the west slopes.

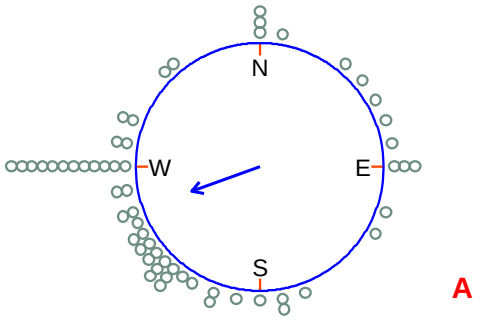

A

mean direction 250.4°: vector strength 0.582

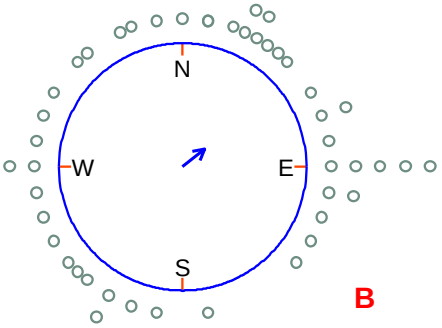

B

mean direction 50.6°: vector strength 0.226

C

D

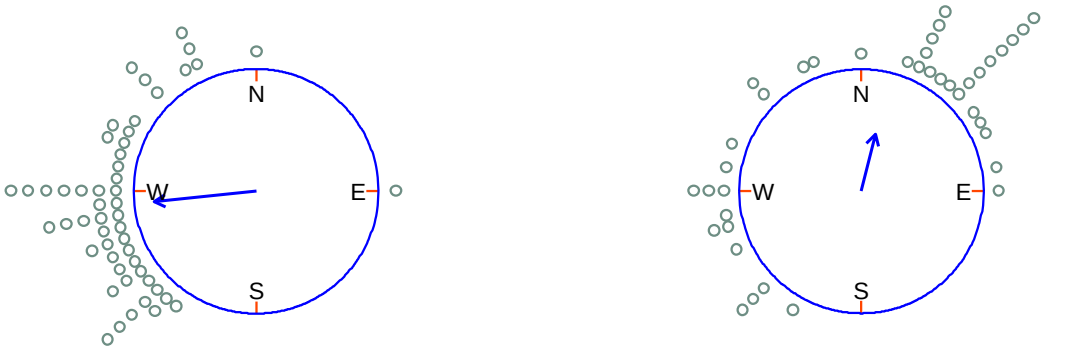

Figure 6.12-Tree curve direction. A and B are the field derived measurements for the east and west bank respectively. C and D are the ArcGIS measurements for the east and west bank respectively.

6.1.7 Rate of Tilt

In order to gather a historical perspective of soil creep throughout the Red House Gill catchment, basal trunk angle and tree age has been used to create an average tilt rate in degrees per year. The equation in Figure 6.7 has been used to calculate average tilt rate for every tree which has a curved base. This calculation produces tilt rate, in degrees per year, which acts as a proxy for soil creep. Figure 6.13, demonstrates the relationship between tree age and rate of tilt. As the graph shows, the relationship appears negative; therefore older trees have a lower rate of tilt. However, the variables on Figure 6.13 aren't independent because tree age has been used to generate rate of tilt. Figure 6.20, demonstrates the relationship between tree age and basal trunk angle, revealing the slightly positive relationship.

Table 6.8 provides summary statistics for the rate of creep for every tree and the individual species. The table demonstrates that the maximum rate of tilt is 1.8 ^{0} yr^{-1} which corresponds to a Sycamore tree whereas the smallest is 0.0068 ^{0} yr^{-1} which corresponds to an Oak tree. The mean rate of tilt between all trees is 0.298 ^{0} yr^{-1}. The data is very variable as the standard deviation for all the trees is 0.35 ^{0} yr^{-1}. Figure 6.14 illustrates the distribution of tilt rates for all trees and the three most common species (Ash, Sycamore and Oak). The graphs show a distinct positive skew. Ash trees appear to have a bi-modal distribution with a peak at 0.3 ^{0} yr^{-1} and 0.75 ^{0} yr^{-1}. Table 6.9 displays the results of t-tests between the three most surveyed species. The rate of tilt is statistically similar for Oak and Sycamore trees. This is

because the t-value is 0.9652. The corresponding two tailed p-value is 0.3368 which is more than the 0.05. However, this isn't the case for Ash and Sycamore trees and Ash and Oak trees as the corresponding p-values of 0.0074 and 0.0479 respectively are smaller than the 0.05 alpha value. These results suggest that soil creep is not the only factor influencing rate of tilt; otherwise all species would be statistically similar therefore biological factors like how different species respond to tilting is important.

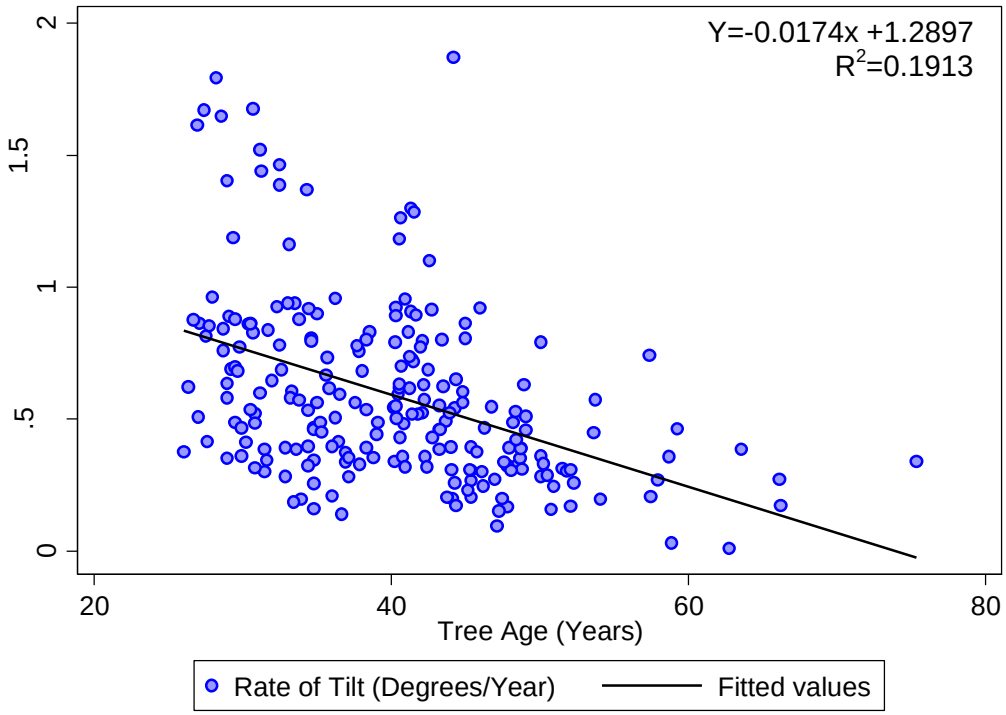

Figure 6.13– Scatter graph demonstrating the relationship between Tree Age and Rate of Tilt

Tree Species	Count	Mean	SD	Min	Quartile 25th	Median	75th	Max
All	225	0.59	0.35	0.01	0.34	0.52	0.79	1.89
Ash	93	0.64	0.38	0.14	0.38	0.53	0.84	1.79
Sycamore	87	0.51	0.30	0.03	0.31	0.46	0.63	1.89
Oak	12	0.42	0.25	0.01	0.31	0.38	0.49	0.95
Beech	9	0.64	0.17	0.34	0.53	0.63	0.79	0.83
Hazel	7	0.75	0.40	0.31	0.45	0.56	1.16	1.37
Bramble	6	0.94	0.26	0.69	0.81	0.89	0.96	1.44
Alder	3	0.48	0.29	0.20	0.20	0.47	0.78	0.78

Elm	3	0.82	0.63	0.20	0.20	0.80	1.46	1.46
Birch	2	0.93	0.47	0.59	0.59	0.93	1.26	1.23
Holly	2	0.61	0.01	0.61	0.61	0.61	0.62	0.62
Elder	1	0.33	n/a	0.33	0.33	0.33	0.33	0.33

Table 6.8– Summary statistics for rate of tilt of every tree and individual species

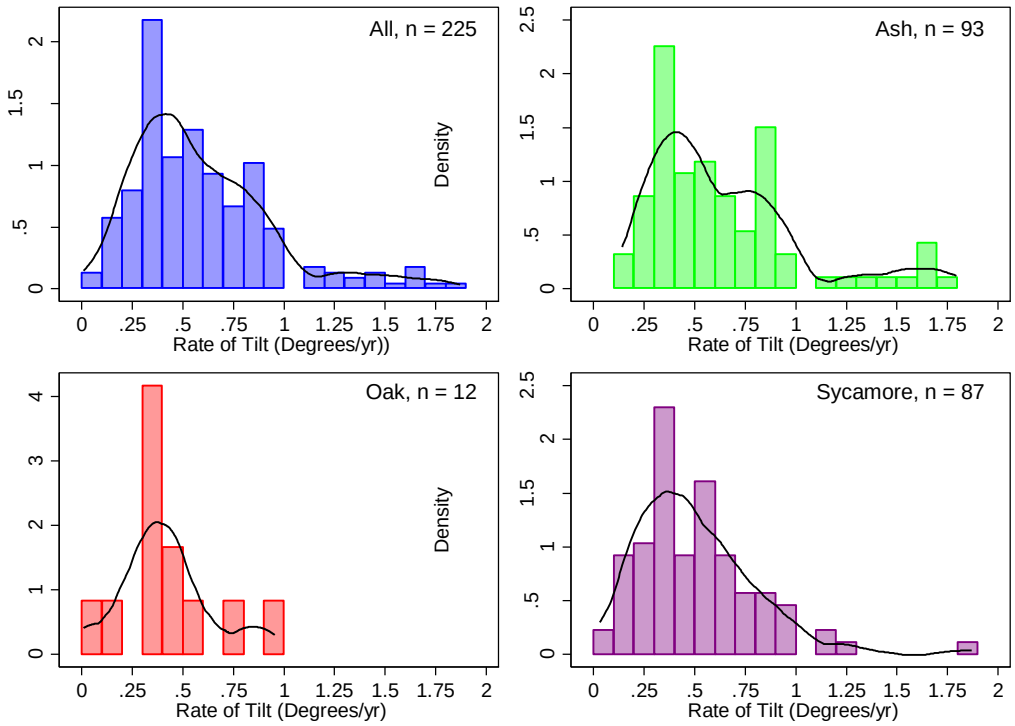

Figure 6.14– Histogram and kernel density plots for all trees and the three most surveyed trees.

	T Value	Degrees of Freedom	P-Value	Alpha Value	Outcome
Ash/Sycamore	2.7082	178	0.0074	0.05	Statistically Different
Ash/Oak	2.0019	123	0.0479	0.05	Statistically Different
Oak/Sycamore	0.9652	97	0.3368	0.05	Statistically Similar

Table 6.9- Students t-test results for rate of tilt

To summarise how the rate of tilt changes spatially the information has been combined with field measurements of aspect to create a vector map (Figure 6.15). This map demonstrates a clear pattern where trees with the highest rate of tilt appear close to the river banks, whereas trees with a smaller rate of tilt appear to

occur in more stable areas of the landscape. However, there are quite a few trees with a small rate of tilt close to the river banks. The map also demonstrates that in most places, trees are moving directly downslope. However, there are a few occurrences where trees do not follow this trend and these tend to be in parts of the catchment with complex micro-topography. Trees with the highest magnitude of tilt rate appear to always curve downslope, whereas trees with smaller magnitudes of tilt rates demonstrate greater spatial variability.

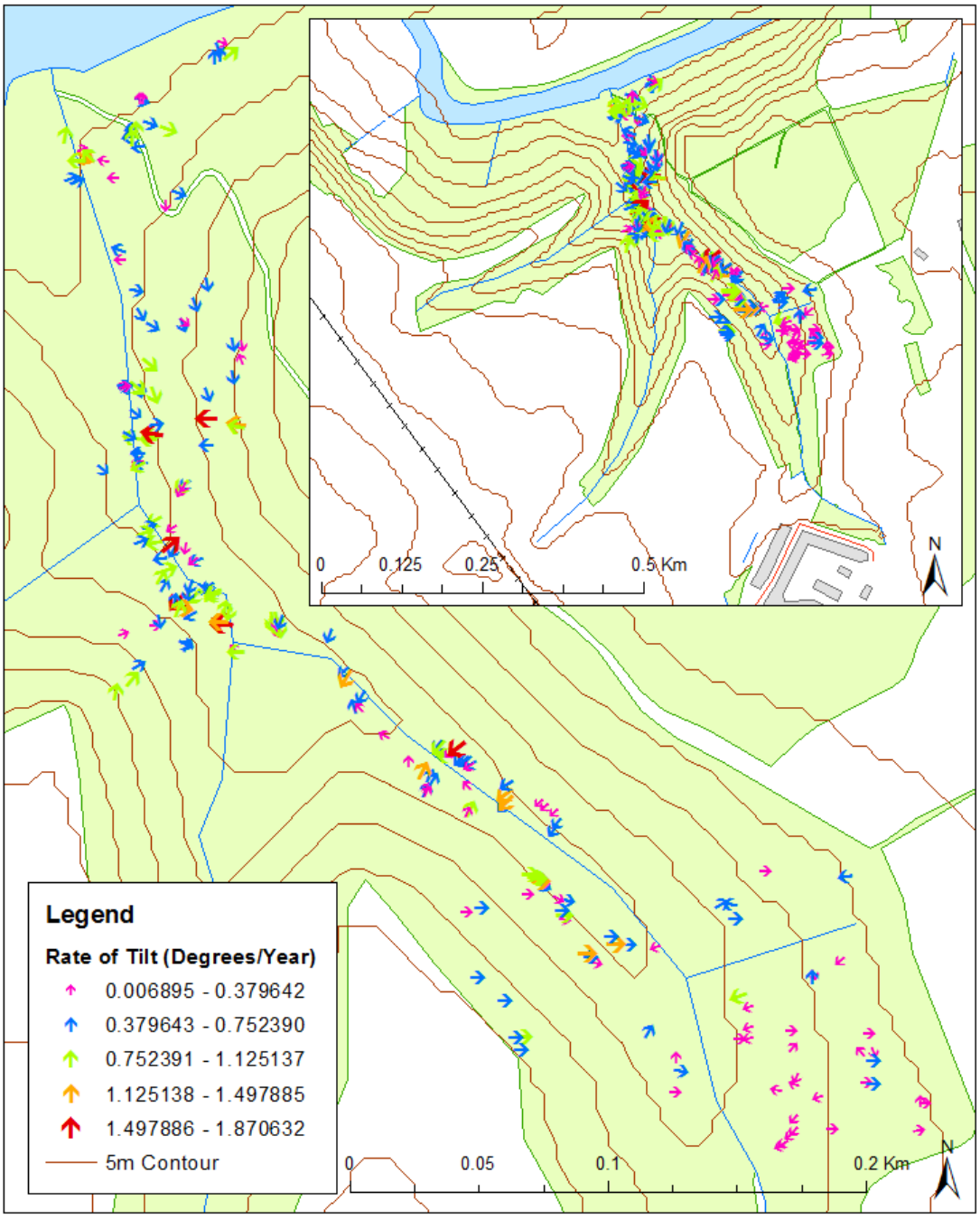

Figure 6.15-Vector map of the tilt rate which is a proxy for soil creep within the Red House Gill catchment. 5m contours have been added.

6.1.8 Active and Stable Areas

An aim of this analysis was to assess whether basal trunk angle could be used to determine different areas of geomorphic activity in the Red House Gill catchment. A review of soil creep measurements by Jahn (1989), demonstrated that rates of soil creep were higher for steeper slopes: 5-10^0 slopes on average had soil creep rates of 8 mm yr^{-1} whereas 13-24^0 slopes produced an average soil creep rate of 9 mm yr$^-$

[1]. More recently, Winchester et al. (2006) suggested that trees growing in steeper areas have a more pronounced tilt (deviation from 90^0). In the Red House Gill catchment, geomorphic activity varies remarkably from the river to the top of the hillslope and along the stream courses. Three different classes of geomorphic activity have been defined in relation to local geomorphology:

- Active- Trees residing in active geomorphic areas next to the river bank and therefore closest to active areas of mass movement (river bank collapse and landslides) or within sections of the hillslope which are $>20^0$ (trees marked in red on Figure 6.16). This category contains 163 trees.

- Semi Active- Trees growing in semi-active geomorphic areas, located on slopes between $10\text{-}20^0$ (trees marked in orange on Figure 6.16). This category contains 116 trees.

- Stable- Trees have been located in stable sections of the catchment on slopes $<10^0$ and away from mass movement disturbances (trees marked in green on Figure 6.16). This category contains 51 trees.

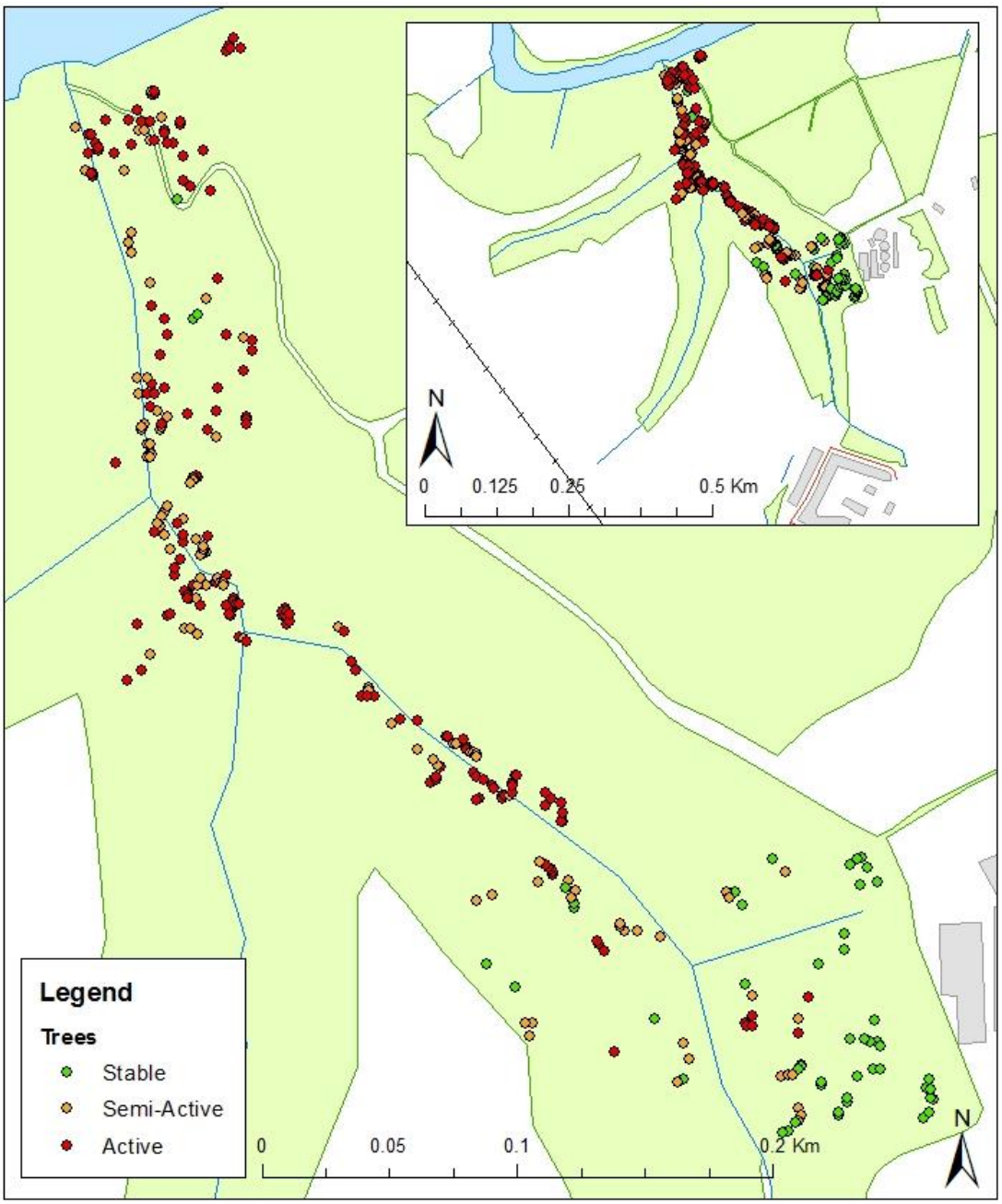

Figure 6.16-Map of Red House Gill demonstrating areas classified as Active (red), Semi-Active (orange) and Stable (green).

It is hypothesised that active geomorphic areas will involve frequent mass movements and therefore high rates of tree regeneration and on steeper slopes, rates of soil creep will be much faster producing greater rates of tree tilt. While on the other hand, trees within the stable areas will be older and straighter as they aren't being influenced by rapid mass movements and long term soil creep. Table 6.10, provides summary statistics for tree age, base angle and rate of tilt divided by geomorphic category. As the table demonstrates, the active category has the

youngest average tree age of 39 years. However this is only slightly older than the semi-active category, while the stable category has the highest average age of 43 years. This agrees with the hypothesis, that the active geomorphic category has the highest rate of tree regeneration. Table 6.10 also demonstrates that the active geomorphic category has the smallest mean basal trunk angle and also contains the tree with the smallest basal trunk angle recorded (7.3^0). Whereas the stable category, which isn't influenced by rapid mass movements and soil creep, has a much larger mean basal trunk angle. Rate of tilt has also been included in Table 6.10 and demonstrates that the active category has the largest average rate of tilt at $0.68\ ^0\ yr^{-1}$. The active category contains both the highest and lowest rates of tilt recorded in Red House Gill and therefore has a high standard deviation. Figure 6.17, visually demonstrates how disperse the rate of tilt is in the active category. The semi-active category is also well dispersed, whereas the stable category isn't. Table 6.11 demonstrates that the rate of tilt in the active, semi-active and stable geomorphic conditions are all significantly different to each other. This result suggests that trees growing in active areas have a different rate of tilt to those in semi-active and stable areas, which suggests all three areas are influenced by different rates of soil creep.

Tree Species	Count	Mean	SD	Min	25th	Median	75th	Max
				Tree Age				
Active	163	39.91	8.36	26.02	33.24	40.35	45.19	75.37
Semi	116	40.12	8.71	26.33	32.87	40.38	45.80	66.21
Stable	51	43.31	7.95	28.70	35.00	46.12	50.11	56.47
				Basal Trunk Angle				
Active	156	72.89	16.41	7.37	63.53	74.06	90.00	90.00
Semi	116	73.22	11.92	36.68	64.71	73.17	81.62	90.00
Stable	51	80.45	8.59	59.23	75.10	79.45	90.00	90.00
				Tree Rate of Tilt				
Active	104	0.68	0.42	0.01	0.38	0.58	0.87	1.87
Semi	89	0.54	0.27	0.02	0.35	0.48	0.70	1.49
Stable	32	0.39	0.17	0.17	0.27	0.32	0.50	0.79

Table 6.10-Summary statistics for tree age, basal trunk angle and tree rate of tilt divided into the three geomorphic categories.

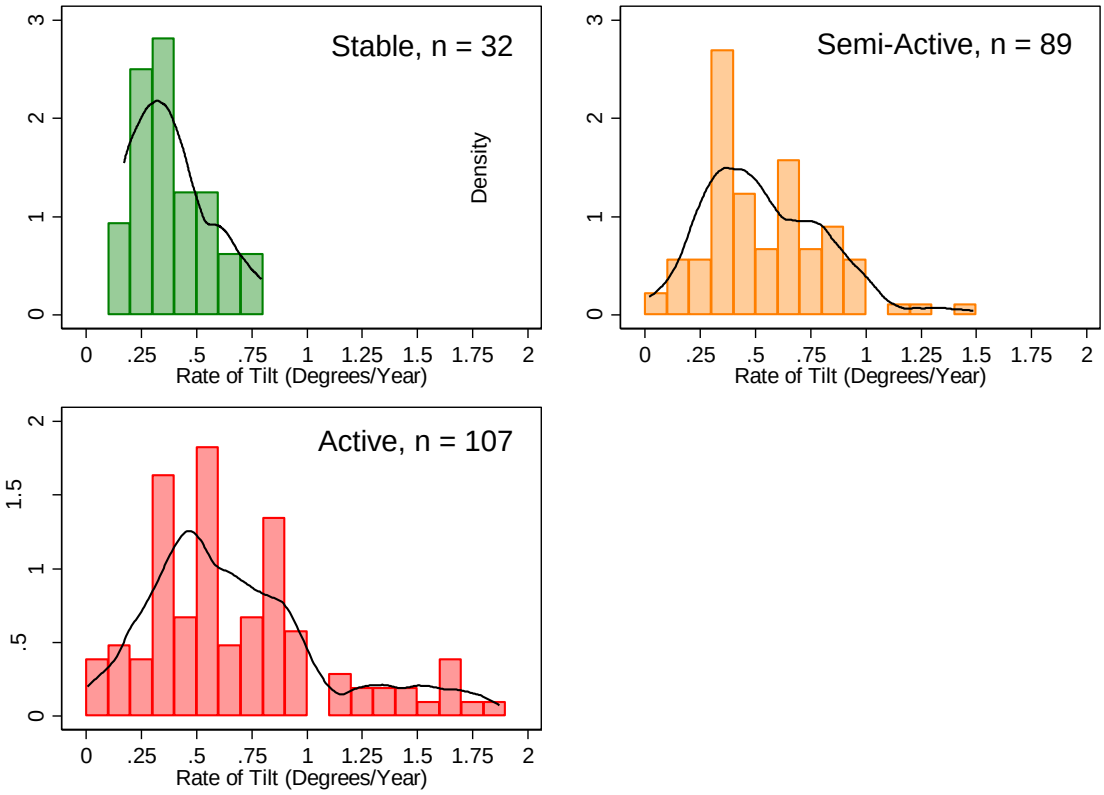

Figure 6.17– Histogram and kernel density plot for rate of tilt divided into active, semi-active and stable geomorphic conditions.

	T Value	Degrees of Freedom	P-Value	Alpha Value	Outcome
Active/Semi	2.711	191	0.073	0.05	Statistically Different
Active/Stable	3.9105	134	0.0001	0.05	Statistically Different
Stable/Semi	3.0188	119	0.0031	0.05	Statistically Different

Table 6.11– Student t-test results for tree basal trunk angle

6.1.9 Slope and Basal Trunk Angle

It has been hypothesised that soil creep increases with slope angle (Jahn, 1989), and trees growing on steeper slopes generally have a more pronounced tilt (deviation from 90^0) (Winchester et al., 2006). This has been tested using data collected from the Red House Gill catchment, it is expected that as slope angle increases, the basal trunk angle should decrease, creating a negative correlation. Figure 6.18, is a scatter graph of local slope derived through field measurements and basal trunk angle. The graph demonstrates the weak negative relationship with an R^2 value of -0.1982. The graph is also coloured by geomorphic category. The

stable trees appear to be well clustered, with a small local slope angle. Whereas, the active geomorphic category is well dispersed. Rate of tilt has also been correlated with local slope, hypothesising that as local slope increases, so should rate of tilt, creating a positive correlation. Figure 6.19, displays this weak positive correlation which has a R^2 value of 0.1667. The low correlation agrees with previous work by Mills (1984) who found that trees on steep boulder streams tilted more, than trees on comparably steep side slopes within Virginia. He therefore suggested this simple pattern is complicated by different geomorphic settings, processes and tree species. Figure 6.19 has also been coloured by geomorphic category, once again the stable group is well clustered, while the active and semi-active group are more dispersed.

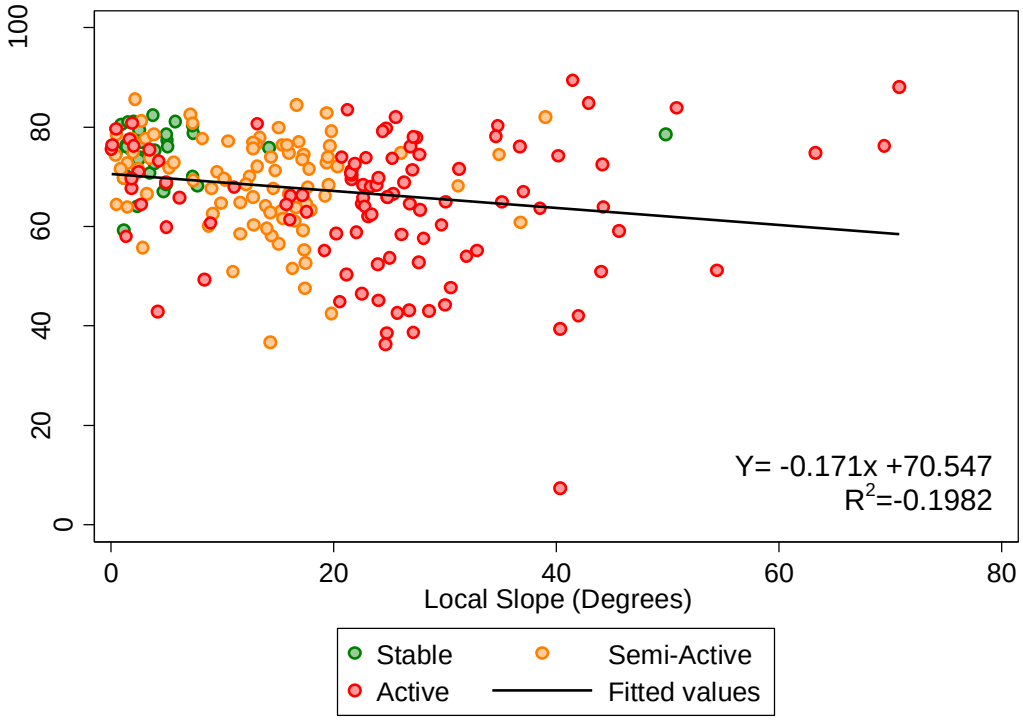

Figure 6.18-Scatter demonstrating the weak negative correlation between local slope and base angle.

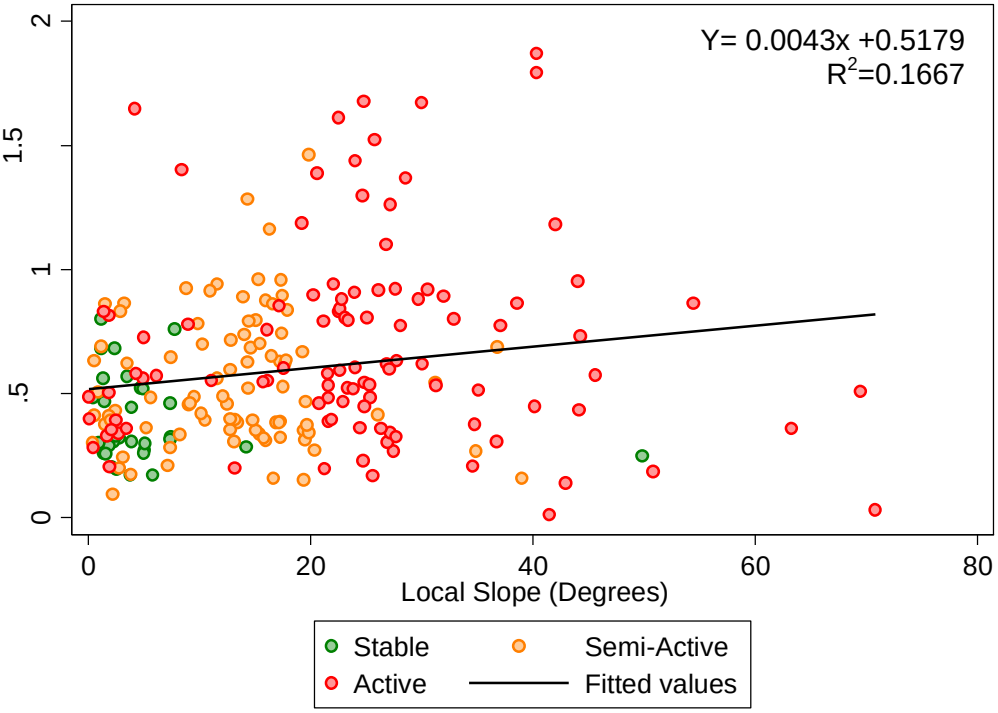

Figure 6.19-Scatter demonstrating the weak positive correlation between local slope and rate of tilt.

6.1.10 Tree Age and Basal Trunk Angle.

If soil creep has been active over the lifespan of a tree then older trees should have a smaller basal trunk angle. This is because as the tree is continuously affected by soil creep, the tree deviates more and more from vertical, progressively developing a smaller basal trunk angle. Therefore, as the tree age increases and the tree is continuously under the influence of soil creep, the basal trunk angle will get smaller. Figure 6.20, shows a scatter plot between tree age and basal trunk angle. The trend line demonstrates a weak positive correlation with a R^2 value of 0.1394. The low correlation between tree age and basal trunk agrees with previous work by Mills (1984) who suggested the lack of correlation demonstrates that trees were bent when saplings and have been relatively stable ever since.

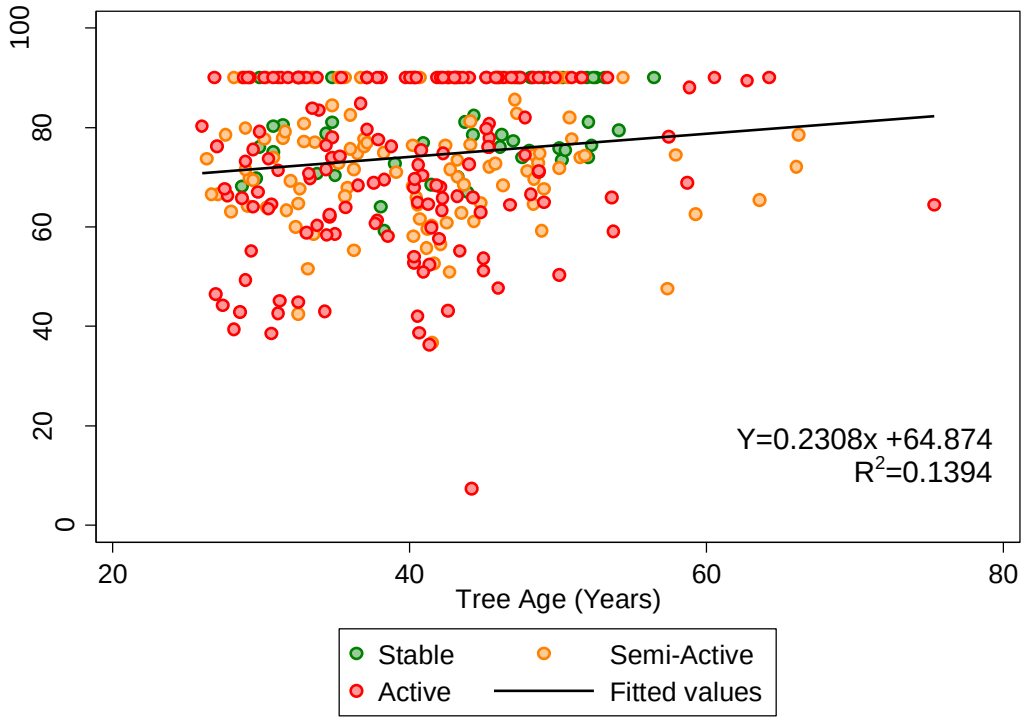

Figure 6.20-Scatter demonstrating the weak positive correlation between tree age and basal trunk angle.

6.2 Tree Rings

Dendrochronology has been used to investigate historic occurrences of soil creep within Red House Gill. Eight curved trees along with four references trees were cored using a 5 mm diameter increment corer (Figure 6.21). This section examines the temporal patterns of eccentric growth caused by soil creep (Section 6.2.2) and patterns of eccentric growth in relation to climatic factors (Section 6.2.3).

6.2.1 Disturbed and Reference Trees

Given high slope inclination, the mixture of poorly drained gley soils and sandy soil, combined with a history of high levels of precipitation, soil creep is potentially a significant geomorphic process in Red House Gill (Kirkby, 1967, Pawlik et al., 2013). A sample of eight trees with a significantly curved base were cored on the upslope and downslope side of the tree. Figure 6.21, indicates that all the disturbed trees were cored along a 35 m transect in a section of steep woodland adjacent to the East stream. This section of hillslope was chosen because it didn't show any obvious signs of historic mass movement and therefore appeared to represent soil

creep across the catchment. Four reference trees were also selected and cored in a relatively flat area of woodland where soil creep was assumed to be virtually nil (Figure 6.21). Here one core perpendicular to the hillslope was collected for every reference tree, as it provides better cross-dating results compared to collecting cores parallel to slope (Owczarek, 2013). Table 6.12 provides an overview of tree and site characteristics for disturbed and reference trees. The eight disturbed trees were comprised of six Ash trees and two Sycamore trees which have an average age of 41 years (oldest 46, youngest 37) and therefore provide information over the past four decades. The mean basal trunk angle is 70^0 (biggest 77^0, smallest 59^0), demonstrating that the trees were significantly curved. Two Ash and two Sycamore trees were selected as reference trees and have a mean age of 60 years (oldest 62, youngest 59); therefore they provide a reference chronology longer than the disturbed trees. As the reference trees were straight (90^0), data wasn't collected to calculate basal trunk angle or local slope.

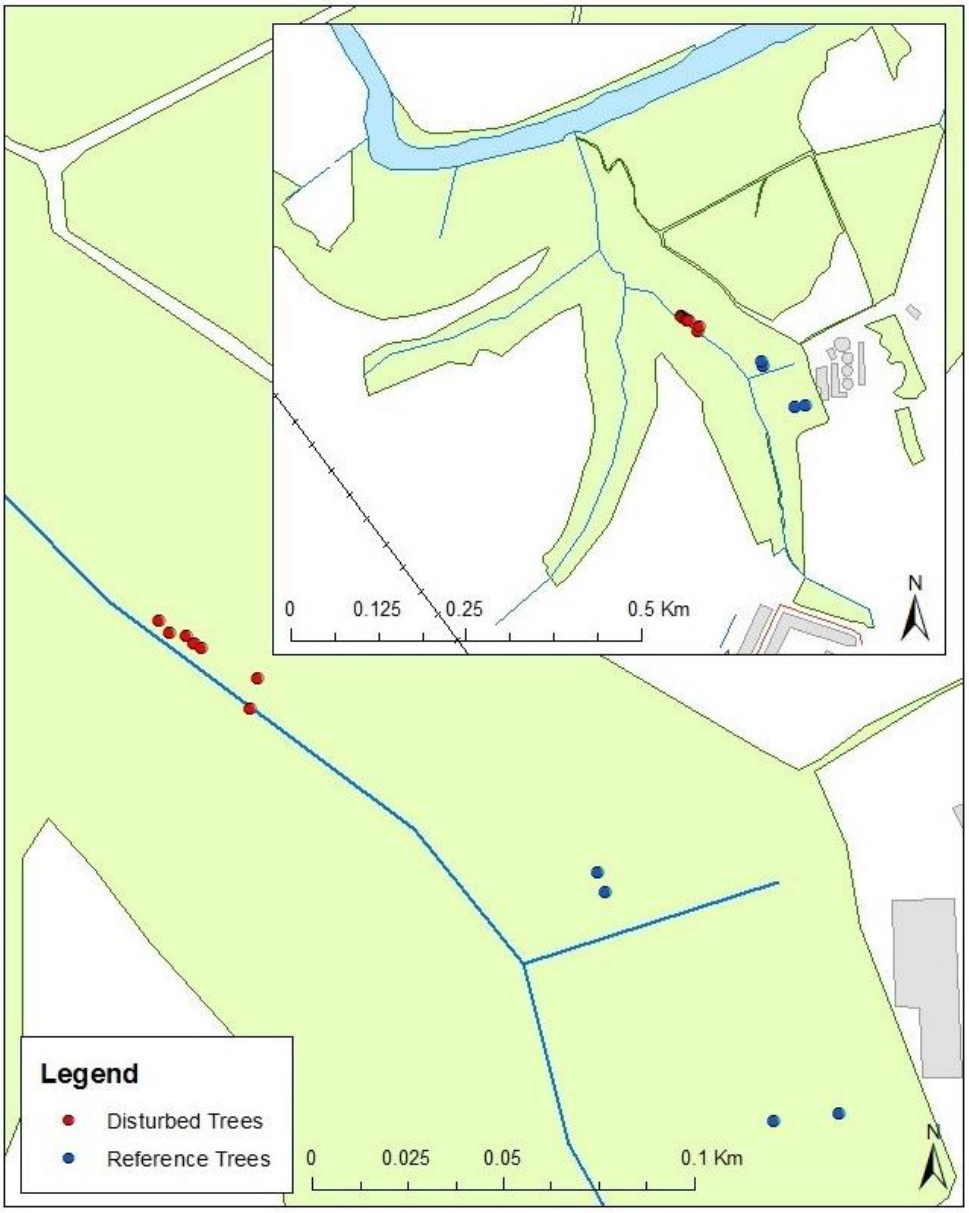

Figure 6.21-The location of all eight disturbed trees which were cored and the location of the four reference trees which were also cored. The inset map demonstrates the location within the wider woodland area.

Tree Number	Species	Age Cored	Age Forestry Commission	Basal Trunk Angle	Local Slope	Aspect	General Site Information
89	Ash	44	35	58	20	220	
193	Ash	46	36	77	8	225	
194	Sycamore	45	41	n.d	n.d	225	Steep section of the hill slope, close to the stream bank. Potentially high levels of soil creep.
196	Ash	37	36	74	26	225	
198	Ash	39	28	n.d	n.d	225	
200	Ash	40	30	73	14	230	
211	Sycamore	39	41	59	14	225	
217	Ash	43	33	70	21	230	
C1	Ash	59	33	n/a	n/a	n/a	Flat terraced section of the hillslope
C2	Ash	62	29	n/a	n/a	n/a	
C3	Sycamore	60	44	n/a	n/a	n/a	Flat area of land at the top of the hillslope
C4	Sycamore	60	46	n/a	n/a	n/a	

Table 6.12-Information regarding the disturbed trees and reference trees sampled at Red House Gill. Please note, no data (n.d) exists for two disturbed trees (194 and 198), as a full set of measurements was not determined in the field. For the reference trees, the three length measurements weren't recorded, as they were growing in a stable part of the catchment, consequently basal trunk angle and local slope cannot be calculated.

6.2.2 Eccentric Growth

When a tree is affected by soil creep, to help regain stability it creates reaction wood (Figure 4.5). In deciduous trees, reaction wood is produced on the uphill side of the tree and is called tension wood (Speer, 2010). Therefore when a tree is affected by soil creep, ring widths on the upslope side of the tree are wider than the downslope ring width for a given year. All eight disturbed trees shows signs of eccentric growth where the upslope tree ring is wider than the downslope tree ring width, suggesting the occurrence of soil creep. However, episodes of eccentric ring growth caused by soil creep within the trees are not identical. For trees 89 and 196, the upslope ring width is consistently bigger than the downslope ring width, suggesting that both of these trees are constantly affected by soil creep. This isn't the case for trees 193, 194, 198, 200, 211 and 217, which only appear to be intermittently affected by soil creep. Figure 6.22, provides an example tree ring series for tree 193 (a) and tree 89 (b). For tree 193, the downslope ring widths are bigger than the upslope ring widths for three years (1989, 1996, and 2012) when it appears soil creep wasn't a major influence on the tree, whereas for tree 89 the upslope ring width is bigger than the downslope ring width for every year, suggesting the tree has constantly been affected by soil creep. Appendix C provides the tree ring width series for all of the sampled trees.

There are a few periods temporally when soil creep doesn't appear to affect every tree, which is demonstrated in Figure 6.23a. There are seven key periods when soil creep isn't affecting every tree 1971-1972, 1975-1977, 1989-1990, 1995-1997, 2000-2005, 2007-2008 and 2011-2012. The full reference chronology can be seen in Appendix D and demonstrates that between 1970-1985, there is a reduction in tree ring width for C1, C2 and C3.

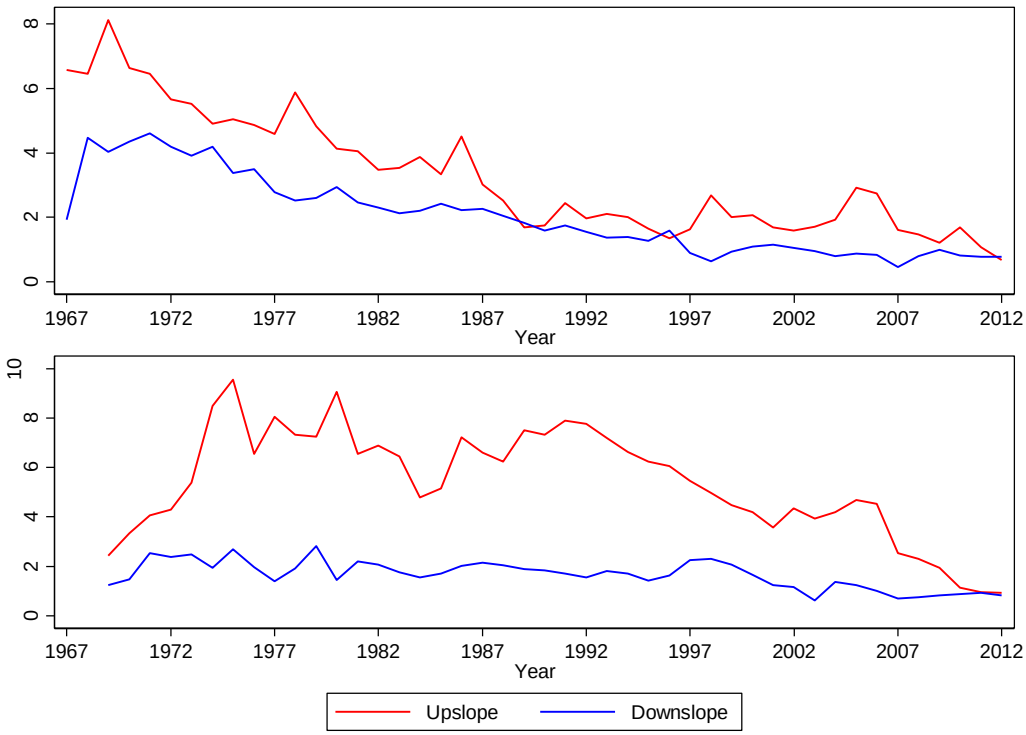

Figure 6.22- Example tree ring data for Tree 193 (top) which shows no soil creep in 1989, 1996 and 2012 and for tree 89 (bottom) which shows a consistent soil creep signal as the upslope ring width is always wider than the downslope ring width.

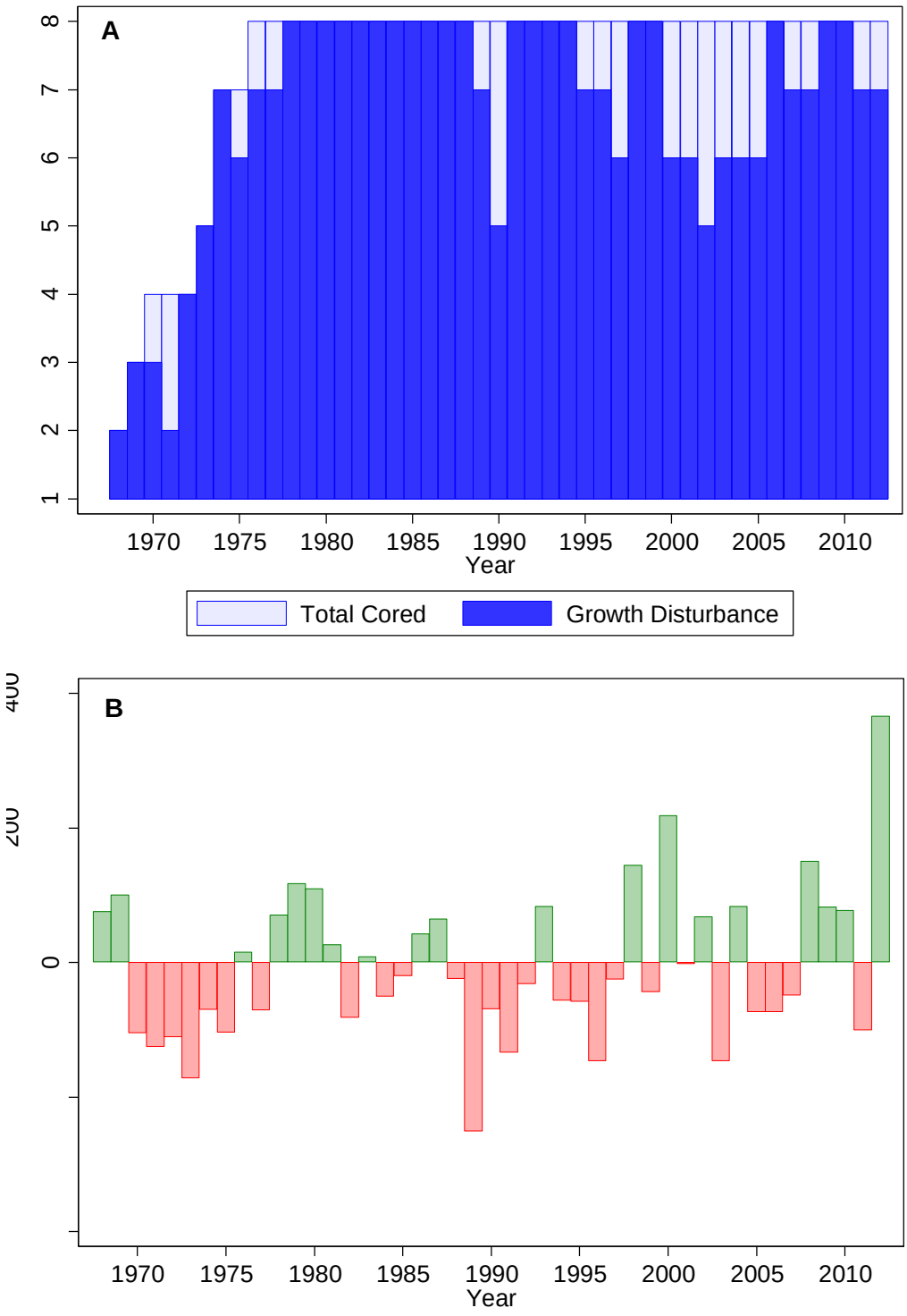

Figure 6.23- A)The number of trees showing eccentric growth (dark blue) from 1968 to 2013 compared with the total number of trees sampled in each year (light blue). B) Precipitation difference from the mean annual precipitation of 666.5mm. Green bars, demonstrate a positive year, while red bars show years with less than average precipitation.

6.2.3 Precipitation

Although soil creep displacement appears almost continuous according to the tree ring record, there are seven key episodes where soil creep doesn't appear to affect every tree (Figure 6.23a). Figure 6.23b, demonstrates the difference between annual precipitation for that year, and the long term average of 665 mm from Durham University Observatory. As the graph demonstrates, there are several key periods when precipitation is below average, 1970-1975, 1988-1992, 1994-1997 and 2005-2008. When reviewing Figure 6.23, there is a clear connection between years with a below average rainfall and a reduction in the soil creep signal recorded from the tree cores. A good example is the dry period between 1988-1992, which contains the driest year on record (1989); in 1989 one tree didn't record a soil creep signal, which increased to three in 1990. These results agree with previous work by Denneler and Schweingruber (1993), who found that reduced signs of soil creep is associated with periods of low precipitation. In some cases, there is a time lag between below average precipitation and fewer signals of soil creep recorded from the tree cores, for example there was below average precipitation in 1970 however trees only recorded signs of reduced soil creep the year after in 1971. Timell (1986) suggests this is because once a tree starts to produce reaction wood, it can continue for years, even if precipitation reduces helping to stabilise the slope.

6.3 Summary

The results presented in this chapter use tree form characteristics as a proxy for spatial and temporal patterns of soil creep and catchment instability. As part of this research information on 340 different trees was gathered. This suggests that the majority of old trees grow in flatter areas of the catchment, while younger trees grow on steeper slopes, where due to rapid mass movements, bank collapse and tree throw many trees collapse into the stream. Trees with the highest rate of tilt generally grow near the streams in the steepest area of the catchment. These trees generally tilt directly downhill whereas trees with a smaller rate of tilt growing within flatter areas of the catchment don't always show a preferred direction of tilt. Slope and basal trunk angle along with tree age and basal trunk angle, both have negative correlations which agree with previous work by Mills (1984). The tree cores demonstrate that within the active geomorphic zones of the catchment soil creep is almost continuously occurring. Therefore there is some support for the simple

hypothesis that relates soil creep to steeper slopes but in detail local geomorphic processes and ecological factors complicated such a simple pattern.

7 Discussion

The aim of this chapter is to combine the contemporary results (Chapter 5) and the historic results (Chapter 6) to gain a better understanding of the fine sediment dynamics in the Red House Gill catchment and develop a preliminary sediment budget characterising the main sediment fluxes. The sediment budget will help identify key processes contributing fine suspended sediment to the fluvial system and help determine, when and where these processes predominately occur. This chapter will be divided into three key sections. Firstly, the sediment budget will be defined (Section 7.1) before looking at how this can be used to help inform mangement processes in the catchment (Section 7.2). The last section of the discussion provides a critical review of the work on tree basal trunk angle as an indicator of surface soil instability (Section 7.3).

7.1 Constructing the Red House Gill preliminary sediment budget

Understanding sediment delivery processes at the drainage basin scale remains a challenge (de Vente et al., 2007). For this reason, sediment budgets are created, outlining and quantifing processes responsible for the generation and transport of sediment (Dietrich and Dunne, 1978, Reid and Dunne, 1996). However, it is worth noting that very few studies have taken place using a sediment budget approach to investigate the effects of urban development, especially within the UK. Therefore the conceptual sediment budget for Red House Gill shown in Figure 2.1 has now been further developed into the preliminary sediment budget which is outlined in Figure 7.1. The preliminary sediment budget characterises sediment fluxes from all three tribuarties to the River Wear over the six month monitoring period. As the catchment is underlain by glaciofluvial deposits composed of sand and clays, fine sediment dominates the flux, which is a great concern environmentally to the fluvial system (Wood and Armitage, 1997).

This sediment budget has been created based on direct monitoring and it is important to understand how the conceptual model has been quantified. Sections 7.1.1-7.1.3 characterise erosion from the main hillslope processes identified within the sediment budget while sections 7.1.4 and 7.1.5 explain the main sediment fluxes in the channel system.

7.1.1 Landslide erosion

When estimating the significance of landslide erosion in sediment budgets this is frequently calculated by measuring the quantity of erosion in a small percentage of the catchment before upscaling (Duijsings, 1987, Nelson and Booth, 2002). Although averaging and extrapolation increases uncertainty, monitoring erosion on every landslide feature isn't feasible. A similar approach has been used within Red House Gill. Here the quantity and spatial extent of landslides within the catchment was determined through geomorphic mapping (Figure 5.1). While mapping the catchment, the dimensions of every landslide was also measured. Given the steep V-shape valley and absence of floodplain, the majority of landslides feed material directly to the stream, increasing suspended sediment concentration. The depth of landslide erosion is heavily dependent upon the type of failure (rotational or translational), although mapping revealed that most landslides are shallow varying between 0.3-1.2 m in depth (Table 5.1). As a result a conservative depth of 0.4 m has been used as an average failure depth to calculate volume of eroded material. The volume of erosion has been converted to mass using a bulk sediment density of 1.7 t m^{-3} which is representative of mixed glacial sand and clay exposed in the majority of landslide scars (Selby, 1993).

Results from the static photography demonstrate that landsliding delivers the most fine sediment to the Red House Gill channel (Section 5.1.2) and landslides accounted for 93% of total erosion. This is almost double what was observed by Nelson and Booth (2002) and an even lower percentage was recored by Duijsings (1987) who suggested that mass movements only accounted for 14% of sediment delivery.

7.1.2 Stream bank erosion

Stream bank erosion has previously been calculated by measuring erosion pins (Duijsings, 1987) and predicted from regional discharge values and measured channel dimensions (Nelson and Booth, 2002). However in this research, erosion occuring through lateral bank erosion and collapse and has been calculated using a similar method to landslides. The amount of bank collapse and erosion was determined through geomorphic mapping (Figure 5.1). For bank erosion a depth of 0.05m was assumed whereas for bank collapse an average failure depth of 0.1m has been used. Once again, both of these estimates are at the lower end of the scale for erosion rates observed in the Red House Gill catchment (Table 5.1).

These volume estimates are then converted into mass using a soil bulk density of 1.3 t m^{-3}, which is representative of woodland soils found in the catchment (Jarvis et al., 1984).

In the Red House Gill sediment budget, bank erosion and collapse accounted for only 6% of erosion. This result is highly comparable to results by Walling et al. (2002), who estimated channel bank erosion accounted for 10% and 6% of sediment output from two catchments, one in Herefordshire and one in Derbyshire, UK. However, in other sediment budgets lateral erosion of stream banks has accounted for far more erosion. Duijsings (1987) reported stream bank erosion was responsible for 43% of sediment delivery whereas Nelson and Booth (2002) suggested that stream bank erosion was responsible for 20% of hillslope erosion.

7.1.3 Soil Creep

In this research, rate of tree tilt has been developed as a proxy for soil creep and Figure 6.15 shows that trees with the highest rate of tilt appear close to the stream banks and therefore indicates that soil creep is an important source of sediment supply. Estimating soil creep is notoriously difficult which has previously restricted its use in sediment budgets (Dietrich et al., 1982). However previous work by Anderson (1977) measured rates of soil creep in Durham over a two year period, suggesting an average rate of 1.8 mm yr^{-1} over a depth of 0.25 m. Using these values along with the length of the stream banks (both sides of the river banks), it is possible to estimate the amount of soil delievered to the channel via soil creep. The volume of erosion is then converted into mass using a bulk density of 1.3 t m^{-3} which is typical of the woodland soils found within the catchment (Jarvis et al., 1984).

Nelson and Booth (2002) calculated soil creep using a very similar method and their results suggest that soil creep is responsible for delivering 3% of suspended sediment. While work by Duijsings (1987) suggests that soil creep delivered 0.8% of sediment within the sediment budget. In the Red House Gill sediment budget soil creep delivered approximately 0.5% of sediment. Although, measuring soil creep is difficult, it appears that the Red House Gill sediment budget is in general agreement with other research projects with regard to the magnitude of soil creep sediment delivery.

7.1.4 Stream channel fine sediment flux

Suspended sediment load has been estimated for the catchment based on discharge and suspended sediment concentration monitored at the main stream gauging site (Section 4.3.3 and Section 5.2.1). The total load was then summed for the whole period of monitoring, providing an estimated total suspended sediment load of 493 t.

7.1.5 Estimation of sediment delivery from the wider urban catchment

Sediment load from the wider urban catchment wasn't directly measured at the source of the East and Middle tributary after they emerge from the urban drainage system. However, information has been collected about the spatial pattern of sediment delivery from the network of TIMS. Figure 5.18, shows the average sediment flux over the monitoring period and demonstrates that the upper Middle stream TIMS provides only $1/40^{th}$ (0.025%) of the sediment flux compared to the downstream Middle TIMS. Based on this value, it is estimated that the upper urban catchment provides 12.3 t of fine suspended sediment.

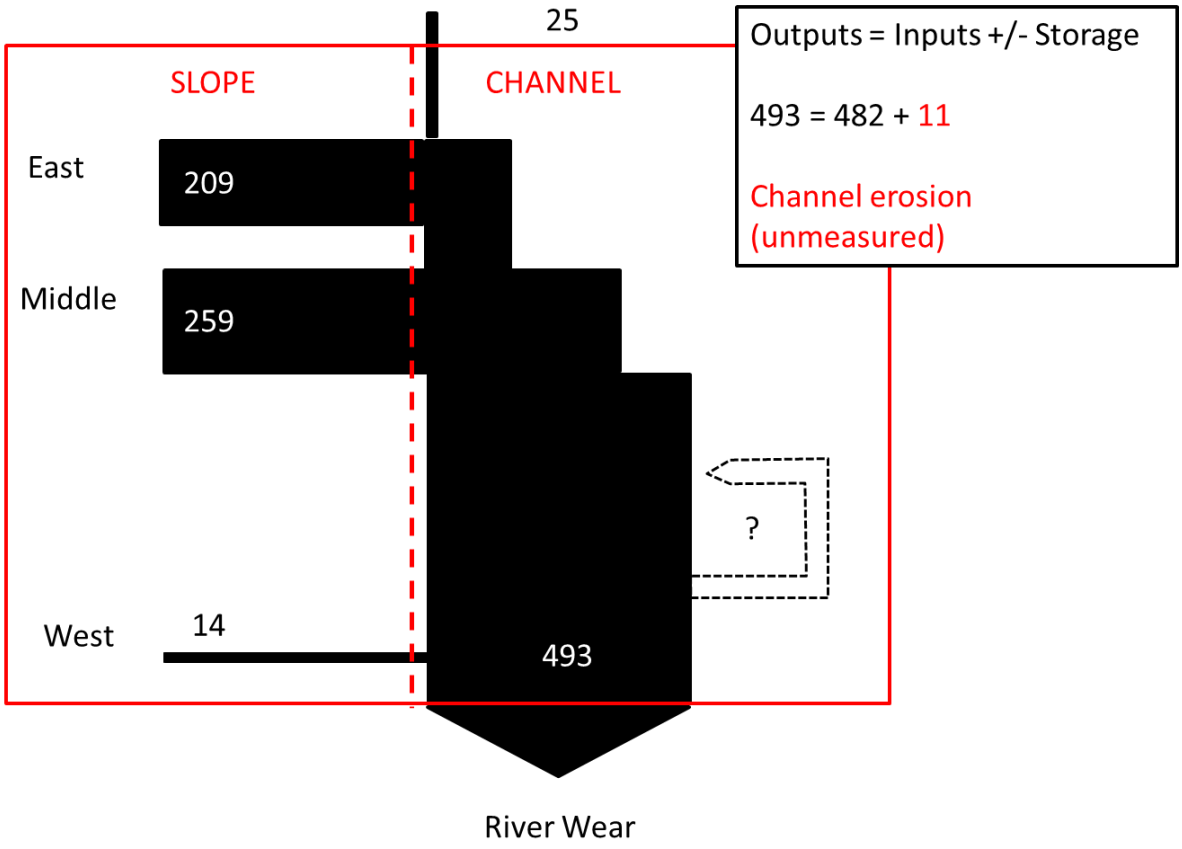

Figure 7.1– Preliminary sediment budget for Red House Gill. The red box denotes the Red House Gill sediment system, divided into the East, Middle and West streams, while the black box explains how channel erosion is estimated in the lower reaches of the channel. All values are in metric tons.

7.2 Interpreting the Red House Gill Sediment Budget

From these calculations, it is possible to construct the preliminary sediment budget which is shown in Figure 7.1. Over the course of the six month monitoring period, 482 t of sediment has been eroded from the hillslopes and supplied to the stream. This quantity of erosion is very high and is roughly balanced by the same amount of suspended sediment being transported by the stream channel which is 493 t. In the absence of other sediment transfer mechanisms, this suggests most of the sediment is being transported in the main channel and therefore ultimately discharged into the River Wear. The 11 t difference between material that has been eroded from the hillslopes and total suspended sediment load is 3%, this is very similar to the 4% difference between material eroded from the hillslopes and total suspended sediment load recorded by Duijsings (1987) in a forested catchment.

In the Red House Gill catchment, there is a clear contrast between the amount of sediment being transported and supplied by each individual sub-catchment. The Middle stream supplies the majority of fine sediment as it is responsible for 55% of the total erosion within the catchment. Although the East stream supplies a similar amount of fine sediment due to hillslope erosion (42%), the West stream is only responsible for supplying 3% of the whole catchment erosion, which is substantially lower. This pattern of sediment transfer suggests a close connection between erosion within the sub-catchments, specifically the East and Middle streams and high levels of suspended sediment delivered to the River Wear.

The three sub-catchments all respond differently to flows generated in the upstream catchment due to the individual geomorphology of each tributary. The Middle stream, drains the second largest area due to the urban drainage systems, it also has a very steep channel, very steep hillslopes defining a V-shaped profile and a lack of a floodplain to store eroded sediment (Table 3.1). The East stream still supplies a lot of sediment due to the moderately steep channel and steep hillslopes. However, the channel is much wider with the development of an intermittent floodplain which can store more eroded sediment (Table 3.1). The West stream is the smallest catchment and has the lowest channel gradient and gentler hillslopes (Table 3.1). These results agree with ideas developed in the classical geomorphology of Schumm and Lichty (1965), who suggested that elevation, relief and channel morphology are important controls on sediment erosion. Also it agrees with more recent research by Wass and Leeks (1999), who found a strong positive correlation between suspended sediment load and catchment area for the sub-catchments of the River Humber.

Many sediment budgets are unable to fully quantify every process in a catchment and therefore some components need to be estimated by subtraction to determine an unmeasured residual in the budget (assuming the sediment budget is a closed system) (Parsons, 2012). Within the lower reaches of the trunk stream in Red House Gill, channel erosion is an active process resulting in local scour and channel deposition. However, within the scope of this investigation it has not been feasible to directly measure channel erosion. Therefore the 11 t (3%) difference (residual) between total suspended sediment load recorded and sediment delivered from the hillslopes has been assumed to be due to channel erosion.

7.3 Moving forward – Implications from the preliminary sediment budget

The sediment budget shown in Figure 7.1, demonstrates that Red House Gill is an actively eroding catchment; which is the result of several key attributes. Firstly, the catchment is comprised of loosely consolidated glacial sand and clay (Section 3.4) which is highly erodible. When coupled with steep channel gradients and V-shaped valleys this greatly enhances sediment transfer (Section 3.3). The catchment displays a very 'flashy' response to rainfall, with just under than 80% of sediment load being transported in four large rainfall events during the monitoring period (Section 5.2.1). As discussed above (Section 7.2) the three tributaries respond in a characteristic way to rainfall events, with the Middle stream supplying the most sediment due to a steep channel, steep hillslopes and no floodplain. While the West stream supplies the least sediment, due to the lower channel gradient, gentle hillslopes and floodplain.

Based on the monitoring results and the constructed sediment budget, it is possible to recommend a number of ideas to help ease environmental problems caused by the high rates of sedimentation within the catchment and downstream River Wear. Erosion could be mitigated by considering two main approaches:

7.3.1 Reducing Flow

Based on a previous modelling study (Table 3.3), it appears that over the six month monitoring period a range of flows which are consistent with storm discharges were experienced. Throughout the monitoring period, four key high flow events occurred (Section 5.2.1) which resulted in extensive erosion which was noted through the static photography (Section 5.1.2). Suspended sediment is generally proportional to flow and therefore as flow increases, so does suspended sediment and as a result a reduction in sediment could be achieved by reducing flow.

It is therefore recommended that peak flows shouldn't be increased and where possible efforts should be made to reduce peak discharges. A range of sustainable urban drainage systems (SUDS) are available and introducing retention ponds within the Red House Gill catchment could significantly attenuate runoff while also improving water quality (Charlesworth et al., 2003). Research conducted by Bressy et al. (2014) in four small Parisian catchments ranging in size between 0.8-1.5 ha compared the efficiency of SUDS (vegetated roofs, underground tanks, swale and grassed retention ponds) and conventional urban drainage for reducing discharge and pollutant loads. Their results demonstrated that the SUDS reduced peak flow by up to 50% while simultaneously reducing run-off pollution by 20-80%.

7.3.2 Erosion and Sediment Control

Historical Ordnance Survey maps (Figure 3.6) demonstrate that over the past 150 years the Red House Gill catchment has had the same general geomorphology with tributary streams being steeply incised. However, fine sediment delivery caused by landsliding and bank collapse triggered by high flows predominately in the East and Middle tributaries has only become a documented environmental concern more recently; largely because fine suspended sediment is transported from the tributary streams to the River Wear.

Reducing sediment supply can be achieved through:

- Hard Engineering – a range of hard engineering options exist to reduce erosion. Slope armour could be used to help reinforce the base of hillslopes which supply large quantities of fine suspended sediment. Debris dams can also be constructed which will help to reduce channel energy and therefore the amount of fine sediment being transported. Previous research by Trimble (1997), looked at the effects of urbanisation on channel erosion and called for the use of hard engineering to manage sediment yields and reduce negative environmental impacts.
- Soft Engineering – typically more environmentally sustainable, soft engineering includes vegetation stabilisation. A large amount of research has looked into the effects of vegetation on stream bank stability, many reporting positive results. Not only does vegetation mechanically reinforce stream bank stability, it also has positive effects on matric suction and therefore soil cohesion helping to increase stability (Pollen-Bankhead and Simon, 2010).

Erosion control measures alone are unlikely to be enough and should therefore be considered as part of a managed flow solution. The West stream is a good model to help guide discharge and erosion control measures, as sediment produced by this stream is far lower compared to the East and Middle streams.

7.4 Critical Review – Basal Trunk Angle and Dendrochronology

One of the aims of this research was to map areas of catchment soil instability using tree deformation and use dendrochronology to determine historical patterns of soil creep. The effects of soil creep on trees is keenly debated, initial work into this topic by Sharpe (1938) suggested that soil creep will make a curve at the base of the

tree. However, this has been contested by Parizek and Woodruff (1957) and Phipps (1974) who believe slow but continuous soil creep will produce a sweeping curve, suggesting a curve at the base of the tree is the result of a sudden mass movement (Section 2.4.1). Both continuous soil creep and more rapid mass movements, highlight soil instability within the Red House Gill catchment and therefore demonstrate the importance of looking at tree deformation to map instability.

It appears that only two previous studies have looked at tree deformation in detail at the catchment scale. Mills (1984) collected information on 210 curved trees in seven different locations, his results revealed that trees on steep boulder streams were tilted more than those with comparable relief on side slopes. No significant correlation was observed between tree age and angle at the base of curved trees. More recent work conducted by Winchester et al. (2006) suggested that trees growing in steeper areas had a more pronounced curve, although it appears that no formal correlation analysis occurred. This idea has therefore been further investigated at Red House Gill to see whether tree form can help map catchment soil instability. Figure 6.9, demonstrates that trees with a smaller basal trunk angle are growing close to the steep stream banks whereas straight trees tend to grow in flatter areas at the top of the hillslope. This map provides further evidence to support the hypothesis that basal trunk angle is associated with slope inclination and position on the slope profile. However, there is only a weak correlation between slope angle and basal trunk angle (Section 6.1.9). In order to take into account tree age and provide a more historical perspective on slope instability, rate of tree tilt was calculated as part of this research. Figure 6.15 combines rate of tilt and aspect, demonstrating that trees with the highest rate of tilt appear close to the river banks and generally curving downslope. However only a weak correlation exists between local slope and rate of tilt (Figure 6.19).

The results of this research highlight the need for further work into the use of tree curvature for determining soil instability either caused by soil creep or rapid mass movements. This research, in common with the two previous studies examining tree curvature (Mills, 1984, Winchester et al., 2006) measure the angle at the base of the tree, however in practice this is very difficult to define and accurately measure. Unlike this research, previous studies have not clearly reported a detailed methodology on how to measure the angle at the base of tree. This is important because a consistent and transparent methodology is required to progress research

in this field. In particular, determining the point at which a tree starts to straighten is somewhat ambiguous (e.g. measurement length A in the current methodology).

A number of previous studies have used traditional dendrochronology (tree cores) to look at the effect of soil creep. Most noticeably Denneler and Schweingruber (1993), collected cores from 36 different trees, with results showing the episodic nature of soil creep, as limited soil creep signals (reaction wood) within the tree cores were observed in years with low precipitation. At Red House Gill, eight tree cores were collected and analysed. Figure 6.23, demonstrates there are seven key periods when soil creep wasn't influencing every tree. There is a clear connection between years with below average precipitation and limited soil creep signal recorded in the tree cores. The results of tree coring within Red House Gill therefore agree with the general finding of Denneler and Schweingruber (1993) that soil creep is less when precipitation, and presumably soil moisture, is reduced.

7.5 Summary

This chapter presents the Red House Gill preliminary sediment budget, which is shown in Figure 7.1. The sediment budget demonstrates that 482 t of sediment has been eroded over the six month monitoring period, which agrees closely with the results from turbidity (SSC) monitoring which estimates 493 t of sediment was transported. This can be extrapolated to an annual load of 962 t of sediment, accounting to an annual sediment load of 386 t km^{-2} yr^{-1}, which is similar to maximum reported sediment yields from UK catchments (Walling and Webb, 1987). If the project were to run again, data should be collected for multiple years. This would allow for an annual sediment budget and would provide a useful comparison between Red House Gill and other UK catchments where similar studies have been undertaken. To continue providing information on the spatio-temporal pattern of sediment delivery within the catchment, static photography should also be continued which will further clarify key erosion processes. The critical review of basal trunk angle and dendrochronology demonstrates the potential importance of this method for providing a historical insight into soil creep. This method could be refined by extending the sampling to include every tree in the catchment which displays a curved trunk with a diameter at breast height greater than 0.2 m. This would provide additional evidence to test the hypothesis that basal trunk angle is associated with local slope angle.

8 Conclusion

The aim of this research was to use a sediment budget approach to assess the impact of urbanisation on sediment delivery in a small peri-urban catchment, while also looking at longer term catchment instability. In order to do this, five research questions were specified (Section 1.3) and these will be used here to frame the main conclusions of this research:

1. *Produce a time series of sediment movement from the catchment to the River Wear; identifying events, periods and conditions leading to enhanced fine sediment delivery.*

The time series of fine sediment movement in Red House Gill has been based on the suspended sediment concentration and load calculated using the turbidity probe situated at the main monitoring site. Suspended sediment delivery was dominated by four key events during the monitoring period on the 18th May 2013, 18th July 2013, 5th August 2013 and 6th September 2013. Each event was associated with a period of heavy precipitation (Section 5.2.1). During these four dates, just under 80% of total suspended sediment load was transported in as little as 2% of the time. This agrees with previous work by Walling et al. (1992), who suggested the majority of sediment transport occurs during high flow events. The network of TIMS has provided detailed information concerning the spatial flux of suspended sediment within the catchment (Section 5.2.2). The Middle stream appears to have transported the most suspended sediment, with the majority being delivered from the hillslopes rather than being supplied to the headwaters by the urban culvert. The total sediment flux from the East, Middle and West streams are all statistically different. The temporal pattern of sediment delivery recorded with the TIMS is in agreement with the concentration time series, as more sediment was collected during sampling periods over the four high rainfall / flow events.

2. *Carry out local surveys using fixed point photography and terrestrial laser scanning (TLS) to characterise hotspots of bank instability and lateral slope instability*.

To assess the impact of high flows on lateral bank stability, static photography and terrestrial laser scanning were used to monitor change. The static photography at a

landslide on the Middle stream (site four) clearly demonstrated the greatest amount of erosion was due to high flows saturating the clay material at the toe of the slope causing upslope instability and eventual failure (Figure 5.3). The fortnightly observations also demonstrated the gradual process of bank undercutting due to high flows (Figure 5.5). The static photography also broadly correlated with the sediment supply data from the network of TIMS; when there was a peak in erosion noted from the static photography, there was also a peak in the amount of sediment collected in the TIMS. The most erosion occurred in the two weeks leading up to the 6th August 2013, which included a peak in rainfall which occurred on the 5th August 2013 (Section 5.2.1). Terrestrial laser scanning was also used to look at feasibility of monitoring erosion in a steep wooded catchment. Results, demonstrated the process of erosion on a landslide face; whereby material was eroded from the top of the landslide face and deposited at the toe, until the next high flow event when the material is eroded away downstream. However, surface vegetation on the landslide slope, masked the bare soil surface, increasing uncertainty in erosion estimates (Section 5.1.3). Although terrestrial laser scanning is conceptually elegant, it isn't always easily executed either in the field or in later processing stages.

3. *Map areas of catchment slope instability using dendrochronology to determine historical patterns of slope movement.*

In order to investigate the spatial and temporal patterns of slope instability a detailed investigation looking at tree basal trunk angle and tree rings (dendrochronology) was undertaken. Key results demonstrate that trees growing in flatter areas of the catchment are older than trees growing in steeper areas which are prone to landslides (Figure 6.6). Catchment maps suggest that trees growing in steep areas of the catchment tend to show larger rates of tilt, which is assumed to be a proxy for soil creep (Figure 6.15). However, there is only a very weak correlation (R^2 0.1667) between rate of tilt and local slope (Section 6.1.9). This agrees with previous work by Mills (1984). No significant correlation was also observed between tree age and tree basal trunk angle (Section 6.1.10), which also agrees with Mills (1984). When the 340 trees are classified into active, semi-active and stable areas, depending on local slope and proximity to mass movements, t-tests demonstrate that the rate of tree tilt is statistically different (Section 6.1.8). This suggests that the rate of creep occurring in areas designated as active, semi-active and stable are different to each other. Results from the tree ring analysis indicate that soil creep is relatively

constant within Red House Gill. The lowest annual precipitation on record from the Durham Observatory was in 1989 and a year later, three trees show signs of no soil creep (Figure 6.23). This agrees with previous work by Denneler and Schweingruber (1993), who found that reduced soil creep is associated with periods of low precipitation. More work is needed to understand the connection between tree curvature caused by soil creep and how this affects tree rings.

4. *Produce a geomorphic map summarising key sediment sources within the eroding catchment.*

The geomorphic map (Figure 5.1) demonstrates that main sediment sources in the Red House Gill catchment are landslides, bank erosion and bank collapse. The three key sources are distributed throughout the catchment although there frequency varies spatially, as it appears that bank collapse is more frequent at the head of the streams, followed by landslides in the middle reaches and bank erosion in the lower stream course. Results from the static photography demonstrate that landslides generally produce the most sediment. This agrees with previous work by Nelson and Booth (2002) who used a sediment budget approach to look at sources of suspended sediment in an urbanising catchment. Information collected as part of the research into tree basal trunk angle, suggests that soil creep is also a source of sediment within the catchment and is spatially very variable (Figure 6.15).

5. *Use the data to assess the longer term spatial and temporal context of observed sediment delivery patterns and construct a preliminary sediment budget characterising fine sediment delivery.*

The sediment budget for Red House Gill demonstrates that hillslope processes (landsliding, bank collapse and soil creep) have delivered 482 t of sediment over the six month monitoring period (Figure 7.1). Assuming a similar sediment yield for the full year this would result in a load of approximately 962 t which equates to a specific annual sediment load of 386 t km^{-2} yr^{-1} a figure which is close to the maximum reported sediment yields from UK catchments (Walling and Webb, 1987). From the static photography analysis, it is clear that the majority of hillslope erosion has come from landslides. By looking at the results from the TIMS for each tributary, it is clear to see that the Middle stream delivers the most sediment, which is reflected in the sediment budget. This is primarily because the Middle stream drains the second largest area and has a steep channel with very steep valley side slopes

with no floodplain to help store eroded material (Table 3.1). The West stream provides the least sediment due to its smaller catchment size and gentler slopes and greater potential for floodplain storage (Table 3.1). Results from the tree coring (Section 6.2.1), suggest that over the past 45 years soil creep has almost been continuous, with only small hiatuses in creep following dry periods. This suggests that historically, soil creep is a slow but continuous source of sediment to the channel.

8.1 Opportunities for future research

In order to extend this research a number of opportunities for future research have been defined.

8.1.1 Tree Basal Trunk Angle

The purpose of the research on tree basal trunk angle was to develop a proxy for assessing soil instability in the Red House Gill catchment. In this proof of concept investigation the whole catchment could not be mapped in the time available. Therefore future research should be focused on gathering information with a greater spatial coverage. This should be coupled with a detailed geomorphic map of the whole catchment so rates of soil creep can be more closely correlated with active and inactive geomorphic zones and process regimes.

8.1.2 Time Integrated Mass Samplers (TIMS)

TIMS are a useful cost effective device for determining spatial patterns of relative suspended sediment flux however they have several limitations. The device only samples a small cross-section of the river channel, the inlet tube can also be easily blocked by debris and changes in stage can also change local flows leaving the device exposed from the flow (Phillips et al., 2000). Along with these well-known issues, the location of each device in the field is often a compromise due to the number of samplers in the network and when access to the river is limited. For example, the River Wear downstream TIMS recorded less suspended sediment than the River Wear Upstream TIMS (Figure 5.18), which was due to the location of the downstream TIMS next to the gravel bar which helped to divert flow away from the device. Figure 5.18 also demonstrates that the East upstream TIMS recorded a higher average sediment flux compared to the Middle upstream TIMS. This result is because the location of the East upstream TIMS is located halfway down the East stream recording more hillslope erosion compared to the Middle upstream TIMS.

Future research within the Red House Gill catchment using TIMS should aim at a better spatial distribution of samplers. An idea for this would be to move the upstream East sampler closer to the culvert and placing a sampler near the source of the West stream. Placing another sampler on the West stream would help gather information about how much sediment is delivered by the upper agricultural part of the catchment compared to the wooded hillslopes.

Together with achieving a better spatial distribution, the TIMS sediment samples could be used for sediment fingerprinting. Information on suspended sediment sources is crucial for sediment budgets (Dietrich and Dunne, 1978) however few studies have used sediment fingerprinting in urbanised / industrial catchments. Although research by Carter et al. (2003) provided a wealth of information about sediment sources within the River Aire and its main tributary the River Calder. In the upper rural part of the catchment, channel bank erosion delivered the most sediment however, within the lower reaches significant amounts of sediment came from urban sources such as road dust (Carter et al., 2003). At Red House Gill, the use of sediment fingerprinting would provide more information about source type and location, which in turn would aid management strategies.

8.1.3 Turbidity Probe and Stage Recorder

The time series of data provided by the turbidity probe and stage recorder provides a lot of information. However, discharge was created from the stage recorder using the slope area method due to the limited site access and due to the lack of an extensive water sampling program a regional calibration was used to convert SSC from NTU. These are both limitations of the data. As a result of this, continuing research at Red House Gill should aim at developing a site specific calibration between suspended sediment concentration and turbidity units. Previous research by Goodwin et al. (2003), created a catchment specific calibration for Bradford Beck within Yorkshire, by collecting automatic water samples daily and manual samples on a fortnightly basis, achieving an R^2 value of 0.99. Along with this improvement, the monitoring period could be extended providing information on all seasons or extended to multiple years.

8.1.4 Preliminary Sediment Budget

The sediment budget demonstrates that sediment being delivered to the stream is well matched to the total sediment load measured although there is a small 11 t

discrepancy. This discrepancy is assumed to be caused by in channel erosion which hasn't been measured. Therefore continuing research into fine sediment movement within the Red House Gill catchment should look at monitoring channel erosion to help further constrain the preliminary sediment budget. To further improve the accuracy of the sediment budget, sediment samples should be taken to provide detailed information on bulk density from a range of soil types in the catchment.

In this research data were collected over a 6 month monitoring period (11th April – 23rd October 2013) and used to generate a preliminary sediment budget. The range of stream flows and weather patterns typical of the annual variability in catchment hydrology, were experienced during the monitoring window. Although further research should focus on extending the period of data collection to generate an annual or multiple year sediment budget the overall conclusions based on the short-term monitoring are unlikely to change substantially. To ensure that the sediment budget investigation is fully representative, instead of providing a snapshot of suspended sediment dynamics, data collection should extend over multiple years (Walling and Webb, 1981) but this is beyond the scope of most studies.

9 Appendices

Appendix Reference	Appendix Name
A	TLS Processing Flow Chart
B	RiSCAN and TerraScan Parameters
C	Disturbed Tree Chronology
D	Reference Tree Chronology

9.1 Appendix A: TLS Processing Flow Chart

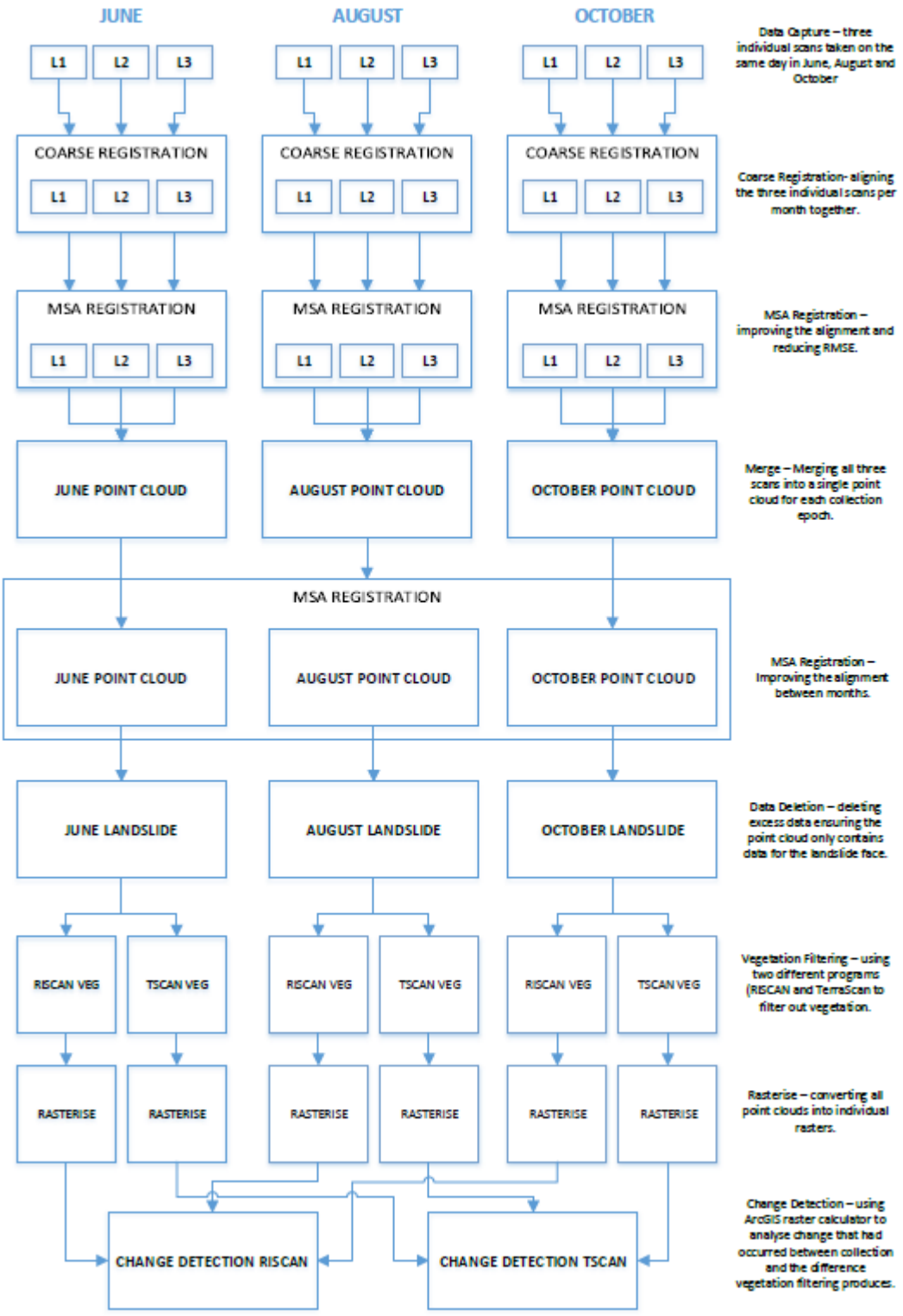

9.2 Appendix B: RiSCAN and TerraScan Parameters

RiSCAN Filtering Parameters

Parameter	Value Used
Base Grid Size (m)	0.05
Number of Levels	8
Tolerance Factor	0.5
Percentile (%)	1
Maximum Slope Angle (^{0})	45
Fine Filter (m)	1

TerraScan Filtering Parameters

Parameter	Value Used
Maximum Building Size (m)	1.0
Terrain Angle (^{0})	90.0
Iteration Angle (^{0})	0.5
Iteration Distance (m)	1.4

9.3 Appendix C: Disturbed Tree Chronology

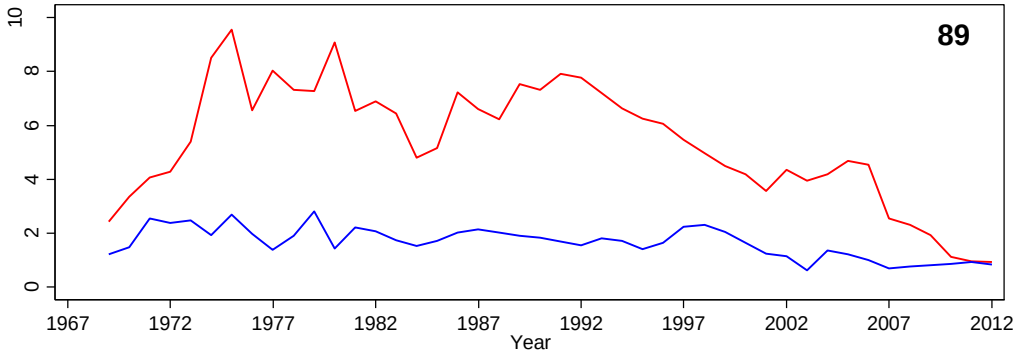

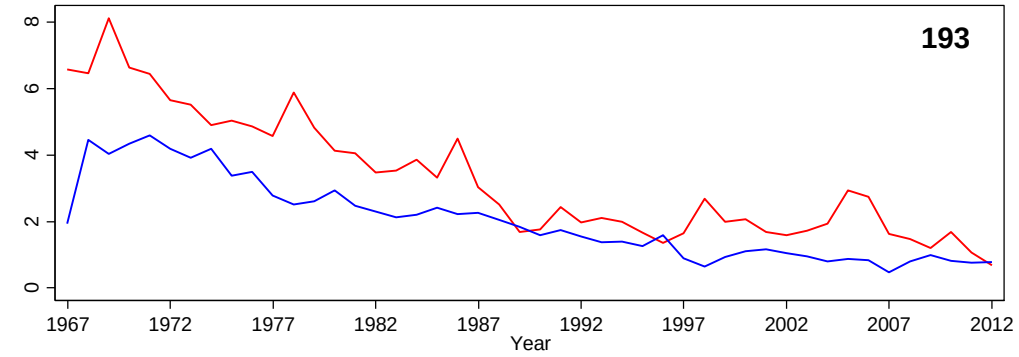

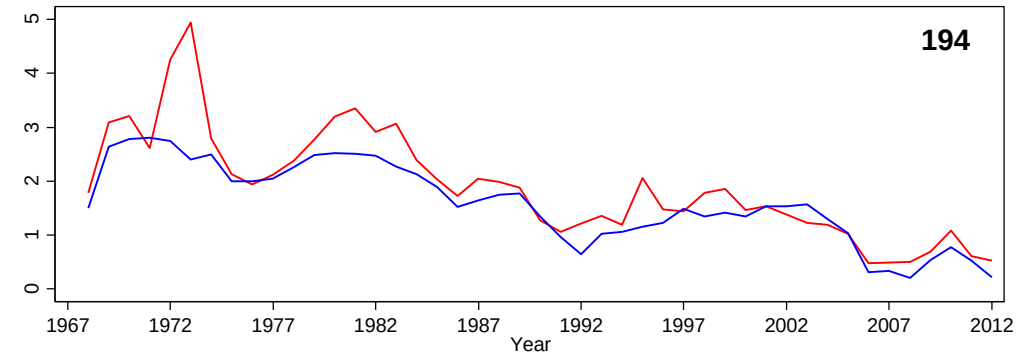

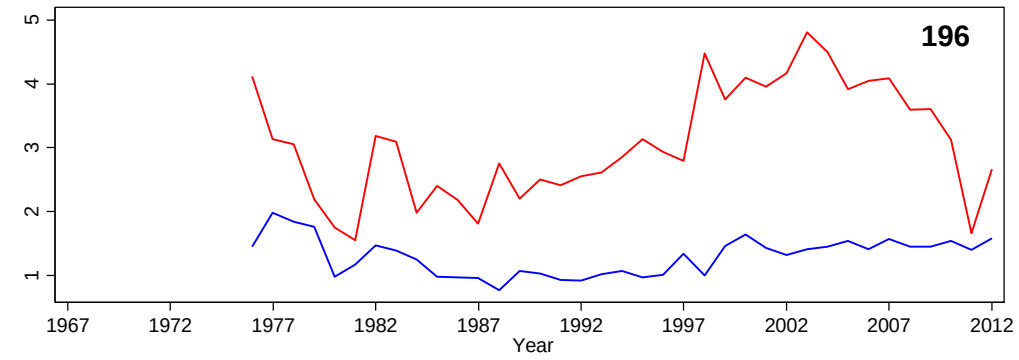

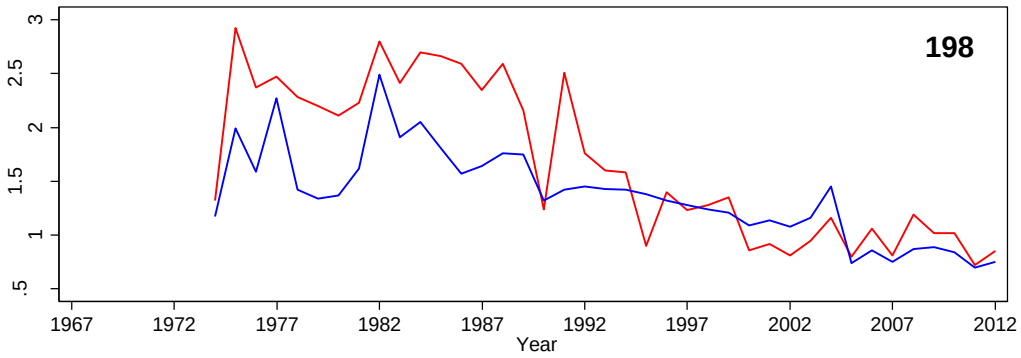
198
.5
1.5
2.5
3
1967
1972
1977
1982
1987
1992
1997
2002
2007
2012
Year

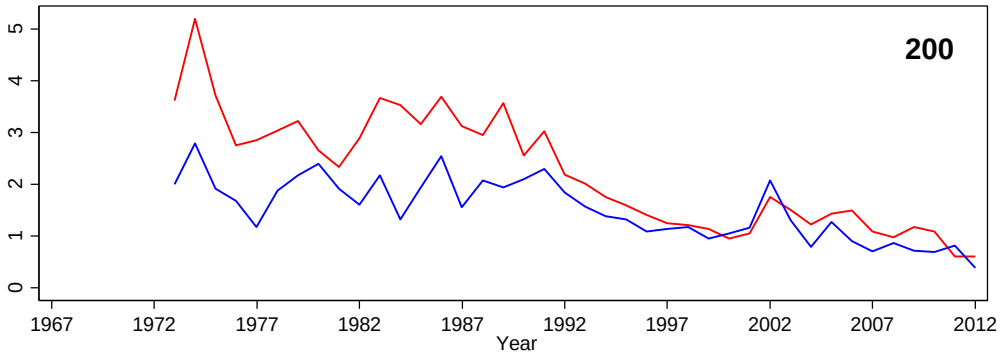
200
0
1
2
3
4
5
1967
1972
1977
1982
1987
1992
1997
2002
2007
2012
Year

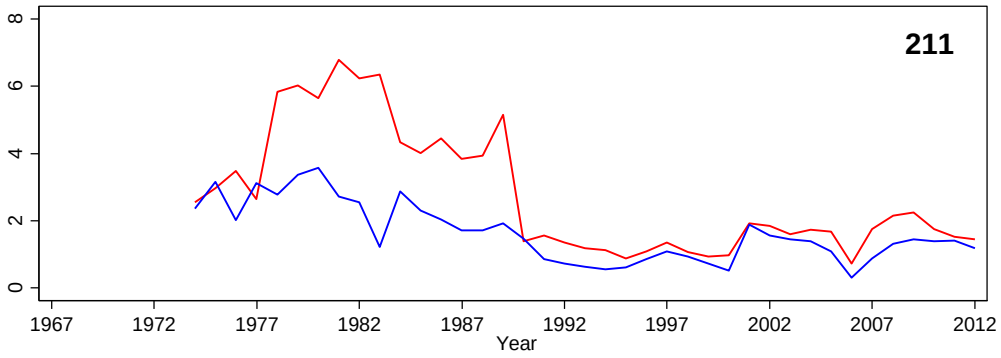
211
0
2
4
6
8
1967
1972
1977
1982
1987
1992
1997
2002
2007
2012
Year

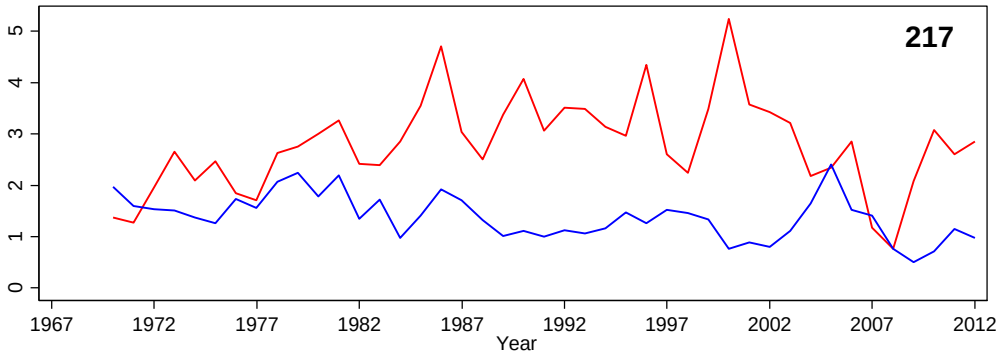
217
0
1
2
3
4
5
1967
1972
1977
1982
1987
1992
1997
2002
2007
2012
Year

9.4 Appendix D: Reference Tree Chronology

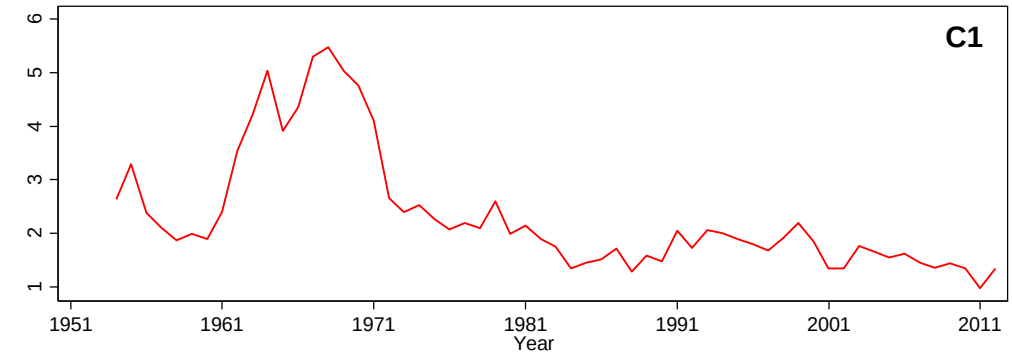

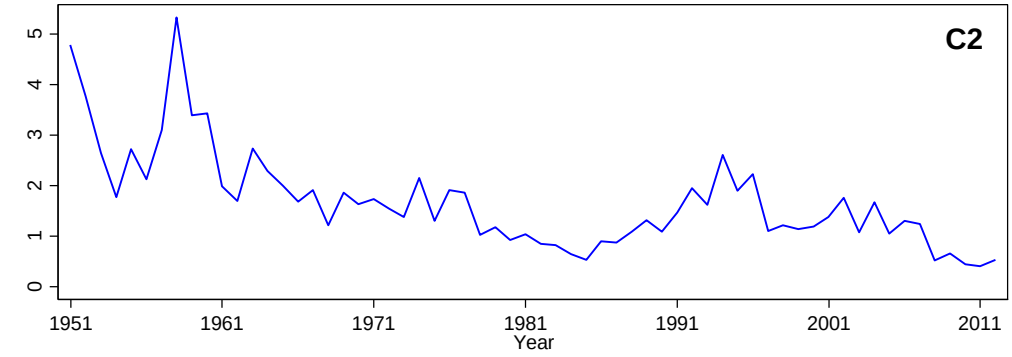

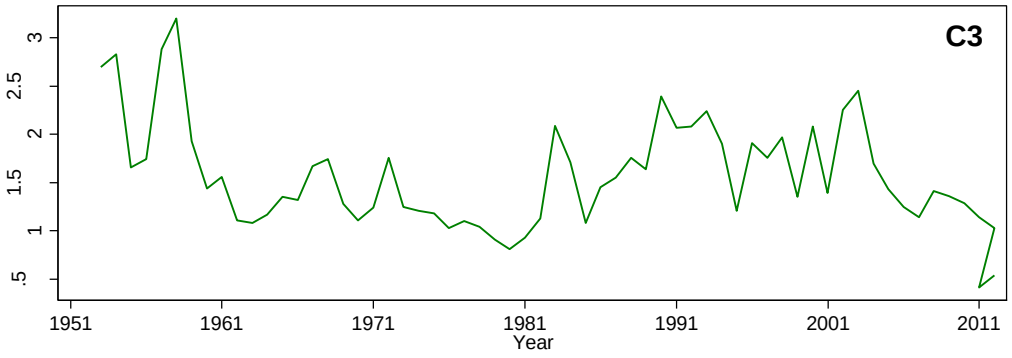

10 References

ALESTRO, J. 1971. Dendrochronological interpretation of geomorphic processes. Fennia, 105, 1-139.

ANDERSON, E., W. 1977. Soil Creep: an assessment of certain controlling factors with special reference to upper Weardale England.

ASSELMAN, N. E. M. 2000. Fitting and interpretation of sediment rating curves. Journal of Hydrology, 234, 228-248.

BBC. 2009. Rare fish 'proves water quality' [Online]. Available: http://news.bbc.co.uk/1/hi/england/wear/8122999.stm [Accessed 20/12 2013].

BITELLI, G., DUBBINI, M. & ZANUTTA, A. 2005. Terrestrial Laser Scanning and Digital Photogrammetry Techniques to Monitor Landslide Bodies. Annual congress of the International Society for Photogrammetry and Remote Sensing. Istanbul.

BOLLSCHWEILER, M., STOFFEL, M. & SCHNEUWLY, D. M. 2008. Dynamics in debris-flow activity on a forested cone — A case study using different dendroecological approaches. CATENA, 72, 67-78.

BRAUD, I., FLETCHER, T. D. & ANDRIEU, H. 2013. Hydrology of peri-urban catchments: Processes and modelling. Journal of Hydrology, 485, 1-4.

BRESSY, A., GROMAIRE, M.-C., LORGEOUX, C., SAAD, M., LEROY, F. & CHEBBO, G. 2014. Efficiency of source control systems for reducing runoff pollutant loads: Feedback on experimental catchments within Paris conurbation. Water Research, 57, 234-246.

BURNS, M. J., FLETCHER, T. D., WALSH, C. J., LADSON, A. R. & HATT, B. E. 2012. Hydrologic shortcomings of conventional urban stormwater management and opportunities for reform. Landscape and Urban Planning, 105, 230-240.

CARTER, J., OWENS, P. N., WALLING, D. E. & LEEKS, G. J. L. 2003. Fingerprinting suspended sediment sources in a large urban river system. Science of The Total Environment, 314–316, 513-534.

CASPER, T. 2008. Regulatory Frameworks for Sediment Management. In: OWENS, P. N. (ed.) Sustainable Management of Sediment Resources. SEDNET.

CHARLESWORTH, S., M, HARKER, E. & RICKARD, S. 2003. A review of sustainable drainage systems (SuDS): A soft option for hard drainage questions. Geography, 88, 99-107.

COHEN, J. E. 2003. Human Population: The Next Half Century. Science, 302, 1172-1175.

COOKE, R., U & DOORNKAMP, J., C 1990. Geomorphology in Environment Management: A New Introduction.

COUNCIL, D. C. 2013. North of Arniston Centre and Newton Hall July 2012 [Online]. Available: http://durhamcc-consult.limehouse.co.uk/portal/planning/lp/na_spd?pointId=2173331#document-2173331.

COUPER, P. R. & MADDOCK, I. P. 2001. Subaerial river bank erosion processes and their interaction with other bank erosion mechanisms on the River Arrow, Warwickshire, UK. Earth Surface Processes and Landforms, 26, 631-646.

DE VENTE, J., POESEN, J., ARABKHEDRI, M. & VERSTRAETEN, G. 2007. The sediment delivery problem revisited. Progress in Physical Geography, 31, 155-178.

DENNELER, B. & SCHWEINGRUBER, F., H. 1993. Slow mass movement. A dendrogeomorphological study in Gams, Swiss Rhine Valley. Dendrochronologia, 11, 55-67.

DIETRICH, W. E. & DUNNE, T. 1978. Sediment budget for a small catchment in mountainous terrain. Z Geomorph, 29, 191-206.

DIETRICH, W. E., DUNNE, T., HUMPHREY, N., F & REID, L., M. 1982. Construction of sediment budgets for drainage basins. In: SWANSON, F., J, JANDA, R., J, DUNNE, T. & SWANSTON, D., N (eds.) Sediment Budgets and Routing in Forested Drainage Basins. United States Department of Agriculture.

DUAN, N. 1983. Smearing Estimate: A Nonparametric Retransformation Method. Journal of the American Statistical Association, 78, 605-610.

DUIJSINGS, J. J. H. M. 1987. A sediment budget for a forested catchment in Luxembourg and its implications for channel development. Earth Surface Processes and Landforms, 12, 173-184.

DUNNE, T. & LEOPOLD, L., B 1978. Water in Environmental Planning, H Freeman and Company

DURHAM 2013. Department of Geography, Weather Data. Durham University

EA 2008. River Wear Salmon Action Plan Review.

EA. 2011. Catchment Pilots: an introduction to the Lower Wear Pilot [Online]. Available: http://www.google.co.uk/url?sa=t&rct=j&q=&esrc=s&source=web&cd=1&ved=0CDAQFjAA&url=http%3A%2F%2Fwww.environment-agency.gov.uk%2Fstatic%2Fdocuments%2FResearch%2FLower_Wear_Pilot_An_Introduction.pdf&ei=o1bNUuvaMsap7Ab0qICwCQ&usg=AFQjCNGr1myYnw1C-2XsQ07EptjxrQRy2A&sig2=rMRqD_3eFoerO_fTNDseEA&bvm=bv.58187178,d.ZGU [Accessed 20/12 2013].

FENN, C. R., GURNELL, A. M. & BEECROFT, I. R. 1985. An Evaluation of the Use of Suspended Sediment Rating Curves for the Prediction of Suspended Sediment Concentration in a Proglacial Stream. Geografiska Annaler. Series A, Physical Geography, 67, 71-82.

FERGUSON, R. I. 1986. River Loads Underestimated by Rating Curves. Water Resources Research, 22, 74-76.

FOX, J. F. & PAPANICOLAOU, A. N. 2007. The Use of Carbon and Nitrogen Isotopes to Study Watershed Erosion Processes1. JAWRA Journal of the American Water Resources Association, 43, 1047-1064.

FRENI, G., MANNINA, G. & VIVIANI, G. 2010. Urban Storm-Water Quality Management: Centralized versus Source Control. Journal of Water Resources Planning and Management, 136, 268-278.

GAO, P. 2008. Understanding watershed suspended sediment transport. Progress in Physical Geography, 32, 243-263.

GIPPEL, C. J. 1995. Potential of turbidity monitoring for measuring the transport of suspended solids in streams. Hydrological Processes, 9, 83-97.

GOODWIN, T. H., YOUNG, A. R., HOLMES, M. G. R., OLD, G. H., HEWITT, N., LEEKS, G. J. L., PACKMAN, J. C. & SMITH, B. P. G. 2003. The temporal and spatial variability of sediment transport and yields within the Bradford Beck catchment, West Yorkshire. Science of The Total Environment, 314–316, 475-494.

GORDON, N., D, MCMAHON, T., A, FINLAYSON, B., L, GIPPEL, C., J & NATHAN, R., J 2004. Stream Hydrology: An Introduction for Ecologists, Wiley

GOUDIE, A., ANDERSON, M., BURT, T., LEWIN, J., RICHARDS, K., WHALLEY, B. & WORSLEY, P. 1981. Geomorphological Techniques George, Allen and Unwin.

HARKER, R. I. 1996. Curved Tree Trunks: Indicators of Soil Creep and Other Phenomena. The Journal of Geology, 104, 351-358.

HATFIELD, R. G. & MAHER, B. A. 2008. Suspended sediment characterization and tracing using a magnetic fingerprinting technique: Bassenthwaite Lake, Cumbria, UK. The Holocene, 18, 105-115.

HELSEL, D., R & HIRSCH, R., M 2002. Statistical Methods in Water Resources. Hydrological Analysis and Interpretation. USGS.

HENSHAW, A. J., THORNE, C. R. & CLIFFORD, N. J. 2013. Identifying causes and controls of river bank erosion in a British upland catchment. CATENA, 100, 107-119.

HICKS, D., M & GOMEZ, B. 2003. Sediment Transport. In: KONDOLF, G., M & PEGAY, H. (eds.) Tools in Fluvial Geomorphology. Chichester, Wiley.

HOOKE, J. M. 1979. An analysis of the processes of river bank erosion. Journal of Hydrology, 42, 39-62.

HUPP, C., L & SIGAFOOS, R., S 1982. Plant Growth and Block-Field Movment in Virginia. In: SWANSON, F., J, JANDA, R., J, DUNNE, T. & SWANSON, F., J (eds.) Sediment Budgets and Routing in Forested Drainage Basins. United States Department of Agriculture.

ISCO 2004. 6712 Portable Water Sampler, Installation and Operation Guide.

JABOYEDOFF, M., OPPIKOFER, T., ABELLÁN, A., DERRON, M.-H., LOYE, A., METZGER, R. & PEDRAZZINI, A. 2012. Use of LIDAR in landslide investigations: a review. Natural Hazards, 61, 5-28.

JACOBSON, C. R. 2011. Identification and quantification of the hydrological impacts of imperviousness in urban catchments: A review. Journal of Environmental Management, 92, 1438-1448.

JAHN, A. 1989. The Soil Creep on Slopes in Different Altitudinal and Ecological Zones of Sudetes Mountains. Geografiska Annaler. Series A, Physical Geography, 71, 161-170.

JARVIS, R., A. , BENDELOW, V., C, BRADLEY, R., I, CARROLL, D., M, FURNESS, R., R, KILGOUR, I., N, L & LING, S., J 1984. Soils and their use in Northern England. Bulletin No. 10, 411.

JBA 2012. Red House Gill Surface Water Study.

JOHNSON, R., C 1992. Towards the design of a strategy for sampling suspended sediments in small headwater catchments. IAHS, 210, 225-232.

KIRKBY, M. J. 1967. Measurement and Theory of Soil Creep. The Journal of Geology, 75, 359-378.

KLEIN, R. D. 1979. URBANIZATION AND STREAM QUALITY IMPAIRMENT. JAWRA Journal of the American Water Resources Association, 15, 948-963.

KNIGHTON, A. D. 1999. Downstream variation in stream power. Geomorphology, 29, 293-306.

LAWLER, D. M. 1995. The impact of scale on the processes of channel side sediment supply: a conceptual model. . Boulder Symposium. IAHS.

LAWLER, D. M., GROVE, J. R., COUPERTHWAITE, J. S. & LEEKS, G. J. L. 1999. Downstream change in river bank erosion rates in the Swale–Ouse system, northern England. Hydrological Processes, 13, 977-992.

LAWLER, D.M., PETTS, G.E., FOSTER, I.D.L.& HARPER, S. 2006. Turbidity dynamics during spring storm events in an urban headwater river system: The Upper Tame, West Midlands, UK. Science of the Total Environment, 360, 109-126.

LAWRENCE, D., J, D, VYE, C., L & YOUNG, B. 2004. Durham Geodiversity Audit. Durham County Council.

LUDWIG, K. A. & HANES, D. M. 1990. A laboratory evaluation of optical backscatterance suspended solids sensors exposed to sand-mud mixtures. Marine Geology, 94, 173-179.

MAEGLIN, R., R 1979. Increment Cores - How to Collect, Handle and Use Them. . USDA Forest Service General Technical Report FPL 25.

MCMAHON, G., BALES, J. D., COLES, J. F., GIDDINGS, E. M. P. & ZAPPIA, H. 2003. USE OF STAGE DATA TO CHARACTERIZE HYDROLOGIC CONDITIONS IN AN URBANIZING

ENVIRONMENT1. JAWRA Journal of the American Water Resources Association, 39, 1529-1546.

MEADE, R. H. 1982. Sources, Sinks, and Storage of River Sediment in the Atlantic Drainage of the United States. The Journal of Geology, 90, 235-252.

METOFFICE. 2013. North East England: Climate [Online]. Available: http://www.metoffice.gov.uk/climate/uk/ne/print.html [Accessed 20/12 2013].

MEYER, J. L., PAUL, M. J. & TAULBEE, W. K. 2005. Stream Ecosystem Function in Urbanizing Landscapes. Journal of the North American Benthological Society, 24, 602-612.

MILLER, J.D., KIM, H., KJELDSEN, T.R., PACKMAN, J., GREBBY, S. & DEARDEN, R. 2014. Assessing the impact of urbanisation on storm runoff in a peri-urban catchment using historical change in impervious cover. Journal of Hydrology, 515, 59-70.

MILLS, H. 1984. Effect of hillslope angle and substrate on tree tilt and denundation of hillslopes by tree fall. Physical Geography, 5, 253-261.

MOGGRIDGE, H. 2010. Assessment of the geormorphological and hydrological condition of Redhouse Gill, a tributary of the River Wear, Durham. Catchment Science Centre, University of Sheffield.

NATIONAL STATISTICS, O. F. 2012. House Building in England: July to September 2012 [Online]. https://www.gov.uk/government/publications/house-building-in-england-july-to-september-2012. [Accessed 12/11/2013.

NELSON, E. J. & BOOTH, D. B. 2002. Sediment sources in an urbanizing, mixed land-use watershed. Journal of Hydrology, 264, 51-68.

NELSON, M., E & BENEDICT, P., C 1950. Measurement and analysis of suspended sediment loads in streams. Trans ASCE, 116, 891-918.

OSTERKAMP, W. R. & HUPP, C. R. 1987. Dating and interpretation of debris flows by geologic and botanical methods at Whitney Creek Gorge, Mount Shasta, California. Reviews in Engineering Geology, 7, 157-164.

OSTERKAMP, W. R. & TOY, T. J. 1997. Geomorphic considerations for erosion prediction. Environmental Geology, 29, 152-157.

OWCZAREK, P. 30/10/2013 2013. RE: Surface processes and interactions with forest vegetation on steep mudstone slope, Stolowe Mountains, SW Poland. Type to PETERS, A.

OWENS, P. N. & WALLING, D. E. 2002. The phosphorus content of fluvial sediment in rural and industrialized river basins. Water Research, 36, 685-701.

PARIZEK, E., J & WOODRUFF, J., F 1957. Mass wasting and deformation of trees. American Journal of Science, 255, 60-70.

PARSONS, A. J. 2012. How useful are catchment sediment budgets? Progress in Physical Geography, 36, 60-71.

PARSONS, A. J., ABRAHAMS, A. D. & SIMANTON, R. J. 1992. Microtopography and soil-surface materials on semi-arid piedmont hillslopes, Southern Arizona. Journal of Arid Environments, 22, 107-115.

PAWLIK, Ł. 2013. The role of trees in the geomorphic system of forested hillslopes — A review. Earth-Science Reviews, 126, 250-265.

PAWLIK, Ł., MIGOŃ, P., OWCZAREK, P. & KACPRZAK, A. 2013. Surface processes and interactions with forest vegetation on a steep mudstone slope, Stołowe Mountains, SW Poland. CATENA, 109, 203-216.

PERKS, M. T. 2013. Spatial and temporal dynamics of fine fluvial sediment transfer: implications for monitoring and management of upland river systems PhD Thesis, Durham University

PERKS, M. T., WARBURTON, J. & BRACKEN, L. 2013. Critical assessment and validation of a time-integrating fluvial suspended sediment sampler. Hydrological Processes, n/a-n/a.

PHILLIPS, J. M., RUSSELL, M. A. & WALLING, D. E. 2000. Time-integrated sampling of fluvial suspended sediment: a simple methodology for small catchments. Hydrological Processes, 14, 2589-2602.

PHILLIPS, J. M., WEBB, B. W., WALLING, D. E. & LEEKS, G. J. L. 1999. Estimating the suspended sediment loads of rivers in the LOIS study area using infrequent samples. Hydrological Processes, 13, 1035-1050.

PHIPPS, R., L 1974. The soil-creep tree fallacy. Journal of Research, US Geological Survey, 2, 371-377.

POLLEN-BANKHEAD, N. & SIMON, A. 2010. Hydrologic and hydraulic effects of riparian root networks on streambank stability: Is mechanical root-reinforcement the whole story? Geomorphology, 116, 353-362.

PRASKIEVICZ, S. & CHANG, H. 2009. A review of hydrological modelling of basin-scale climate change and urban development impacts. Progress in Physical Geography, 33, 650-671.

REID, L., M. & DUNNE, T. 1996. Rapid Evaulation of Sediment Budgets, Margot Rohdenburg.

RICKLI, C. & GRAF, F. 2009. Effects of forests on shallow landslides – case studies in Switzerland. Forest and Snow Landscpe Research, 82, 33-44.

RIEGL. 2013. Reigl VZ-1000 [Online]. Available: http://www.riegl.com/nc/products/terrestrial-scanning/produktdetail/product/scanner/27/.

ROBERTSON, D. J., TAYLOR, K. G. & HOON, S. R. 2003. Geochemical and mineral magnetic characterisation of urban sediment particulates, Manchester, UK. Applied geochemistry, 18, 269-282.

ROSE, S. & PETERS, N. E. 2001. Effects of urbanization on streamflow in the Atlanta area (Georgia, USA): a comparative hydrological approach. Hydrological Processes, 15, 1441-1457.

ROY, A. H., ROSEMOND, A. D., PAUL, M. J., LEIGH, D. S. & WALLACE, J. B. 2003. Stream macroinvertebrate response to catchment urbanisation (Georgia, U.S.A.). Freshwater Biology, 48, 329-346.

RUSSELL, M. A., WALLING, D. E. & HODGKINSON, R. A. 2001. Appraisal of a simple sampling device for collecting time integrated fluvial suspended sediment samples. In: M, S. (ed.) The Role of Erosion and Sediment Transport in Nutrient and Contaminant Transfer. IAHS: IAHS.

SADEGHI, S. H. R., MIZUYAMA, T., MIYATA, S., GOMI, T., KOSUGI, K., FUKUSHIMA, T., MIZUGAKI, S. & ONDA, Y. 2008. Development, evaluation and interpretation of sediment rating curves for a Japanese small mountainous reforested watershed. Geoderma, 144, 198-211.

SAUNDERS, I. & YOUNG, A. 1983. Rates of surface processes on slopes, slope retreat and denudation. Earth Surface Processes and Landforms, 8, 473-501.

SCHINDLER WILDHABER, Y., MICHEL, C., BURKHARDT-HOLM, P., BÄNNINGER, D. & ALEWELL, C. 2012. Measurement of spatial and temporal fine sediment dynamics in a small river. Hydrol. Earth Syst. Sci., 16, 1501-1515.

SCHUMM, S. A. & LICHTY, R. W. 1965. Time, space, and causality in geomorphology. American Journal of Science, 263, 110-119.

SEDNET 2004. Contaminated Sediments in European River Basins, European Sediment Research Network

SEDNET. 2013. SedNet: Strategy Paper [Online]. Available: http://www.sednet.org/about.htm Accessed 17/02/2014.

SELBY, M., J. 1993. Hillslope Materials and Processes, Oxford University Press.

SHARPE, C., F, S 1938. Landslides and related phenomena: New York, Columbia University Press.

SHEEDER, S. A., ROSS, J. D. & CARLSON, T. N. 2002. DUAL URBAN AND RURAL HYDROGRAPH SIGNALS IN THREE SMALL WATERSHEDS1. JAWRA Journal of the American Water Resources Association, 38, 1027-1040.

SITHOLE, G. & VOSSELMAN, G. 2004. Experimental comparison of filter algorithms for bare Earth extraction from airborne laser scanning point clouds. Photogrammetry and Remote Sensing, 59, 85-101.

SPEER, J., H. 2010. Fundamentals of Tree Ring Research, The University of Arizona Press.

STAFFORD, S. 2005. Magic Lantern Guides: Nikon D70 and D70s, Lark Books.

STOFFEL, M. & BOLLSCHWEILER, M. 2008. Tree-ring analysis in natural hazards research - an overview. Natural Hazards and Earth System Science, 8, 187-202.

SWANSON, F., J, JANDA, R., J, DUNNE, T. & SWANSTON, D., N 1982. Introduction: Workshop on Sediment Budgets and Routing. In: SWANSON, F., J, JANDA, R., J, DUNNE, T. & SWANSTON, D., N (eds.) Sediment Budgets and Routing in Forested Drainage Basins. United States Department of Agriculture.

TERZAGHI, K. 1950. Mechanisms of Landslides. In: TEZAGHI, K. (ed.) Application of Geology to Engineering Practice Geological Society of America.

THE WOODLAND TRUST. 2013. The Wooldland Trust Nature Detectives - Leaf Hunt [Online]. Available: http://www.naturedetectives.org.uk/download/hunt_leaves.htm [Accessed 01/05/2013.

THEULE, J. I., LOYE, A., LIÉBAULT, F., LAIGLE, D. & JABOYEDOFF, M. 2009. Sediment budget of a debris flow event in the French Prealps. American Geophysical Union, Fall Meeting

TIMELL, T. E. 1986. Compression wood in gymnosperms. Springer-Verlag. Berlin.

TRIMBLE, S. W. 1997. Contribution of Stream Channel Erosion to Sediment Yield from an Urbanizing Watershed. Science, 278, 1442-1444.

TWIDALE 1964. Erosion of an alluvial bank at Birdwood, South Australia. Z Geomorph, 8.

WALKER, L., R & SHIELS, A., B 2013. Landslide Ecology, Cambridge University Press.

WALLING, D. E. 1977. Assessing the Accuracy of Suspended Sediment Rating Curves for a Small Basin. Water Resources Research, 13.

WALLING, D. E. 2005. Tracing suspended sediment sources in catchments and river systems. Science of The Total Environment, 344, 159-184.

WALLING, D. E. & COLLINS, A. L. 2005. Suspended sediment sources in British Rivers. In: WALLING, D. E. & HOROWITZ, A. J. (eds.) Sediment Budgets. IAHS Press

WALLING, D. E., RUSSELL, M. A., HODGKINSON, R. A. & ZHANG, Y. 2002. Establishing sediment budgets for two small lowland agricultural catchments in the UK. CATENA, 47, 323-353.

WALLING, D. E. & WEBB, B., W 1981. The reliability of suspended sediment load data. IAHS, 133, 177-194.

WALLING, D. E. & WEBB, B., W 1987. Suspended Load in Gravel-bed Rivers: UK Experience. . In: THORNE, C. R., BATHURST, J. C. & HEY, R. D. (eds.) Sediment transport in Gravel-bed Rivers. John Wiley and Sons.

WALLING, D. E. & WEBB, B., W 1988. The reliability of rating curve estimates of suspended sediment yield: some further comments. In: BORDAS, M. P. & WALLING, D. E. (eds.) Sediment Budgets. IAHS.

WALLING, D. E., WEBB, B., W & WOODWARD, J., C 1992. Some sampling considerations in the design of effective strategies for monitoring sediment-associated transport. In: BOGEN, J. W., D, E & DAY, T., J (eds.) Erosion and sediment transport monitoring programmes in river basins. IAHS.

WANG, L., LYONS, J., KANEHL, P. & BANNERMAN, R. 2001. Impacts of Urbanization on Stream Habitat and Fish Across Multiple Spatial Scales. Environmental Management, 28, 255-266.

WASS, P. D. & LEEKS, G. J. L. 1999. Suspended sediment fluxes in the Humber catchment, UK. Hydrological Processes, 13, 935-953.

WHITE, J. 1998. Estimating the Age of Large and Veteran Trees in Britain [Online]. Available: http://www.forestry.gov.uk/website/Publications.nsf/WebPubsByISBN/8D19EF378AB5884980256F9E00597BF3 [Accessed 06/06/1998.

WINCHESTER, V., GARTNER, H. & BEZZI, M. 2006. Dendrogeomorphological Applications. In: GOUDIE, A. & KALVODA, J. (eds.) Geomorphological Variations.

WISTUBA, M., MALIK, I. & OWCZAREK, P. 2011. Eccentric growth of trees as a tool for reconstruction of mass movement activity (example from the Carpathian Mountains - Central Europe). . Tree Rings in Archaeology, Climatology and Ecology,, 9, 103-108.

WOOD, P. J. & ARMITAGE, P. D. 1997. Biological Effects of Fine Sediment in the Lotic Environment. Environmental Management, 21, 203-217.

WOODWARD, J. C. & WALLING, D. E. 2007. Composite suspended sediment particles in river systems: their incidence, dynamics and physical characteristics. Hydrological Processes, 21, 3601-3614.

WREN, D., BARKDOLL, B., KUHNLE, R. & DERROW, R. 2000. Field Techniques for Suspended-Sediment Measurement. Journal of Hydraulic Engineering, 126, 97-104.

YAMADA, S. 1999. The role of soil creep and slope failure in the landscape evolution of a head water basin: field measurements in a zero order basin of northern Japan. Geomorphology, 28, 329-344.